FIT Fukuoka Institute of Technology 福岡工業大学

GRADUATE SCHOOL OF ENGINEERING

FUKUOKA INSTITUTE OF TECHNOLOGY

Study of Devised Hall Effect Sensor System for Industrial Measurement and Non-destructive Inspection

by

Witsarut Sriratana

Adviser: Prof. Riichi Murayama

2014

Contents

List of Figures

List of Tables

List of Abbreviation and Symbols

The abbreviations appearing in the dissertation are listed below. Any minor departure from these abbreviations is explained in the text itself.

Abbreviation	Description
a	Acceleration of the reference metal particles moving to permanent magnet (m/s^2)
A	Area of oil containers (cm^3)
A_1	the cross section in cm^2
B	Density of magnetic field (Tesla)
B_m	Phases movement
B_0	Center of the magnetic field
B_X	Phase movement direction X-axis
B_Y	Phase movement direction Y-axis
c	The constant
C_t	Timer capacitor (μF)
d	Distance of the reference metal particles moving to permanent magnet (mm)
d_1	The thickness in cm
D	Distance of the end of shaft from the center of the Helmholtz coil
D_1	Specific gravity of copper ($grams/cm^3$)
Dp	The depth of hole
D_{Si}	The length of sample material
e	An electron of charge
E_H	Hall field
f_o	Output frequency (Hz)
F	Lorenzt force
F_1	The force (N)
ΔH_S	The difference value between the maximum and minimum value of output voltage of each Hall generator
i	The data from the measurement in the one cycle
I	Current through each coil (A)

Abbreviation	Description
l	The length in cm
m	Slope as a function of mass of metal particles and viscosity (s/V)
M	The constant (kg/m) as a function of density of the fluid, distance, and acceleration of the metal particles
n	Number of data in repeated measurement
N	Number of turn of each sub-coil (Turn)
N_1	The number of carriers per cubic centimeter
N_A	The Avogadro constant (6.02×10^{23} mol^{-1})
M_m	The molar mass of copper (63.55 $g \cdot mol^{-1}$)
q	Magnetic field on an electron
r	Distance from the centerline of the conductor to the sensor
R	Coil radius or distance between coils (m)
R_1	Length of shaft
R_e	Resistance in ohm
R_H	Hall coefficient
R_L	Comparator resistor (Ω)
R_s	Bias current resistor (Ω)
R_t	Timer resistor (Ω)
S	The number of Hall generator
$S(x_i)$	Standard deviation
St	The resolution of movement
Sum_S	The summation of data from the measurement of the length of sample material
t	Thickness (cm)
t_m	Time of a given sample passing through Hall Effect sensor (s)
t_{moving}	Moving time to permanent magnet of metal particles (s)
Th	The threshold of voltage (0.15 V)
U_c	Experimental uncertainty
v	Velocity of electron due to electric field
v_1	Moving speed of a sample (mm/s)
V_{max}	The maximum value of output voltage of each Hall generator
V_H	Hall voltage
$V_{S(max)}$	The maximum value of output voltage of each Hall generator
$V_{S(min)}$	The minimum value of output voltage of each Hall generator

Abbreviation	Description
V_{Si}	The output voltage of each Hall generator
w	The width in cm
Wd	The width of hole
x	Displacement of a sample (mm)
x_i	The value of each individual item in the list of number being averaged
$\overline{x}$	Average value or arithmetic mean
X	Distance of shaft from center of the Helmholtz coil direction X-axis

Greek symbols

μ_0	Magnetic permeability (1.26×10^{-6} H/m)
β	Angular of the triangle base
θ	Relative angle
η	Viscosity (Pa.s)
ρ	Density of the fluid (kg/m^3)
σ	The resistivity in ohm-cm

Abstract

This study proposes a new design for a new sensor module for the application of a semiconductor known as a Hall Effect sensor and a measurement method for the angular displacement, the lubricant viscosity and contamination in lubricant, and non-destructive material imperfection. In order to find ways of enhancing the effectiveness of a conventional Hall Effect sensor, this study was divided into 3 parts: 1) the new configuration and its theoretical performance, 2) a consideration of an appropriate placement of a Hall generator, 3) a preliminary experimental test.

With regard to the application of the new sensor module in the measurement of the lubricant viscosity and contamination in lubricant in this study aims to assess the contamination level of metal particles during the work period of an industrial machine. It can also predict the period of lubricant replacement if the lubricant quality is lower than the standard of NAS1638. Analysis of contamination of metal particles in lubricant has a relationship with the output signal of a new sensor module due to the metal particles moving to a permanent magnet. Moreover, this methodology can be effectively applied to examine the viscosity standard of the lubricant used. In this study, dynamic movement and the metal particles with 0.001 g to 1 g of weight and 1 μm to 100 μm of size were used as a case study to simulate the real movement of metal particles in a lubricant during machine operation.

The use of a magnetic field to stimulate a Hall Effect sensor in the case of angular displacement measurement was based on the angular relationship of trigonometric functions. The stimulation was created by an electromagnetic field which was generated by a Helmholtz coil and a magnetic field generated by a permanent magnet. The system was designed by using Helmholtz coil to provide the measuring resolution of 1 deg per step in the measuring range of -15 deg to 15 deg from the normal line with 95 % accuracy. However, the new sensor module was designed by using a permanent magnet to provide the greater measuring resolution of 0.01 deg per step in the measuring range of -20 deg to 20 deg from normal line with 99 % of accuracy.

From empirical study, enhancement of the conventional Hall Effect sensor by determining the appropriate placement of Hall generator and permanent magnet as well as the number of Hall generators in a new sensor module is significant for several

measurements such as the inspection of metal material completion by measuring the dimensions of the holes on the surface of the test specimen. The new sensor module is called the single Hall sensor and is suitable for small slot drilled holes, while 4-crossing Hall sensors are appropriate for large drilled holes or cracks. This is because the output of each Hall generator would be more effective in comparative calculation for determining the perimeter and diameter of drilled holes or cracks in the material, and also depth compared to that of a single Hall sensor. In the case of alternative placement of permanent magnet poles, namely 4-array Hall sensors, it was observed that the disadvantage of flux reversal was caused by suddenly changing the N-poles and S-poles of permanent magnets during measurement.

In the case of signal conditioning, an analysis of the output signal from the new sensor module in the frequency domain was based on the principle of Fourier transform, as used in this study for determining the different diameters and depth of drilled holes on test specimens in order to enhance the efficiency of conventional Hall Effect sensors in being more accurate and reliable. This is because the signal from measurement in frequency form can clearly determine small differences in signals by the measurement of the width and depth of drilled holes. The new sensor module was designed to be clearly distinct at a different depth of 0.5 mm. In comparison, the ultrasonic wave at 1 MHz of frequency generated by electromagnetic acoustic transducer (EMAT) technology Lorentz force was controlled so as to be in parallel with the surface of material which can generate transverse wave detectors for analyzing the wavelength and ratio of signal per noise from experiment under the same conditions. It can be noted that the generation of ultrasonic waves using the EMAT method would not be appropriate for small specimens as the error was greater than 4.51 % and the standard deviation was about 0.279. However, a new sensor module can be effectively used with small specimens as it would cause the error to be less than 0.24 % with a standard deviation of 0.014. Moreover, compared to the ultrasonic wave, the new sensor module could provide the high resolution of measurement at each position, as well as ease of installation and a simple experiment procedure at a reasonable cost.

Chapter 1

Introduction

1.1 General Background

One of the most important factors in guaranteeing the working standard of the instrumentation in the industrial sector is the sensor device, which can be classified by its structure and operating function. The selection of the most effective sensor device in order to make it appropriate for working depends on several factors such as the type and the quantity of variables to measure, the range of measurements and the conditions of the environment (temperature, vibration, humidity, etc.). In case of the industry sector, it was found that one of the most significant factors was the performance of instruments used for detection and measurement, including the process of overall system.

The basic concept of the Hall Effect sensor can be exhibited in an equivalent circuit as shown in Figure 1.1. Figure .1.1 (a) shows the connections between the terminals of a semiconductor, namely the Hall generator and the constant power supply, in this case supplied by a DC power supply. A Hall generator, which is the shape of a thin plate, is made of conductive material, like copper that is carries a current. The direction of flow of a constant current through the Hall generator depends on the polarity of the induced voltage. The terminals of a Hall generator, when it is perpendicular to the direction of a current flowing through a thin plate, are connected to a voltmeter in order to measure its output voltage. In this case the voltage of Hall generator will still be zero due to the absence of a magnetic field around a thin plate. On the other hand, a small voltage appears across a thin plate when is stimulated by magnetic field, then the measurement of Hall generator terminals using the voltmeter found that a small voltage is generated due to a magnetic field being perpendicular to the direction of flowing current as shown in Figure 1.1 (b). However, the direction of polarity of induced voltage will depend on the direction of the magnetic field. If we reverse the direction of the magnetic field, the polarity of this induced voltage will also be reversed. This phenomenon is called the Hall Effect, and was named after Edwin Hall. (*Original by Edward Ramsden: Hall-Effect Sensor Theory and Applications; Elsevier Inc. 2006*) [1].

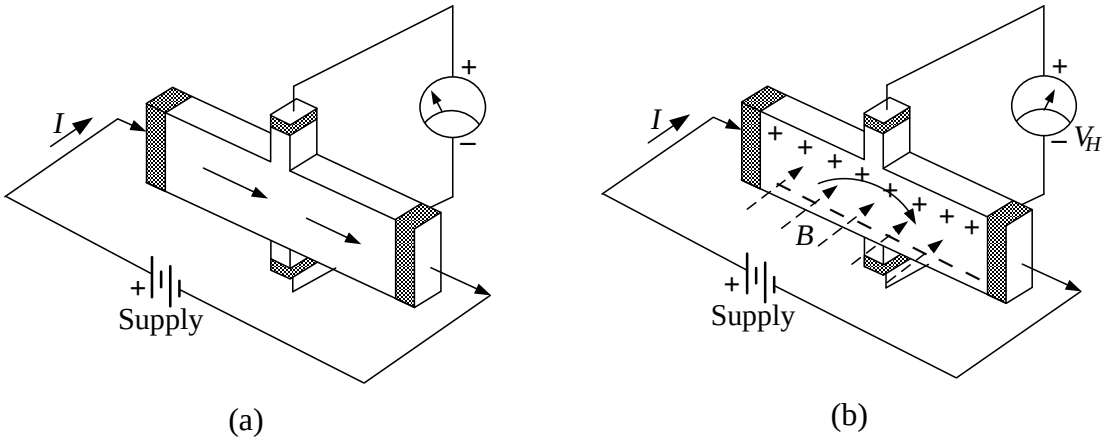

Figure 1.1: Physical principle of a Hall Effect sensor.

The Hall Effect sensor is a methodology which can be applied to a sensor device that involves assembling industrial instrumentation in order to detect, measuring, and control several variables in the industrial fields. This because the Hall Effect sensor is a small semiconductor, which can provided the high accuracy and reliability. Moreover, it is easy to operate along with a general electronics circuit, and also provides good sensitivity for measurement. The phenomenon of Hall or the Hall Effect was discovered by Edwin Hall in 1879. This phenomenon occurs when the current flowing through a conductive material has the presence of a magnetic field around a conductor. If the direction of the flowing current and the magnetic field are perpendicular, the Lorentz force of magnetic flux will divert the direction of an electron, so the electric charge will appear to the opposite side of conductor. On the contrary, these Lorentz force causes the potential and is perpendicularly to both the current of flowing direction and the magnetic field. This is known as called Hall voltage.

1.2 Statement of Problem and Research Questions

The Hall Effect sensor is one of the most commonly used forms of sensor equipment, and is used for detection work, for example; displacement detection and position detection. Moreover, it also functions as speed detection such as clutch detection, automatic gear position, a differential gear tooth sensor, a DC brushless fan, and a speed sensor for encoders. Most signals will be in the term of Logic state, and will be in the condition “Turn ON and Turn OFF”. Thus, the Hall Effect sensor does not cover all the industrial variables, but it is sometimes necessary to use its signal output, measured in term of linearity signals, to analyze and control the process. Therefore, the way to improve the efficiency of a conventional Hall Effect sensor and effectively measure the industrial variable fields in this research will focus on the alignment of Hall generator and magnet, including increasing

the Hall generator and permanent magnet alignment as an array and a crossing. Moreover, there will be on the possibility of working with a magnetic field to stimulate a Hall Effect sensor to work effectively when analysing output signals, by making comparisons between voltage and frequency domain under the same condition in order to assess the system.

1.3 Literature Reviews in Development of Hall Effect Sensor

This section presents the details to clarify the background and rationales discussed in the previous studies as follow:

1.3.1 Angle Measurement Using a Miniature Hall Effect Position Sensor

The origin of this paper is presents to the various methods of angle measurement as well as the miniature Hall Effect angle measuring sensor and a special test stand for it. Similar sensors are going to be used to measure the angle of rotation of the mobile parts of the artificial human hand-shape manipulator that is just being designed in the Bialystok Technical University, as shown in Figure 1.2. (*Original by Karol Bieilczyk, IEEE, 2009*) [2].

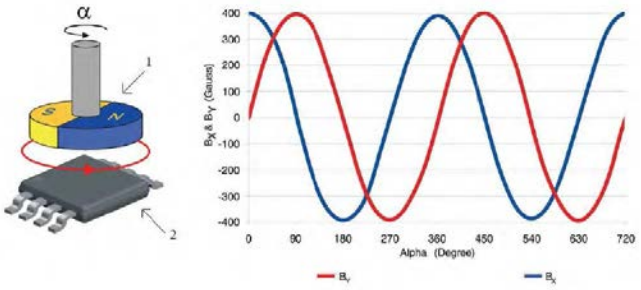

Figure 1.2: Cooperation between magnet and MLX90316:1-small magnet, 2-MLX90316 sensor and sensing signals.

1.3.2 Applications of Linear Hall-Effect Sensors on Angular Measurement

The origin of this paper is presents to the non-contact type application on the permanent magnet and linear Hall Effect sensor gauging rotary system. For such a contactless case, there is no wear. This provides a longer life span in association, and in particular, high reliability to achieve continuous use. The main component of the angular position estimation system is the linear Hall Effect sensor. The angle gauge depends on the Hall voltage at the rotation of the magnetic induction. The advantage of the system is its reliable operation in special environmental conditions, such as high vibration, humidity, or dust. Higher accuracy and precision will be achieved, as shown by the experimental results, and

it can be widely used in the angular measurement field, as shown in Figure 1.3. (*Original by Yun Yao Lee, IEEE, 2011*) [3].

Figure 1.3: Schematic view of the angular position device containing two semi-ring shaped magnets, connected with attractive poles and double linear Hall sensor.

1.3.3 Magnetic Sensor Array for Investigations of Magnetic Field Distribution

The origin of this paper is presents to the various magnetic sensor arrays are described - GMR sensor array, Hall sensor array and AMR sensor array. The applications of this last one are presented. The sensor matrix was designed for three various purposes: a) for test of the steel strip in n × 16 points, b) for increase of the sensor output signal and to obtain the averaging effect, c) for improve of the speed of the scanning device, ad shown in Figure 1.4. (*Original by Slawomir Tumanski, FEI STU, 2006*) [4].

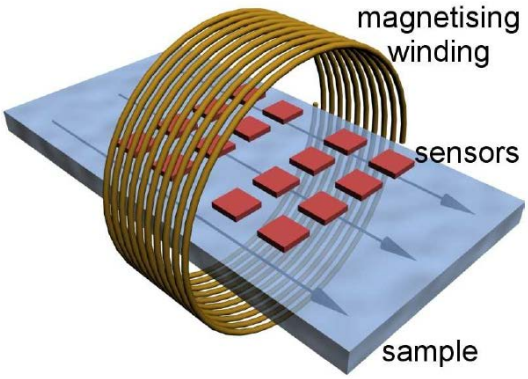

Figure 1.4: The arrangement of the sensor matrix for testing of electrical steel strip magnetized by the magnetic field generated by the coil.

1.4 The Originality of the Study

The main idea, a challenging and interesting one for this study, was the idea of using a conventional Hall Effect sensor in the form of a semiconductor device, which may be small, but provides high quality and reliability at a reasonable cost compared to other

methodologies. In order to apply the measurements in a way that is appropriate for the variables in industrial fields, it is necessary to design and develop measuring instruments which are based on the fundamentals of a magnetic field. Moreover, it can be designed instruments for calibrating the relationship between trigonometric functions in terms of the angles and the remaining length of the measured triangle using an electromagnetic field, which can be generated by the conductor coil to stimulate the Hall Effect sensor. The new sensor module has been designed to detect the material imperfections in the methodology of non-destructive inspection (NDT), based on the fundamental elements of a conventional Hall Effect sensor, then compare to the methodology of an EMAT in terms of performance, ability, and appropriateness for use. It is classified as a new technique of measurement using a Hall Effect sensor, due to the need for measuring and testing the materials which, in this case, need to have a high resolution. A Hall Effect sensor has the ability to provide good resolution and high levels of accuracy as intrinsic properties. Importantly, the performance of a Hall generator will depend on the placement of stimulation by magnet and measurement systems, which in this study are referred to as the new sensor module.

1.5 Objectives of the Study

This study aims to design and develop a new non-destructive measurement using a new sensor module as a sensor device in order to measure the imperfection of metal materials using, in some cases, the methodology of non-destructive inspection. It shows how a conventional Hall Effect sensor can be replaced by other methods such as an EMAT method [5], a radiographic method, an eddy current method [6], a magnetic particle method and a positive material identification method, due to the system it uses for instruments, a Hall Effect sensor has rather high flexibility, using small sizes for simplicity of installation, and it is also easier to setup and calibrate as a sensor device than other methodologies.

1.6 Scope and Limitations

The scope of the study is as follows:

(1) An explanation of the placement of a Hall generator, examining the use of a Hall generator and a permanent magnet in a variety of ways in order to decide on the appropriateness of its use in a number of versions, such as the signal Hall sensor, the 4-array Hall sensor, the 5-array Hall sensor, and the 4-crossing Hall sensor.

(2) An examination of an application of a Hall Effect sensor in the industrial sector. This study was designed to assess a measurement system using a Hall generator and

a magnetic field to activate a Hall Effect sensor. The main electromagnetic field, which was generated by a Helmholtz coil, and another magnetic field which was generated by a permanent magnet, can be divided into four systems which involve the application of angular displacement, lubricant viscosity and contamination in lubricant, and the application of material imperfection.

(3) An analysis of the output signal from a Hall Effect sensor based on the fundamentals of its frequency domain. This study also involves designing and developing a signal conditioning circuit which consists of an instrumentation amplifier and a voltage to frequency converter circuit. The transformation of the frequency will transform the time domain to a frequency domain in this study, using MATLAB software as a case study.

(4) A comparison of the operating systems of a Hall Effect sensor and an EMAT method under the same condition of measuring the material imperfection by non-destructive inspection. This was carried out in order to evaluate the performance of the overall system, the appropriate measurements and the effectiveness of the installation and the initial setup of a sensor device.

(5) An improvement of a new non-destructive measurement using a conventional Hall Effect sensor as a sensor device will replace the EMAT technology for the purpose of inspection of non-destructive materials, which in some cases depending on the appropriateness of the form of the variables and the kind of materials used.

1.7 Organization of the Dissertation

The dissertation is organized in 11 chapters, as follows:

Chapter 2 presents the basis of the methodology used here, such as the physical effects of the Hall Effect sensor, the practical transducers, the principle of the Hall Effect sensor, and the general sensing device using the Hall Effect sensor.

Chapter 3 discusses the main objectives and improvements in the conventional Hall Effect sensor and approach used in the study such as specific objectives, work procedure, and planning of experiment study for applying in different variable.

Chapter 4 presents the study of devised of Hall Effect sensor system for industrial measurement and non-destructive inspection. The typical new sensor modules were considered in this chapter. Moreover, in this chapter explains the fundamental of each sensing mode of Hall Effect sensor such as a single Hall sensor, a Hall Effect sensor with Helmholtz coil, the two flat-curve permanent magnets, the 4-array Hall sensor, the 5-array Hall sensor and the 4-crossing Hall sensor.

Chapter 5 presents an experimental study of the Hall Effect sensor to industrial field. An experimental study in lubricant degradation using the conventional Hall Effect sensor is also explained here, along with a design of a new sensor module used for the measurement of lubricant viscosity and contamination in lubricant.

Chapter 6 presents an experimental study of Hall Effect sensor to industrial field. An angular displacement using the conventional Hall Effect sensor with Helmholtz coil was considering in this study. In this chapter is starting from design of the Helmholtz coil then analysis of angular displacement with the aim of error analysis use results from experiment are discussed.

Chapter 7 presents an experimental study of Hall Effect sensor to the industrial field which continued the development from the previously mentioned application (chapter 6) using the same methodology. In this chapter an angular alignment using two flat-curve permanent magnets is considered. There is also an explanation of the design of a new sensor module, simulating the magnetic field by COMSOL multiphysics, and an experiment with a new sensor module in angular displacement with the aim of error analysis. The results from this experiment are then discussed.

Chapter 8 presents an experimental study of non-destructive inspection for detecting the material imperfection based on time domain. In this chapter the number of Hall generators and number of permanent magnets will be increased in order to enhance the performance of the sensor module for a wider detection area, and then compare the result from measurement in each Hall generator in order to select the best of signal to analyze.

Chapter 9 presents an experimental study of material imperfection based on the frequency domain. This chapter begins by discussing from how to transfer the time domain into the frequency domain. Moreover, the content of this chapter consists of a measurement process, an experiment in frequency waveform and error analysis of measurement.

Chapter 10 presents a comparison of the performance of a Hall Effect sensor and an EMAT a condition of the material imperfection non-destructive. This chapter also provides the details of experimental setup for empirical analysis of a Hall Effect sensor in voltage form and also a frequency domain and empirical analysis of EMAT are analyzed.

Finally, Chapter 11 presents the conclusions of this study.

Chapter 2

Methodology

2.1 Introduction

This chapter presents the history of a Hall Effect sensor from the beginning by starting with the physical Hall Effect sensor. It also describes of the type of materials used for making a Hall generator, which in this study were divided into two types of material: metals and semiconductors. There is also some discussion of the practicality of transducers, the principle of the Hall Effect sensor, and the typical characteristics of Hall Effect sensor, respectively. Finally, examples of the application of the Hall Effect sensor in the industrial sector are given in order to give a basic explanation of the structure and overall process of the Hall Effect sensor. This will be beneficial for those engaged in designing and developing instrumental systems for sensor devices.

2.2 Physical of Hall Effect Sensor

2.2.1 Hall Effect Sensor in Metals

Actually, the first priority for estimating the sensitivity of Hall generator should be to find the value of average charge carrier velocity. Normally, the movement of electrons in metal material will be random with freedom to move due to the thermal energy. However, the thermal velocities will be relatively high in value rather than there being a given value for each electron, because the electrons move in random pattern. The motion of individual electrons will be equal to a zero net motion, resulting in no current. Therefore, when stimulated to conduct by the electric field, there will be a drift of electrons in the same direction as the electric field, while the average rate of motion from an electric field is called ‘drift velocity’. The benefit of drift velocity, when considering the case of the highly conductive metals can be used in order to calculate the density of carriers per unit volume. In case of material such as copper, it was established that every atom of copper has only one atom in its outer shell, which was available for conducting an electric current. Therefore, the volumetric carrier density depended on the number of atoms per unit of weight and specific gravity can be calculated by Equation 2-1.

$$N_1 = \frac{N_A}{M_m} D_1 \tag{2-1}$$

Moreover, the carrier density is also available to estimate carrier drift velocity based on the electric current in unit of amperes (A) was given as about ~ 6.2 × 10^{l8} charge carriers per second which was equal to 1/*q*0. Considering the case of a piece of conductive material (the cross-section area is A_1), in this case the carrier velocity will be proportional to the electric current. Anyhow, the volumetric electric current will double when many carriers through per unit time. Assuming that the carrier density is constant, and the carriers look like an incompressible fluid, it was found that the velocity would be inversely proportional to the cross-section. This means that if the cross-section is large then the carrier velocity will be low, which can determine the carrier drift velocity by means of Equation 2-2.

$$v = \frac{I}{q_0 N A_1} \tag{2-2}$$

Another result is the average of carriers drift velocity in metals while the electric field which causes charge carriers to move is propagated through the conductor at approximately half light speed at about 300 × $l0^6$ m/s. On the other hand, when considering the case of copper wire (#18) together with the electrical current 1 A, it was found that this kind of copper wire was commonly used for wiring lamps and also other home appliances, was and had the cross-section of about 0.0078 cm^2. Normally, 100 W lamps with need to use an electric current of about 1A, which can be calculated in terms of carrier drift velocity from the carrier density of copper material which was equal to 0.009 $cm.s^{-1}$. However, the carrier drift velocity was considerably slower than the speed of light. Therefore, the sensitivity of the Hall generator was a function of cross-sectional dimensions, the electric current, and carrier density and could be determined by Equation 2-3. (*Original by Edward Ramsden: Hall-Effect Sensor Theory and Applications; Elsevier Inc. 2006*) [1].

$$V_H = \frac{IB}{q_0 Nd} \tag{2-3}$$

2.2.2 Hall Effect Sensor in Semiconductors

In the previous section, it was observed that enhancement of the performance of a Hall Effect sensor could be achieved by changing the kind of materials that do not have as many carriers per unit of volume. Therefore, material with low carrier density could provide more of an electric current. Therefore, the most appropriate materials would be semiconductors such as silicon, germanium, or gallium-arsenide. These semiconductors can provide carrier

densities as low as needed. Anyhow, carrier densities have usually occurred from semiconductor materials and will require carrier concentration.

Table 2.1: Intrinsic carrier concentration at 300 K or 26.85 °C [Soc185].

Material	Carrier concentration (cm^{-3})
Copper (est.)	8.4×10^{22}
Silicon	1.4×10^{10}
Germanium	2.1×10^{12}
Gallium-arsenide	1.1×10^{7}

Table 2.1 shows the carrier concentrations of semiconductor materials in different types of material, which can be noted that these semiconductor materials have a magnitude lower than metal materials due to the mostly atoms in metal materials which will contribute a conduction electron. On the other hand, the conduction electrons in semiconductors are more tightly adhesive. Therefore, the electrons in semiconductors need to be available for conduct when the sufficient thermal energy to reach a conduction state was obtained. This was because the carrier concentration would be highly dependent on the temperature. Normally, the use of the semiconductor materials are not popular used in pure form, but will doped by addition the carrier concentration to a required level such as adding a substance like phosphorous which has five electrons in valence (appears in column fifth of periodic table), the result is known as an N-type semiconductor. Similarly, the P-type can be performed by doping a semiconductor with a substance like boron which has the electrons in valence (appears in column third of periodic table).

Making a Hall generator by using doped semiconductor materials has several advantages. The first is that pure semiconductors have low intrinsic carrier concentrations if such materials can be obtained at the levels of one part per-trillion purity. The second reason for choosing the methodology was using doped material which could not selected the predominant charge carriers of electrons in metal materials, which are different to semiconductor materials. The semiconductor materials can select to either electrons or holes due because electrons tend to be faster than holes under the same specific conditions. Moreover, making a Hall generator more sensitive can be carried out by using carried electrons in an N-type material which has a majority carriers rather than a P-type material in which the current is carried by holes. The third reason for using doped materials is that the pure semiconductors have a function that is not very influenced by to the variation of temperature. The resulting of carrier concentration deriving from the addition of a dopant is mostly a function of dopant concentration, from which the results are not varied by

temperature. However, using a highly adequate concentration of dopant can provide relatively stable carrier concentrations in periods of temperature variation, because Hall voltage is a function of carrier concentration.

One of the reasons this is popular is for making integrated circuits (IC) for a Hall generator using doped silicon material and also almost all of the Hall generator as a silicon IC. Considering the internal structure it was found that the various silicon layers used in normal IC process are doped with difference levels of N-type and P-type materials, depending on the design of the intended function. However, it does not commonly used pure silicon as a component of a standard IC. (*Original by Edward Ramsden: Hall-Effect Sensor Theory and Applications; Elsevier Inc. 2006*) [1].

2.2.3 Silicon Hall Effect Sensor

Considering the structure of Hall generator which was made from N-type silicon and doped to a level 3×10^{15} cm^3 with 25 μm of thickness, the current source is 1 mA. The output voltage for the 1 T of a magnetic field from a Hall generator can be calculated by substituting the values into Equation 2-3 as being equal to 0.0083 V. It can be noted that the result of output voltage as calculated would be rather than 20,000 times of the output signal from copper transducer, as described previously. The bias current to the copper transducer must be used at a rate of 1/1,000. Therefore, the case of semiconductor materials will be given at the level of both output signals; output voltage and electrical current; as mV and mA, respectively for use of a sensor device. Normally, the sensitivity calculation of a transducer is considered to be affected by geometry, doping levels and bias current. However, one detail we may ignore is the resistance of the transducer. In fact, it is possible to obtain the great sensitivity from thinly doped semiconductor transducers for a unit in the mA of a bias current. It is necessary to use a high voltage in order to control the current flowing through the transducer. Therefore, the resistance of the Hall generator as functions in terms of conductivity and geometry. It can be calculated with regard to the resistance of semiconductor materials, which was represented as a of rectangular slab pattern in Equation 2-4.

$$R_e = \frac{\sigma \times l}{w \times d_1} \tag{2-4}$$

When considering the meaning of σ between metal materials and semiconductor, it was found that the meaning of σ in metal materials is a characteristic of the material, but in the case of semiconductor, σ meaning a function of both the doping and the property is called ‘carrier mobility’.

In this case the carrier mobility refers to how to measure how the speed charge carriers move in response to electric field and the difference in kinds of semiconductors, the level of dopant concentration, the carrier type (N or P type), and the temperature.

In the case of a silicon Hall generator with 25 μm or 0.0025 cm of thickness, which was making a N-type silicon be doped to a level of 3×10^{15} cm^{-3}, $\sigma \approx 1.7$ Ω-cm under the condition of temperature control at room temperature. Assuming that the dimensions of transducer are 0.1 cm of length and 0.05 cm of width, it can be calculated the resistance of transducer was equal to 1.36 kΩ. From the result, it was necessary to take the voltage supply of 1.36 V, the electric current of 1 mA flowing through the sensor and the power 1.36 mW. These values are generally sufficient for use in the electronics system. Therefore, the sensitivity and power, which was generated by Hall Effect transducers from silicon or other semiconductors for use as a sensor device, could be applied for practical measurements. (*Original by Edward Ramsden: Hall-Effect Sensor Theory and Applications; Elsevier Inc. 2006*) [1].

2.3 Practical Transducers

2.3.1 Key Transducer Characteristics

With regard to the design and development of the Hall Effect sensor for measuring the variables in the industrial sector, the guidelines for assembling and applying a sensor device with the fully performance are known as the 'key characteristics' of the Hall Effect transducer. The benefits of the key characteristics will describe the behaviour of a Hall Effect generator for uses including the effects from external environment, which consists of sensitivity, the temperature coefficient of sensitivity, the ohmic offset, the temperature coefficient of ohmic offset, linearity, the input and output resistance, the temperature coefficient, and electrical output noise. (*Original by Edward Ramsden: Hall-Effect Sensor Theory and Applications; Elsevier Inc. 2006*) [1].

2.3.2 Thin-Film Transducers

A sensor device in kind of a thin-film transducer has been constructed by depositing thin layers of metal materials and semiconductor materials. Each of the doped layers was supported by insulation such as alumina ($A1_2O_3$) or some other ceramic material. Normally, the thickness of films was used as an artificial sensor device and was about 1 μm smaller, as shown in Figure 2.1.

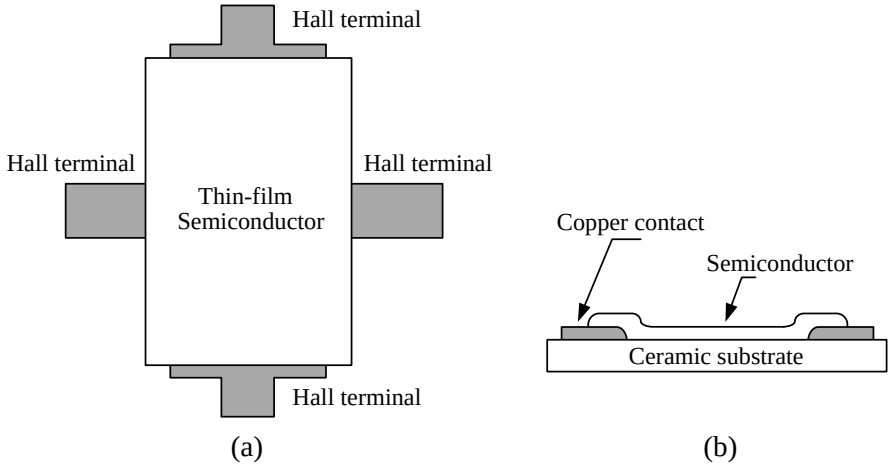

Figure 2.1 Simple structure of thin-film Hall Effect sensor:
(a) Top view;
(b) Side view.

When considering the advantages of sensor device in construction of a thin-film, it can be noted that it is possible to be flexible in choosing the type of material, making sensor sizes smaller and providing a high level of output signal from the Hall generator by using less bias in the current, while the production of the sensor device can be performed by mass production. (*Original by Edward Ramsden: Hall-Effect Sensor Theory and Applications; Elsevier Inc. 2006*) [1].

2.3.3 Integrated Hall Transducers

The production of a Hall Effect transducer from a silicon semiconductor using standard integrated circuit processing techniques will make it possible to build a complete sensor system on a chip. In cases of bias, the circuit of the transducer, the front-end amplifier, and the signal processing can be combined with other cases in a single reasonable cost, but with high quality and reliability. Moreover, the production of the sensor device in the form of an electronic device will allow the manufacturers to enhance the potential of a sensor device in response to the diverse needs of consumers. However, this can be made to be affordable. In addition, the production of a Hall generator from a semiconductor in the industrial sector would take the form of a single wafer. It is reasonable to economically produce large numbers of sensors (IC) at the same time. Finally, constructing a Hall generator in this form can also provide high quality sensors, a feature of silicon wafers as illustrated in Figure 2.2. (*Original by Edward Ramsden: Hall-Effect Sensor Theory and Applications; Elsevier Inc. 2006*) [1].

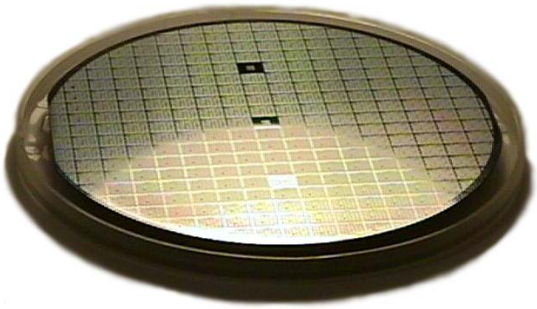

Figure 2.2: Hall Effect sensor ICs on a silicon wafer.
(*http://fusion-xhd.blogspot.jp/2011/09/manufacturing-semiconductor.html*)

2.3.4 Variation on the Basic Hall Effect Transducers

Considering the fundamental limitations of a traditional Hall generator which was produced from a semiconductor, it was found that the Hall generator can provide the results of sensitivity on only one axis, which indicates that the axis is perpendicular to the surface of the materials (IC). Therefore, if the sense field components are needed in more than one axis a Hall generator must combine the use of more than one sensor (IC) and each sensor (IC) should be individually mounted.

Using a sensor in type of vertical Hall Effect transducer [Baltes94] to provide multi-axis sensing ability on a single silicon die, as shown in the basic structure in Figure 2.3 may be a fundamental limitation. The operations of vertical Hall Effect transducer starting from bias current will be connected to an N-well at the centre of terminal 3, while the direction of flow of the current would be collected by ground terminals 1 and 5. In case of the magnetic field absence around a sensor, the electric potential at the terminals 2 and 4 would be symmetrical. This value is set as a point to operate a sensor device. When the magnetic field presence is applied across the surface of chip, perpendicular to the flowing direction of the current through device, a result has occurs which would involve deviation from the electric current due to the Lorentz forces. These forms of behaviour are fundamentals of the traditional Hall generator, often resulting here in electrical potential differences between terminals 2 and 4. Although the potential of voltage would be exhibited with a small difference, the voltage signal will be assumed to be amplified by the instrumentation amplifier into a usable signal level.

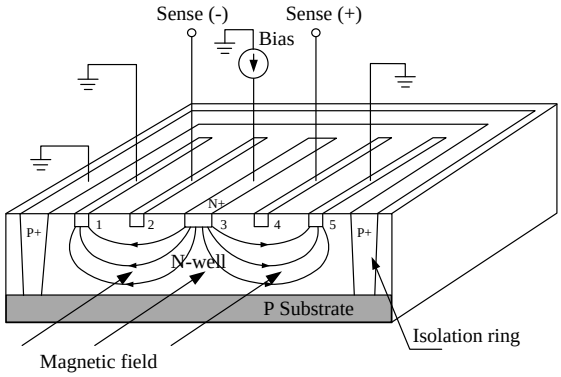

Figure 2.3: Vertical Hall Effect transducer (after Baltes et al.).

However, one of disadvantages of the structure of the vertical Hall Effect transducer is that it may be defective in four-way symmetry, while the sensor device has been symmetrical and would benefit from reducing the ohmic effects and by offset the error of the voltage signal. (*Original by Edward Ramsden: Hall-Effect Sensor Theory and Applications; Elsevier Inc. 2006*) [1].

2.4 Principle of Hall Effect Sensor

A Hall Effect sensor as a sensor device is a kind of proximity sensor. It is a small and can be applied in several measurements for detection such as position and distance detection, speed sensors (rpm), linearity displacement and angular displacement. The output voltage of a Hall Effect sensor will be generated when the constant current flowing through it deviates from the direction of a flowing current, as illustrated in Figure 2.4 (a). Also, the deviation of the electric current will be dependent on the magnetic field of a magnet that is installed at both sides of the generator as a current carrying conductor through it, as shown in Figure 2.4 (b). However, the results of the magnetic field being perpendicular to the flowing direction of the electric current would be proportional to the multiplication of magnetic field density and the electric current.

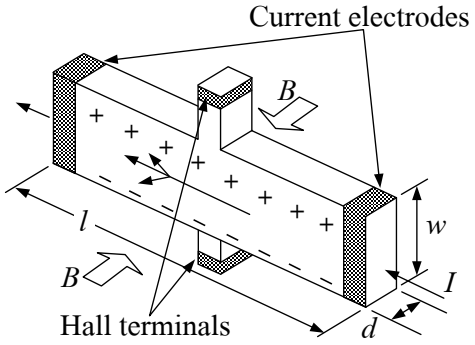

(a)

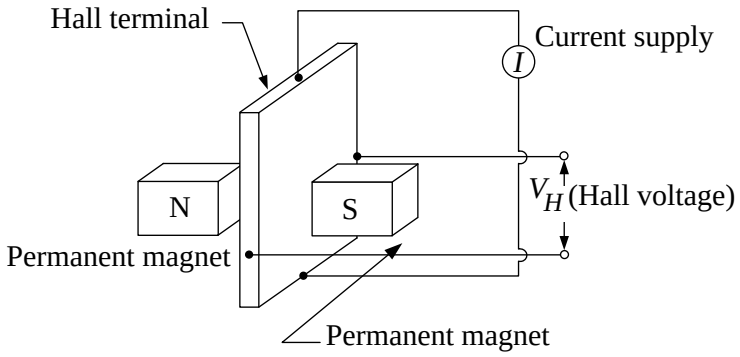

(b)

Figure 2.4: Physical structure of Hall Effect sensor;
(a) Flowing direction of electric current through a Hall generator;
(b) The output voltage generated by a Hall Effect sensor.

Conceptually, defining the flowing direction of electric current through a Hall generator and the output voltage of a Hall Effect sensor would depend on the voltage power supply and also the direction of the magnetic field which stimulates the surface of the Hall generator, as shown in Figure 2.5. Reversing the direction of output voltage of a Hall Effect sensor can be performed into two ways; the first is by reversing the voltage power supply that supplies a Hall generator and the second is reversing the magnetic field that is used to stimulate a Hall generator, as shown in Figure 2.5 (a). Figure 2.5 (b) shows how the reversing of the output voltage of a Hall Effect sensor can be brought about by reversing the direction of the voltage power supply, while the direction of the magnetic field may still be constant. The deviation of the current flowing through a Hall generator was influenced by magnetic flux, resulting in a small voltage appearing across the pole that is perpendicular to the direction of the electric current being carried. On the other hand, Figures 2.5 (c) and 2.5 (d) indicate the reverse of output voltage of a Hall Effect sensor by reversing the direction of voltage power supply and reversing the direction of the magnetic field at the same time. This will show the deviation of the current flowing through a Hall generator with in various directions.

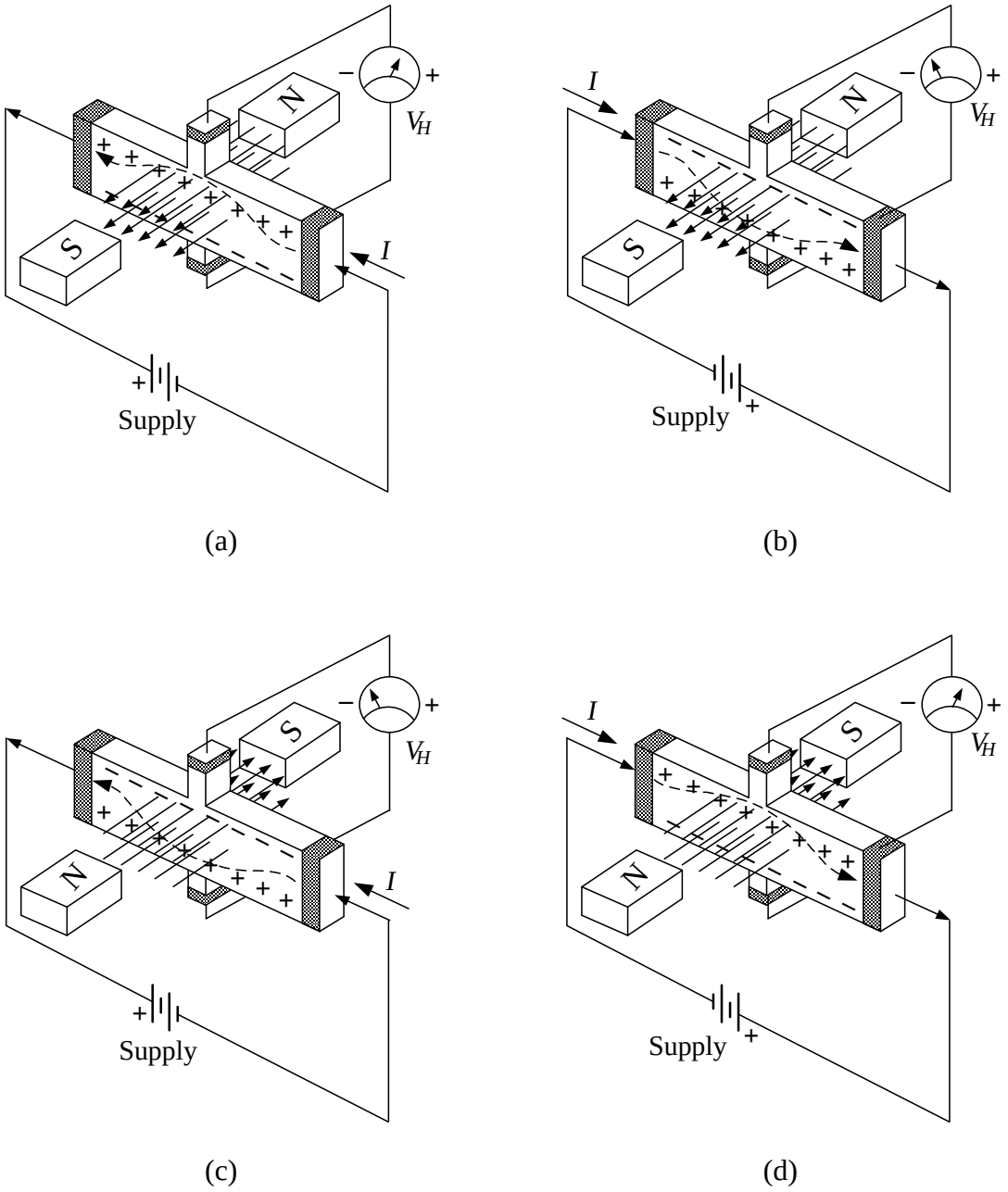

Figure 2.5: Deviation of electric current which was flowing through a Hall generator.

An electron of charge, which is the net electric current moving in a magnetic field at a particular velocity, can be used to analyse the Lorentz force of the magnetic field by means of Equation 2-5.

$$F = e\,(vB) \tag{2-5}$$

The basics of a Hall Effect sensor begin from an electric current flowing through a Hall generator, which will be constrained by the structure of a semiconductor which is being used as a Hall generator, while the electrons will be deflected by the density of the

magnetic flux. However, the build-up of the charges towards one side of the Hall generator will also be increased by an electric current as well. This concept is called a 'Hall Field'. Moreover, the flow of electric current will be through in the original direction, while the effect of the variation of the magnetic field can be determined by Equation 2-6.

$$E_H = vB \tag{2-6}$$

Where ρ and e represent density and the charge of the carriers, the density of the electric current can be determined by Equation 2-7.

$$i = \rho v \tag{2-7}$$

When E_H exhibits single electron velocity, it can be calculated by Equation 2-8.

$$E_H = \frac{1}{\rho} iB \tag{2-8}$$

The factor $1/\rho$ in terms of Hall coefficient will be inversely proportional to the density of carrier depending on the kind of a semiconductor used as a Hall generator. When considering the operations of a Hall Effect sensor it was found that $V_H = wE_H$ and $I = iwd_1$. Therefore, the level of the Hall voltage can be calculated by Equation 2-9.

$$V_H = \frac{R_H}{d_1} IB \tag{2-9}$$

The balance between the Lorentz force and Hall field could only be obtained by current carriers with a single velocity. Anyhow, the electric current in Hall element will be defined by thermal dissipation and permissible temperature rise to maximum level of power output, the majority of Hall element will be making from the material types of Indium Antimonide and Indium Arsenide. (*Original by C. Rangan, G. Sarma, V.S.V. Mani: Instrumentation: Devices and System; Tata McGraw-Hill Publishing Company Limited, 2004*) [7].

Figure 2.6 and 2.7 shows examples of testing the properties of measurement by using different forms of a Hall generator which was mounted to consider the responding of output signal from measurement within the laboratory. Figure 2.6 (a) shows the installation of Hall generator in order to measure the variables in a pattern of linearity displacement, using the slide-by sensing mode, resulting from measurement that would be exhibited in the form of voltage, as illustrated in Figure 2.6 (b). From the graph, it can be observed that the position of a permanent magnet in close proximity to the centre of a Hall generator would provide the maximum value of output voltage from a Hall Effect sensor. On the other hand, if a permanent magnet move away from a Hall generator then the output voltage from the Hall

Effect sensor would also be decreased. Therefore, the output voltage of a Hall Effect sensor will also be inversely proportional to the moving distance of a permanent core magnet.

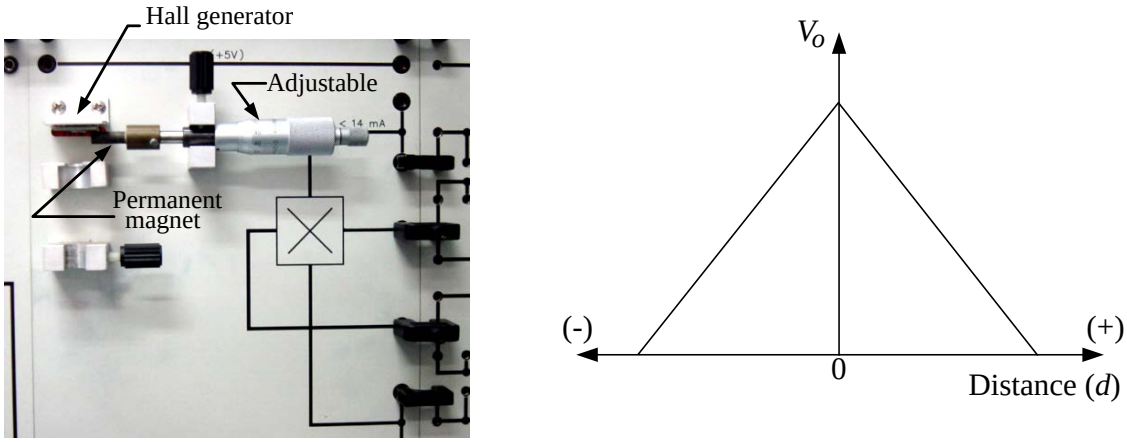

(a) (b)

Figure 2.6: Installation of permanent magnet using slide-by sensing mode for measuring the linearity movement;
(a) Placement of permanent core magnet;
(b) Relationship between output voltage and distance from measurement.

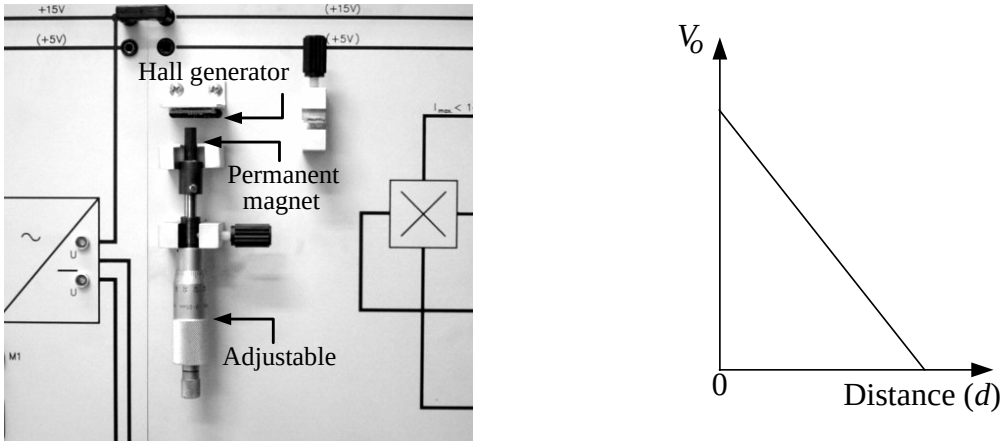

(a) (b)

Figure 2.7: Installation of permanent magnet using head-on sensing mode for measuring the linearity movement;
(a) Placement of permanent core magnet at a perpendicular angle to a Hall generator;
(b) Relationship between output voltage and distance are measured only the positive values.

Figure 2.7 (a) shows the installation of Hall generator in order to measure the variables in a pattern of linearity displacement using the head-on sensing mode, resulting from measurement that would be exhibited in the form of voltage, as illustrated in Figure 2.7 (b). It can be noted that, when a permanent magnet is in close proximity to the centre of a Hall generator, the output voltage from Hall Effect sensor will increase. On the other hand, if a permanent magnet move away from a Hall generator, then the output voltage from Hall Effect sensor would be decreased in a similar way to that of the installation by using the slide-by sensing mode. Figure 2.8 and 2.9 shows the installation of a Hall generator in a case of angular measurement in order to detect the motion and speed sensor of a motor. The placement of a Hall generator of both patterns would be exhibited with various voltages. Figure 2.8 (a) shows the placement of two Hall generators for detecting the position and speed in angular displacement, while the results of the experiment were exhibited in the form a voltage signal and the waveform in the output voltage condition as a binary signal or logic state, which indicate a turned-ON and turned-OFF state, as shown in Figure 2.8 (b).

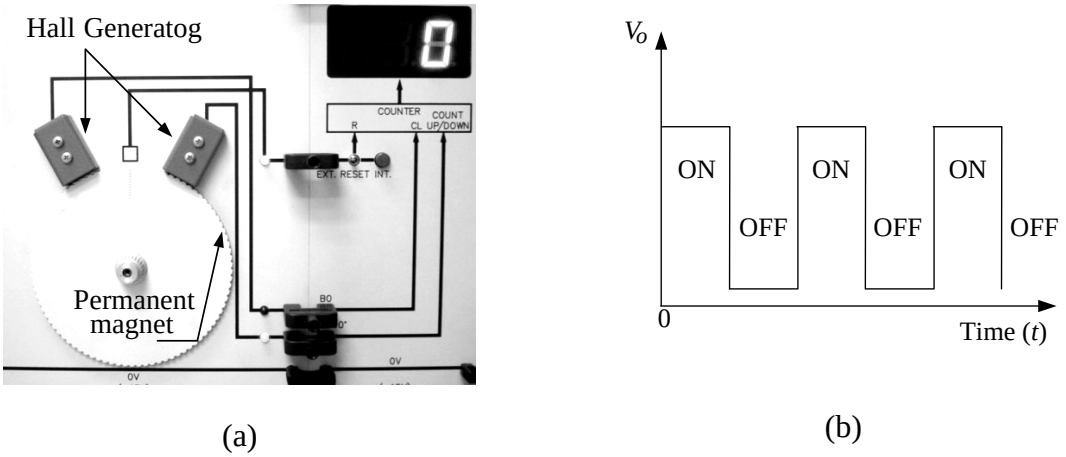

(a) (b)

Figure 2.8: Installation of Hall generator for measuring the angular movement;
(a) Placement position in case of angular;
(b) Relationship between output voltages in the form of a square wave.

2.5 General Sensing Device Using Hall Effect Sensor

This section presents a review of the literature on the Hall Effect sensor device and considers a few examples of most common applications and design of sensing devices in the industrial field.

a) Turbine Flow Meter: This is an instrument for measuring flow rate that can be also use a Hall Effect sensor as a sensor device. The fundamentals of the turbine flow meter involves converting the flow rate of fluid into an electrical signal by detecting

the motion of the propeller which installed on the rotor, as shown in Figure 2.9 (a). The output signal from the Hall Effect sensor will be generated when the fluid flowing into the housing through the propeller will be installed on the rotor. In this case, the propeller would be rotated at a speed that was proportional to the flow rate of fluid. The rotation of the propeller can activate the Hall generator, which was mounted on the top of the housing, and then a hall generator will generate the output signal in the form of pulse wave. The variation of frequency would be proportional to the speed of propeller rotation due to the flow of the fluid, as shown in Figure 2.9 (b). (*Original by James W. Dally, William F. Riley, Kenneth G. McConnell: Instrumentation for Engineering Measurements; John Wiley & Sons, Inc., 1993*) [8].

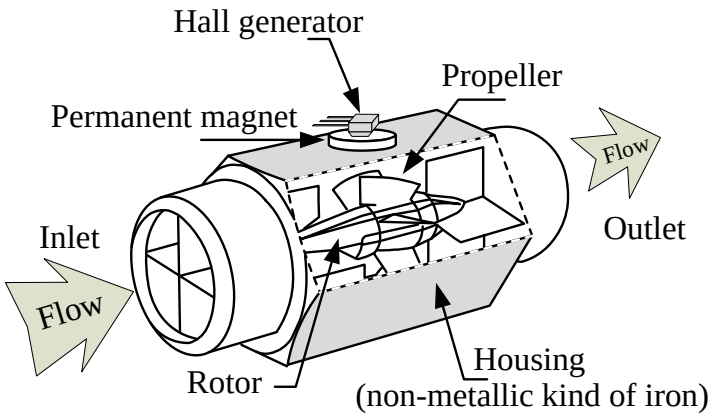

(a)

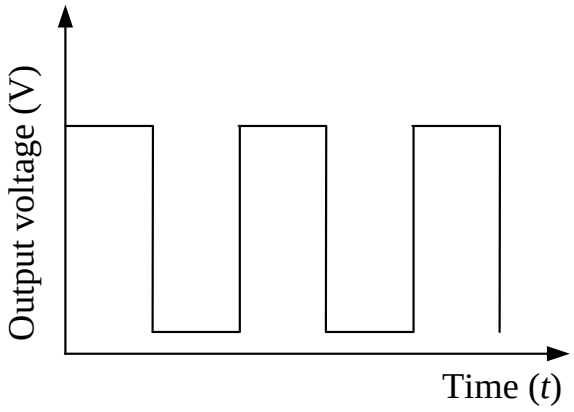

(b)

Figure 2.9: Structure of Turbine flow meter;
(a) Installation of Hall generator and magnet;
(b) Output signal from measurement.

b) Transmission Mounted Speed Sensor: Conceptually, design of a transmission speed sensor, in this case used a digital output bipolar sensor is actuated by sensing the magnetic field created by a rotating ring magnet driven by the speedometer output shaft. This phenomenon the frequency of the output signal is proportional to speed as shown in Figure 2.10. (*Original by Honeywell Inc.: Hall Effect sensing and application; MICRO SWITCH Sensing and Control, www.honeywell.com/sensing*) [9].

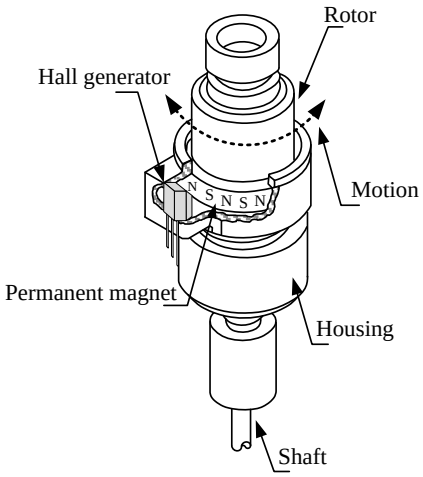

Figure 2.10: Speed sensor used Hall Effect sensor device.

c) Brushless DC Motor Sensors: Installation of Hall Effect sensors in this case are starting to consider an electronic commutation was performed by three digital output bipolar sensors. Permanent magnet materials mounted on the rotor shaft operate the Hall generators. The Hall generators sense the angular position of the shaft and feed this information to a logic circuit. The logic circuit encodes this information and controls switches in a drive circuit. Appropriate windings, as determined by the rotor position, are magnetic field generated by the windings rotates in relation to the shaft position. This reacts with the field of the rotor's permanent magnets and develops the required torque. Since no slip rings or brushes are used for commutation; friction, power loss through carbon build-up and electrical noise are eliminated. Also, electronic commutation offers greater flexibility, with respect to direct interface with digital commands as shown in Figure 2.11. (*Original by Honeywell Inc.: Hall Effect sensing and application; MICRO SWITCH Sensing and Control, www.honeywell.com/sensing*) [9].

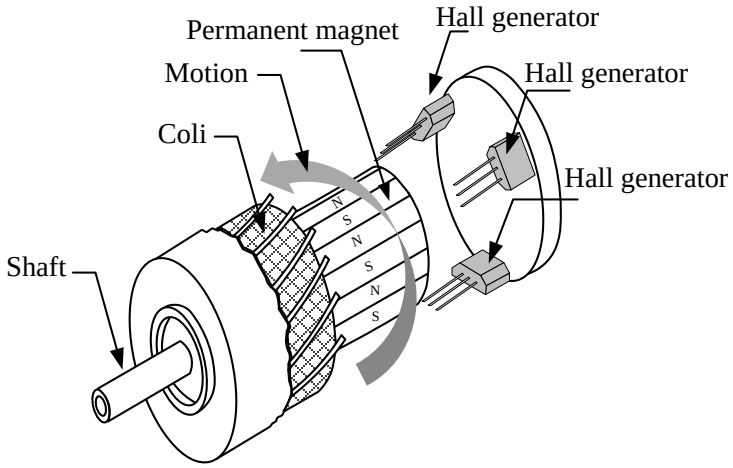

Figure 2.11: Brushless DC motor sensors using Hall Effect sensor.

2.6 Conclusion

The details of all the sections in this chapter will be summarized to describe how a Hall Effect sensor works as a sensor device. It has an uncomplicated structure and is also easy to use with an electronics circuit. A Hall Effect sensor can be used to activate an electrical current and can also operate a voltage power supply at a low level. However, here the Hall Effect sensor was to be doped from a semiconductor which mainly used silicon. The production of a Hall Effect sensor through the technology processing of a semiconductor benefits the manufacturer in enhancing the potential of the sensor device in order to respond to the diverse needs of consumers. It will also be affordable for them. It is also as a sensor device for IC and its small size is appropriate for installation with an electronics device.

Chapter 3

Main Objectives and Improvements in The Conventional Hall Effect Sensor

3.1 Introduction

This chapter describes the specific objectives of this study. Details of the work procedure are develop to implement the objectives, including the development of a new sensor module and some experimental studies of various application of the different variables are then discussed.

3.2 Main Objective

The main objective of the study is to focus on using of the conventional Hall Effect sensor in several operations in a way that may be appropriate for the variables in industrial fields, by considering the output signal in the form of a linearity signal. The use of a magnetic field to stimulate of a Hall Effect sensor in this study is divided into two types: the first is stimulation of a Hall Effect sensor by an electromagnetic field which was generated from conductor coil. Here, two Helmholtz coils were used. The second will be stimulated by a magnetic field generated from the permanent magnet. The results of the experiment involved making comparisons under the same specific conditions, and then analysing the installation of a Hall generator together with the Helmholtz coils (in case of stimulation by using electromagnetic field), and placing of a Hall generator together with the permanent magnet in various of formats including a single Hall sensor, the 4-array Hall sensor, the 5-array Hall sensor, and the 4-crossing Hall sensor [10]. With regard to comparing the appropriateness of measurement, the conditions of variables, and also the limitation of placing a Hall generator in various patterns, the results of output signal from the analysis were exhibited in the form of the voltage variation, which is related to the quantity of the variables various. An analysis of output signal from the measurement of a Hall Effect sensor in the form of a frequency domain can help estimate and enhance the performance by means of measurement processing, while the output signal from a new sensor module in the form of voltage will be converted into the frequency in the form of a time domain by

using the voltage to frequency converter circuit. The frequency in time domain will then be transformed into the frequency domain by using MATLAB software. Finally, the results of the experiment will be compared with those for the ultrasonic sensor, by which the ultrasonic wave was generated by the EMAT under the same specific conditions, in order to consider the efficiency and ability of a measurement system, the simplicity of an installation system and a measurement process at a lower cost. The design and development of a 'new non-destructive measurement' used a conventional Hall Effect sensor device to replace the EMAT [5, 11] in some cases of non-destructive testing. This was because of the system including a Hall Effect sensor would be flexible, simple to install and easy to set up and calibration its sensors.

3.3 Specific Objectives

Various ways to improve a conventional Hall Effect sensor were studied with regard to three specific objectives in order to perform the evolutionary sequence. The conceptual basis of study involves the improvement of a conventional Hall Effect sensor as a new non-destructive measurement so that it can use a Hall Effect sensor to obtain the most benefit. The details of specific objectives are presented as follows:

3.3.1 Improvement of a Conventional Hall Effect Sensor Device

These specific objectives aim to estimate the performance results of new sensor module in terms of developing the process and the system:

3.3.1.1 The patterns and how to use the magnetic field to stimulate a Hall Effect sensor.

3.3.1.2 The patterns and how to place a Hall generator and permanent magnet installation together and also the number of Hall generators per number of magnets.

3.3.1.3 The patterns of signal processing and output signal analysis of both formats of voltage signal and frequency signal.

3.3.2 Analysis and Comparison of the Operation of New Sensor Modules for Each Method

These specific objective aim to compare the performance of the New sensor module in a different format under the same specific conditions as the comparison of the advantages and the disadvantages of magnetic field in order to activate a Hall Effect sensor between a permanent magnet and Helmholtz coil, and comparing this with the result of placing a Hall generator and a permanent magnet in the various patterns of array and crossing also the number of Hall generators with the permanent magnets which were installed together, and

comparing the signal processing by considering the output signal analysis of a new sensor module in terms of measurement between the voltage and the frequency signal.

3.3.3 Industrial Application of New Sensor Module

These specific objective aim to uses a new sensor module to develop and applying several variables in industrial fields. The main objectives are to evaluate the performance of new sensor module and the reliability of the measurement system, which are consists of angular measurement, measurement of the industrial machine alignment in the production line, measurement of the contamination level of metal particles in industrial machine lubricant and also a comparison of the performance of the new sensor module and EMAT under conditions of non-destructive testing.

3.4 Work Procedure

The procedure to accomplish the overall objective of the study is presented in Figure 3.1.

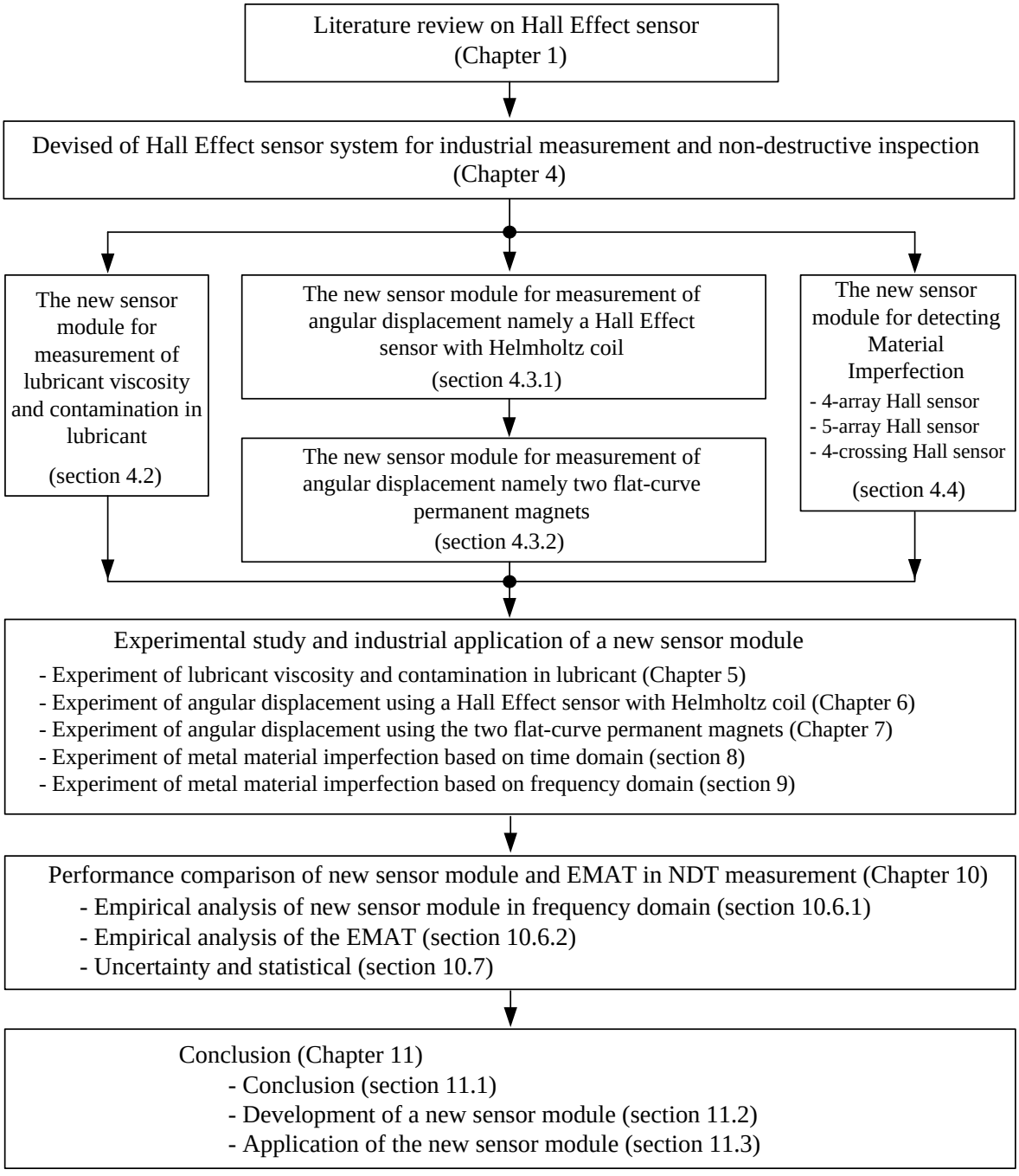

Figure 3.1: Work procedure of the study.

3.5 Planning of Experiment Study for Application to Different Variables

The detailed experiment study and analyses were originally performed for the study in chapter 1, and also the methodology of Hall Effect sensor, as described in chapter 2. Details of the study are summarized as follows:

Step 1: The experiments were set up to compare the performance of electromagnetic fields generated by coil and magnetic field generation by permanent magnets. The purpose was also to invent and design the new sensor module for application to several variables, an application of the new sensor module for any measurement of variables such as measurement of lubricant viscosity and contamination in lubricant, the measurement of angular displacement, and inspection for any defects in materials.

Step 2: The results of the experiment were then compared to those from output voltage of the new sensor module as well as those from the output signal in frequency. An analysis of the uncertainty of the experiment was conducted. Furthermore, the results of experimentation between a new sensor module and EMAT method in the same sample materials were compared. The performance and restrictions of each method were also considered.

3.6 Conclusion

Defining the objectives and scope of studies are necessary as guidelines to manage the process and sequence of the research. Achieving the targets can also involve assessing the quality of research and how satisfactory the results are. The specific objective in this study was divided into three steps: the first step was the is operation of a conventional Hall Effect sensor device, the second step involved analysis and comparison of the operation of new sensor module for each method, and the last step was the industrial application of the new sensor module. Moreover, it also exhibited the details of work procedure of the study in section 3.4 as well as the structure and overall process of research.

Chapter 4

Devising a Hall Effect Sensor System for Industrial Measurement and Non-destructive Inspection

4.1 Introduction

This chapter presents the new technique for stimulation of the conventional Hall Effect sensor as a new sensor module for industrial measurement and non-destructive inspection. In this study, the design of the new sensor module will be divided into four types which are based on the different standard types. Firstly, a single Hall sensor used for the measurement of lubricant viscosity and contamination in lubricant. Secondly, a Hall Effect sensor with a Helmholtz coil and two flat-curve permanent magnets will be used for the measurement of angular displacement; and then the detection of material imperfection will be made with a 4-array Hall sensor, a 5-array Hall sensor, and a 4-crossing Hall sensor. Thirdly, in the case of generating a magnetic field, a permanent magnet will be used for the placement of a Hall generator and a permanent magnet to be installed together using techniques such as a head-on sensing mode, a slide-by sensing mode, and a null-point sensing mode. Finally, we need to consider the format of the Hall generator placement and permanent magnet, which are installed together in the most appropriate order for measuring several variables.

4.2 Typical New Sensor Module for Measurement of Lubricant Viscosity and Contamination in Lubricant

Viscosity is one of the vital parameters that play an important role in the characteristics of industrial lubricant. Normally, viscosity has been directly related to the flow rate of lubricant. If the viscosity of lubricant is lower than the specified value under normal operation, the efficiency of the machine can also decrease, which leads to machine failures. This section discusses the design of the new sensor module for the simultaneous measurement of lubricant viscosity and contamination in lubricant. The new sensor module, namely the single Hall sensor, consisted of a conventional Hall Effect sensor mounted on a permanent magnet based on the principles of the head-on sensing mode.

4.2.1 Objectives of Design for the New Sensor Module

The objectives of this section were to improve a conventional Hall Effect sensor by designing a new sensor module to be applied for measuring the contamination in lubricant and lubricant viscosity of several industrial lubricants and engines. The sensor module was selected in this study for several reasons such as it being theoretically necessary to replace the new lubricant to prevent damage to the machinery because of the wear and tear of industrial machine components during operation time [12]. It can be noted that more than 50 percent of lubricant replacement would be performed although the lubricant is still in good condition, which lead to significant business waste [13, 14]. The sensor module consists of a Hall generator and a small permanent magnet. The measurement of lubricant degradation was performed under the conditions of magnetic flux density which was generated by a permanent magnet. Moreover, a sensor module would be applied to examining the lubricant contamination of metal particles based on NAS 1638 standard. The measurement system can be divided into two major parts: the first is a sensor module; the second is the signal conditioning circuit and the display on a computer. The results of measurement in error analysis are discussed. The major benefit of this methodology is the reasonable cost of sensor as well as the ease of use and installation.

4.2.2 Design of the New Sensor Module for the Measurement of Lubricant Viscosity and Contamination in Lubricant

Design of a new sensor module in this study was performed by considering the placement of Hall generator together with the permanent of magnet based on the fundamental of head-on sensing mode. In this sensing mode, a Hall generator for the beginning of the operation involves placing the pole of permanent magnet in close proximity to the area at the centre of a Hall generator for activation. Normally, the actuation of a Hall Effect sensor in this case was called ‘head-on sensing’, as shown in Figure 4.1 (a). Head-on sensing is one of basic methods mostly commonly used for actuation of a Hall generator in order to detecting the variables which require the output signals to respond in the format of the binary signal state. Considering the actuation of a Hall generator by using the head-on sensing mode, it was found that the sensitive axis of a Hall generator and the axis of magnetization are co-linear. Therefore, the curve line which represents the relationship between flux density and variation of displacement is called a ‘flux map’ or a ‘magnet map’, as shown in Figure 4.1 (b). (*Original by Edward Ramsden: Hall-Effect Sensor Theory and Applications; Elsevier Inc. 2006*) [1].

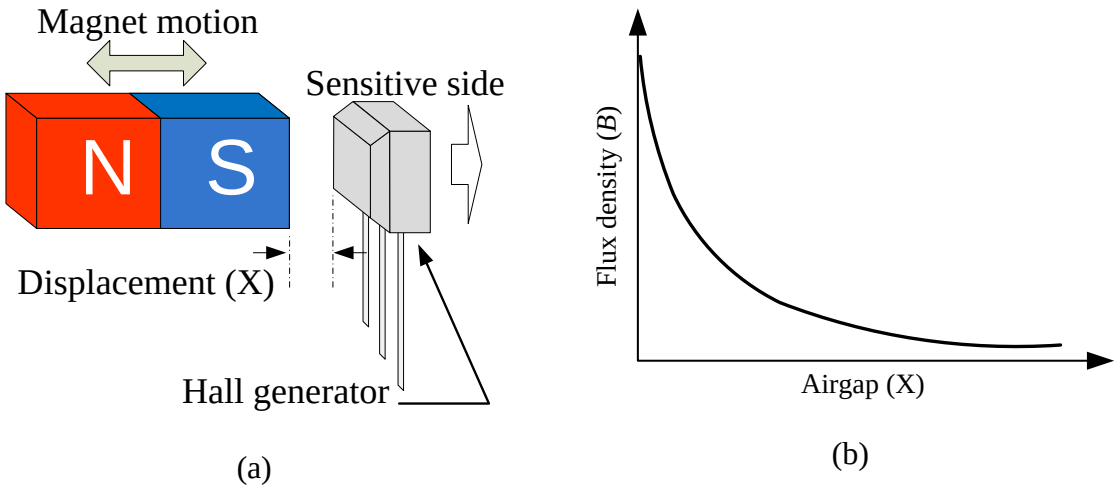

Figure 4.1: The head-on sensing mode;
(a) Placement of a Hall generator and permanent magnet;
(b) Relationship between the flux density and airgap.

4.2.3 Generation of Output Voltage Using the New Sensor Module

This section discusses the placement of a Hall generator and permanent magnet combination in order to assemble the sensor module as well as operate the sensor module for detecting metal material using the magnetic field generated by the permanent magnet. A Hall Effect sensor can only detect the material which was influenced by the magnetization of the magnetic field and cannot be used for detection of materials that are not influence by the magnetization of the magnetic field, whether it is a metal or non-metal such as copper, aluminium, acrylic, and ceramic. A Hall Effect sensor for detection of a metal material was used by taking the Hall generator mounted on the front surface of magnetic pole (S-pole) as shown in Figure 4.2 (a). In this case, the sensitive axis of a Hall Effect sensor appeared at the rear of a sensor device. Considering the output signal in the format of voltage, it was found that the voltage could be in a turned off state when there was an absence of metal material in the area of the sensitive axis, as shown in figure 4.2 (b).

On the other hand, when the metal material moved in close proximity to the area of the sensitive axis of a Hall generator, as shown in Figure 4.3 (a), it was found that the magnetic flux would be of high intensity, unlike the normal flux at the surface of a permanent magnet. Therefore, the output voltage of the Hall Effect sensor will be turned on as shown in Figure 4.3 (b), and the status of this detection will be in the format of a binary signal. (*Original by Edward Ramsden: Hall-Effect Sensor Theory and Applications; Elsevier Inc. 2006*) [1].

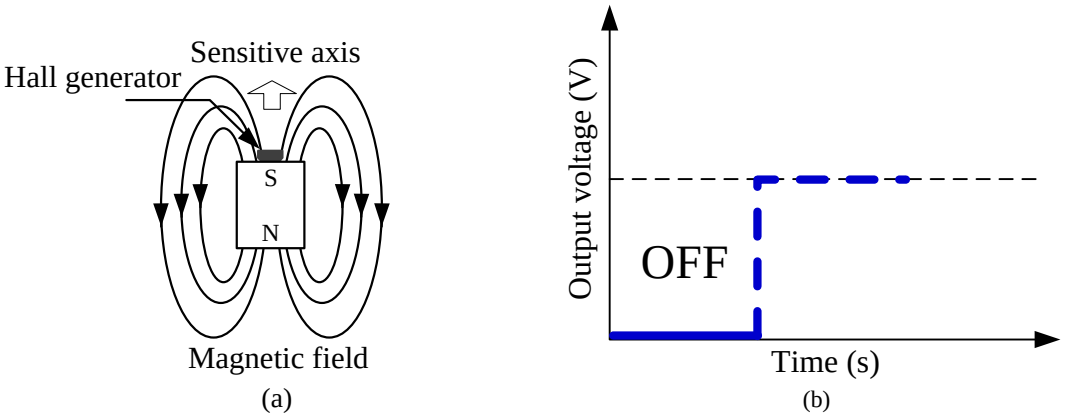

Figure 4.2: The Influence of sensor placement;
(a) Flux around magnet when the metal material target was absent;
(b) The output voltage was turned OFF.

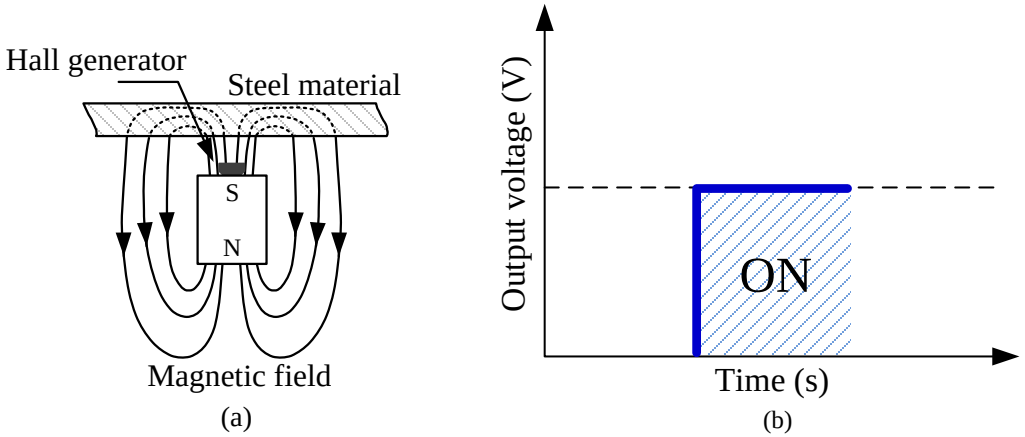

Figure 4.3: Operation of the Hall Effect sensor;
(a) The flux around the magnet by presence of the metal material target;
(b) The output voltage was turned ON.

Figure 4.4 shows the placing of a sensor module before testing the metal particles in the lubricant. The deviation of the current flowing through a Hall generator was influenced by magnetic flux, resulting in a small voltage appearing across at the output terminals of Hall generator. When the metal particles is moved to a sensor module, the output voltage of Hall generator will increase to the maximum value, and then were saturated when the status of metal particles is stop-motion as shown in Figure 4.5. This means the output voltage of a sensor module will be proportional to the moving distance of the metal particles, and were also dependent on the velocity of the metal particles moving to a sensor module.

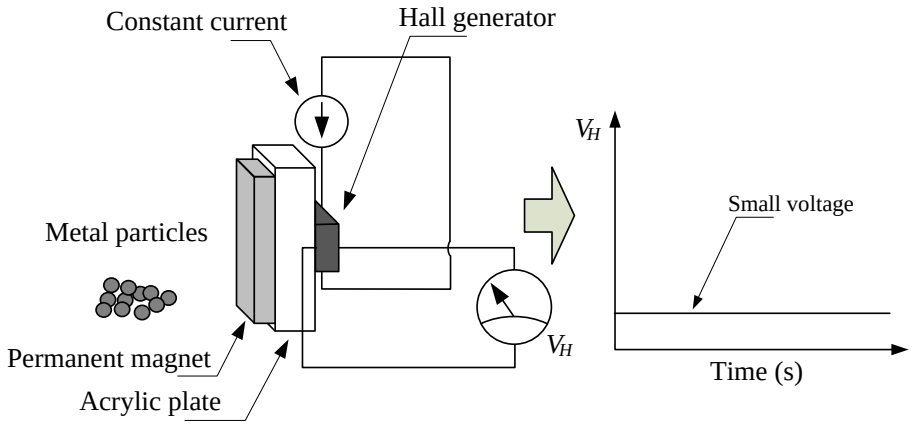

Figure 4.4: Output voltage from a sensor module initially at 3.736 V before testing.

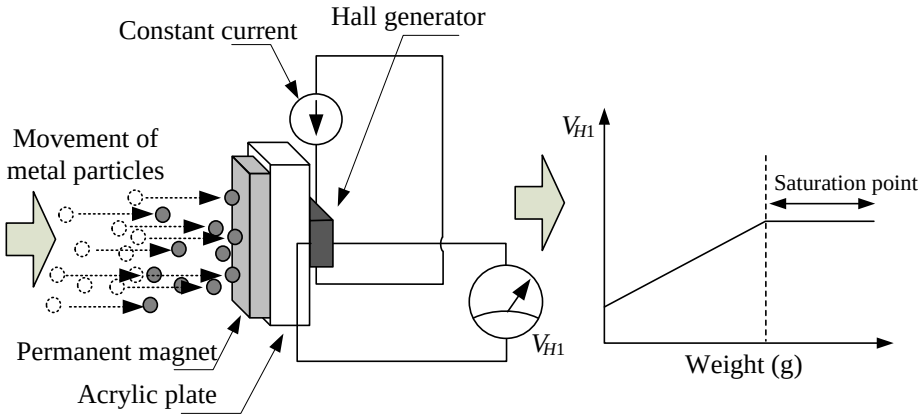

Figure 4.5: Increase of output voltage from a sensor module when metal particles are moving to permanent magnet.

New sensor module used for measuring the contamination in lubricant consisted of a conventional Hall Effect sensor mounted on a permanent magnet (0.17 T) which size is 12 mm of width 15 mm of length and 2 mm of thickness. The gap between Hall Effect sensor and permanent magnet is 3 mm in order to protect the saturated output voltage of Hall Effect sensor in case of the magnetic field over the range. The output voltage from the conventional Hall Effect sensor was therefore constant and used for comparing to the sensing output voltage, which was generated when metal particles move to a permanent magnet [15], as shown in Figure 4.6.

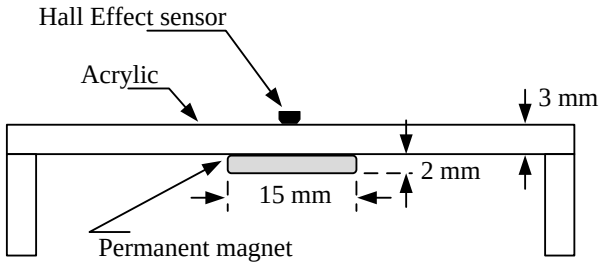

Figure 4.6: Installation of a Hall generator and a permanent magnet in top view.

The permanent magnet generates a magnetic field, which can be effect to metal contaminants in the lubricant that is cause of the magnetic field changed according to the weight of the contaminants. The conventional Hall Effect sensor can detect changing of magnetic field and generate the voltage output to the 12 bit-analog to digital convertor for sending data to the data acquisition based on microcontroller then it passes data to store on the computer and data analysis.

4.2.4 The Basic Idea for the Measurement of Lubricant Viscosity and Contamination in Lubricant

The relationship of the metal particles the factors and the viscosity can be determined from the Newton's Law of viscosity in case of dynamic and kinematic viscosity by Equation 4-1.

$$\eta = t_{moving} \frac{F_1}{A} \rho \tag{4-1}$$

Figure 4.7 shows the different levels of contamination in the lubricant. Typically, the contamination in the lubricant of industrial machines as rust is caused by machine wear itself or exterior contamination such as the contamination inside pipelines, which was installed together with the industrial machine. Therefore, when the quantity of metal particles has been contaminated in a lubricant to reach the standards set. Theoretically it is necessary to be replaced the new lubricant to prevent the damage to the machinery because of wear and tear of industrial machine components during operation time. With regard to lubricant degradation and the quantity of metal particles, it can be noted that the quantity of metal particles will be proportional to lubricant degradation. It means, in beginning to increase metal particles, the lubricant degradation will be changing rapidly until it reaches saturation point. With regard to this point, it was considered necessary for the lubricant to be replaced (more than 50 percent of metal particles based on NAS 1638 standard) as shown in Figure 4.8.

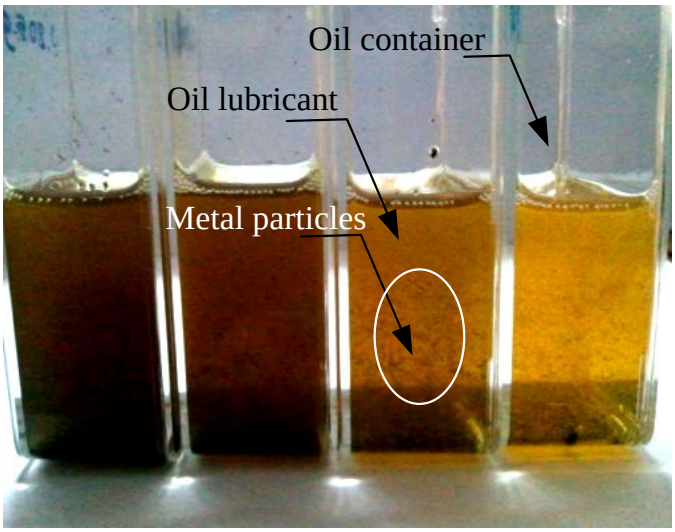

Figure 4.7: Different levels of contamination in lubricant degradation.

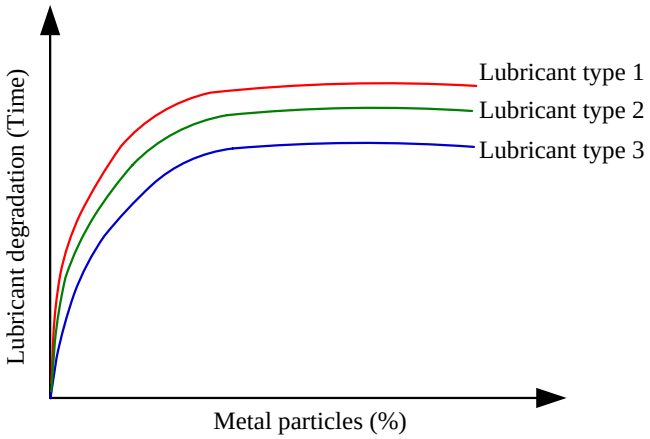

Figure 4.8: Relationship between lubricant degradation and the quantity of metal particles.

Conceptually, when we can measure the quantity of metal particles in the lubricant, we can know the level of lubricant degradation. Therefore, from the relationship between metal particles and magnetization of magnetic field, the conventional Hall Effect sensor can be applied to measure variables in this case. However, in this study, a methodology is presented which is based on the variations of saturation time and maximum output signal intensity of lubricant degradation. These variations in both factors were dependent on the quantity of metal particles as shown in Figure 4.9 and Figure 4.10, respectively. Because of the reasons we stated, we can evaluate the lubricant degradation using the output signal from Hall Effect sensor by considering the quantity of metal particles on acceptable levels of reliability for the industry as shown in Figure 4.11.

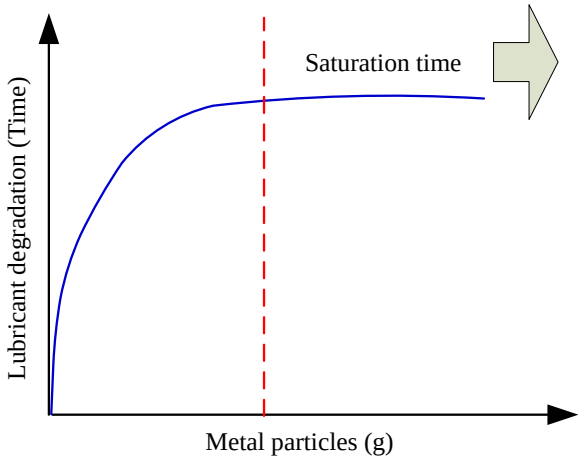

Figure 4.9: The saturation time of signal depends on the quantity of metal particles.

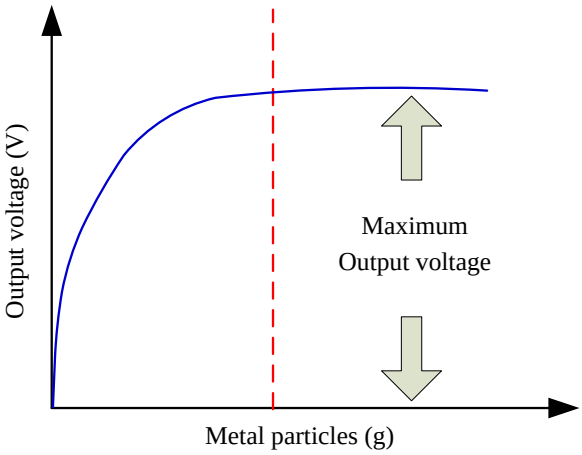

Figure 4.10: The maximum signal intensity depends on the quantity of metal particles.

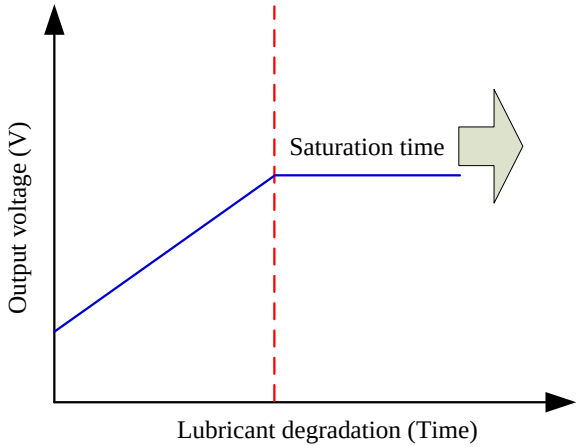

Figure 4.11: Evaluate the lubricant degradation using output voltage of Hall Effect sensor.

4.3 Typical New Sensor Module for Measurement of Angular Displacement

In this section, the type of sensor module used for the measurement of angular displacement will be divided into two types: the first is the new sensor module, namely a Hall Effect sensor with Helmholtz coil, and the second is the two flat-curve permanent magnets. The measured results will then be used to compare the performance of each technology in the same specific condition.

4.3.1 Measurement of Angular Displacement Using a Hall Effect Sensor with Helmholtz Coil

4.3.1.1 Objectives of Design for a Hall Effect Sensor with Helmholtz Coil

The objectives in this section aim to design a sensor module to examine the angular displacement of shaft declination angle on X-axis by starting from perpendicularly with ground surface. The conventional Hall sensor would be used as a sensor device, and an electromagnetic field was generated by induced in the coil of wire has chosen the Helmholtz coil due to its high stability with an electromagnetic field generated. The assumptions of the study will be influenced by the characteristic of Helmholtz coil that is the density of electromagnetic field of Helmholtz coil would be distributed and flowing direction to be stable at the center of first coil through the center of second coil. When considering the distribution of the electromagnetic field density out of the center of coil, it was found that the intensity of density will decrease proportional to the distance between of center of coil. The conventional Hall sensor was used as a sensor for analyzing the relationship of trigonometric functions in terms of angle and remaining length of the measured triangle. In this study, the declined angle of shaft on X-axis was assessed despite measurement and analysis of angular position [16-18]. Output voltages from the sensor module were also available for real time collection via PC which can be then used for further analysis

4.3.1.2 Design of a Hall Effect Sensor with Helmholtz Coil

Design of new sensor module in this study was performed by using the fundamental of slide-by sensing mode. This sensing mode was performed by sliding the permanent magnet at a perpendicular angle through the Hall generator, as shown in Figure 4.12 (a). Considering the movement of a permanent magnet, the axis of magnetization of a permanent magnet will be parallel to the sensitive axis of a Hall generator, while the movement of direction of a permanent magnet will be perpendicular to the axis of

magnetization. The operation of a Hall Effect sensor uses slide-by sensing, which has benefited in terms of safety for a device rather than the head-on sensing method due to the scenario of practicality, while the permanent magnet may be moved over the end point or release points. In the case of head-on sensing, the permanent magnet could be bumped with a Hall generator, which was damaged by the Hall generator, the permanent magnet, or both.

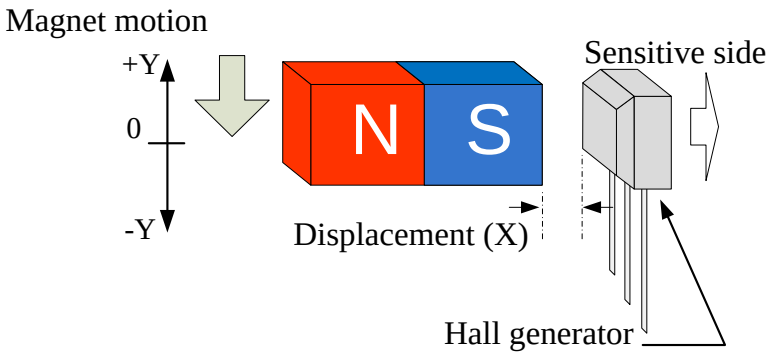

(a)

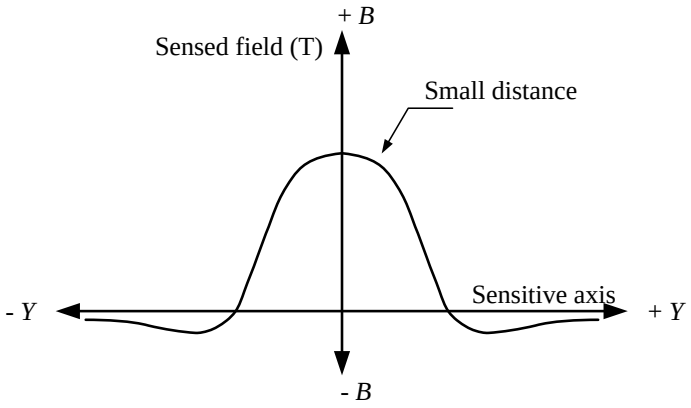

(b)

Figure 4.12: Slide-by activation mode;
(a) A magnet placing at the center of a Hall generator;
(b) The maximum value of resultant flux.

Moreover, it can be observed that there are some advantages of the slide-by sensing method which was superior to the head-on sensing method. This is the movement of a permanent magnet from the centre position, which was that the sensed magnetic field could be reducing a slightly negative field towards at the end of the movement. Therefore, when a permanent magnet moved into the centre position at the same level as a Hall generator the maximum value of the output signal from a Hall Effect sensor as shown in Figure 4.12 (b) would be obtained.

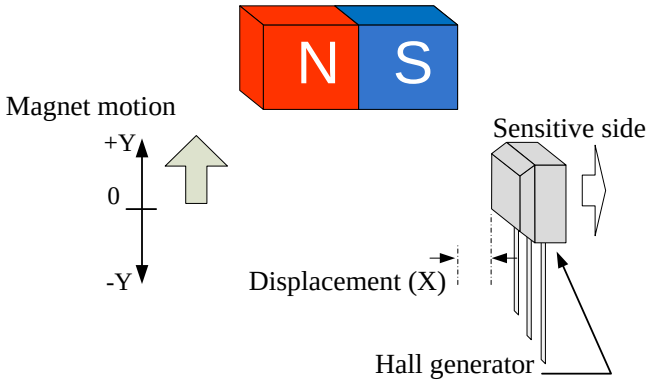

(a)

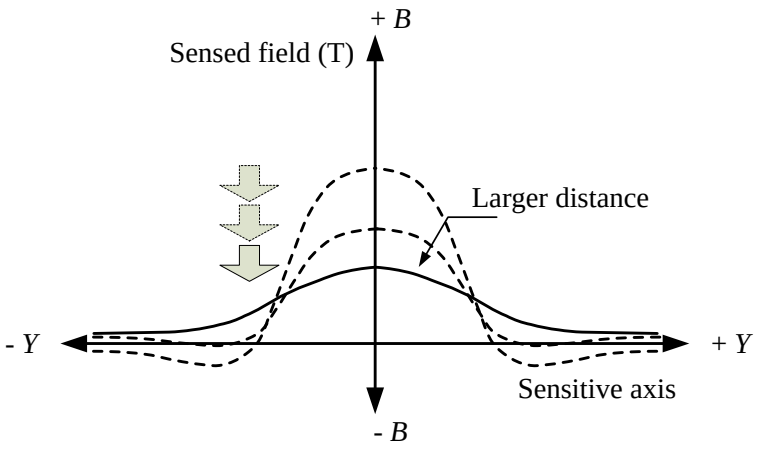

(b)

Figure 4.13: Slide-by sensing mode;
(a) A magnet move away from a Hall generator;
(b) The minimum value of resultant flux.

When a permanent magnet moves through the centre of a Hall generator, it will be transmitting the return of the magnetic field to the rear pole of a permanent magnet. This guarantees the performance of turn-off for application for a Hall Effect sensor as an electronic switch-type. The effect has occurred from this phenomenon will be used more clearly when the distance between a permanent magnet and a Hall generator decreases. This means that the 'ON' status will be reasonable and will approximate the width of a magnetic pole, although it depends on the variation in the condition of the distance between a Hall generator and a permanent magnet. This is because the negative field which was passing the edge of a magnet might be lower in relation to the position of the magnetic field in the area at front of a permanent magnet. Therefore, when the permanent magnet moved in direction of perpendicular to a Hall generator, as shown in Figure 4.13 (a), it was found that the effect of the magnetic field density on a Hall generator would be decreased. This also

had the effect of decreasing the output signal of the Hall Effect sensor. The relationship between distance and the movement position of a permanent magnet is shown in Figure 4.13 (b). (*Original by Edward Ramsden: Hall-Effect Sensor Theory and Applications; Elsevier Inc. 2006*) [1].

4.3.1.3 The Basic Idea for the Measurement of Angular Displacement Using a Hall Effect Sensor with Helmholtz Coil

The design of a sensor module applies the conventional Hall Effect sensor for measurement of angular displacement based on the relationship between the electromagnetic field density at any point within Helmholtz coil radius and the declined angle of a shaft. Figure 4.14 shows the relationship between the trigonometric function and the electromagnetic field, which from conception can be determined by the current flowing into the coil in one cycle, as shown in Figure 4.14 (a). Also, an analysis of phase movement can be determined by means of Equation 4-2.

$$B_m = \sqrt{B_X{}^2 + B_Y{}^2} \tag{4-2}$$

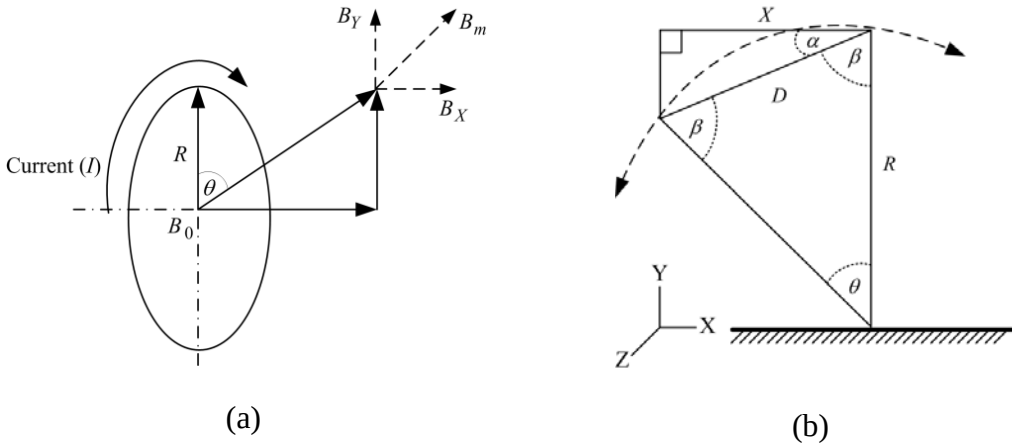

(a) (b)

Figure 4.14: Relationship between the trigonometric function and the electromagnetic field;
(a) Relationship between electromagnetic field and current flowing into the coil;
(b) Relationship of the trigonometric function compared with the centre of Helmholtz coil.

An analysis of angle due to shaft declination on X-axis compared to the center of Helmholtz coil was performed as shown in Figure 4.14 (b). The distribution properties of magnetic field density at a given point within Helmholtz coil radius can be estimated by Equations 4-3 to 4-5.

$$\frac{\sin\theta}{D} = \frac{\sin\beta}{R} \tag{4-3}$$

$$D = \frac{\sin\theta}{\sin\beta} \times R_1 \tag{4-4}$$

$$X = D \times \cos\alpha \tag{4-5}$$

Normally, the Helmholtz coil was used in biological research due to its having a stable electromagnetic field in distributed and flowing directions. The basic structure of a Helmholtz coil consists of two circular coils in windings connected in series and parallel with the gap which is equal to radius of the coil, as shown in Figure 4.15 [1].

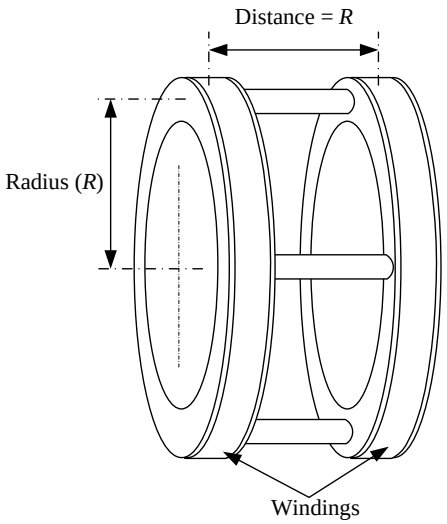

Figure 4.15: The Helmholtz coil in ideal.

This study used the standard Helmholtz coil of LEYBOLD DIDACTIC GMBH [19] as a reference to design the sensor module, which has a spec with a radius of 6.8 cm from 320 turns of 0.8128 mm copper wire (AWG 20 standard) and which can support the current supplied constantly at 1.5 A, as shown in Figure 4.16.

Figure 4.16: The standard Helmholtz coil of LEYBOLD DIDACTIC GMBH.

The Helmholtz coil was named in honour of its inventor, a German physicist named Hermann Ludwig Ferdinand von Helmholtz (1821-1894). The major reason to choose Helmholtz coil in order to generate an electromagnetic field to stimulate a Hall Effect sensor is because the electromagnetic field generated at the centre of Helmholtz coil was found to be stable. Figure 4.17 shows that the structure of Helmholtz coils used for generated the electromagnetic field in this study were suitable for use.

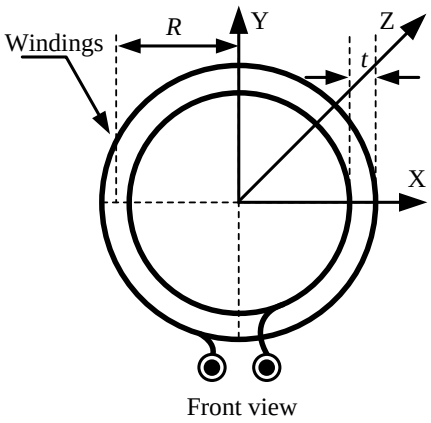

Figure 4.17: The basic structure of a Helmholtz coil used for generating an electromagnetic field.

A Helmholtz coil consists of two circular coils mounted symmetrically and parallel to the gap based on the conditions of the diameter of coils, the diameter of copper wires, the number of turns of wire, and the external constant current. It also has the currents in both coils which were flowing in the same direction. Figure 4.18 shows the operation of Helmholtz coils and Hall generator together. A Hall generator was placed at the top of shaft and in the centre between two Helmholtz coils. The electromagnetic field generated at the centre of the coil was found to be stable and a magnetic flux was distributed from the centre of the coils.

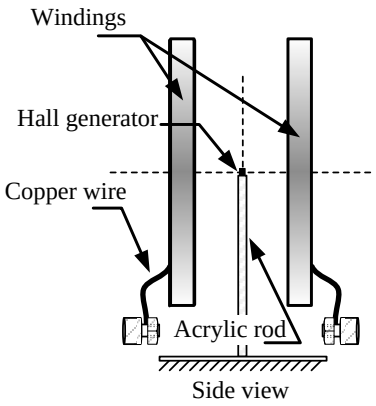

Figure 4.18: Hall generator position at the centre between two Helmholtz coils.

Two Helmholtz coils, in the form of serial wires, were used in this study. These coils were installed parallelly with the gap as equal to the coil radius. The electromagnetic field generated at the centre of Helmholtz coil was found to be stable and magnetic flux was distributed from the centre of the coil [20]. The density of the electromagnetic field was proportional to the number of wire turns and was induced by a constant external current. The relationships between a current supplied constantly to a Helmholtz coil and the density of electromagnetic field can be expressed by Equation 4-6.

$$B = \left(\frac{5}{4}\right)^{\frac{3}{2}} \times \frac{\mu_0 NI}{R} \tag{4-6}$$

4.3.1.4 The Performance of Stimulation by Helmholtz Coil

The advantages of activating a Hall Effect sensor using an electromagnetic field which is generated by a Helmholtz coil:

a) Ease of determining the size and also controlling the density of the electromagnetic field.
b) Ease of determining and controlling the flow direction of electromagnetic flux.
c) Ease of determining the feature and the density of magnetic field with requirement by designing and developing the shape of a wire coil.
d) A simple structure which can be self produced.

The disadvantages of activating a Hall Effect sensor using an electromagnetic field which is generated by a Helmholtz coil:

a) It requires an external constant current with high values (1 ampere and more) to excite a Helmholtz coil.

b) The constant supply of the high current into the coil can also cause the heat to accumulate in the Helmholtz coil.

c) It has been found that the deadband of range measurement is in the area at the centre of the Helmholtz coil.

d) The size of Helmholtz coil would not be reasonable for installation in a limited space.

e) The limitation of remote sensing measurement because of the generation of electromagnetic field by Helmholtz coil would be rather low in terms of flux density.

f) In some cases, the electromagnetic field which was generated by Helmholtz coil might be not smooth and unstable.

g) The range of measurement would be narrow (depending on the diameter of the coil).

4.3.2 Measurement of Angular Displacement Using Two Flat-Curve Permanent Magnets

4.3.2.1 Objectives of Design for the Two Flat-Curve Permanent Magnets

The objectives in this section are to improve the new sensor module by conducting continuous development and by examining the angular displacement of the shaft declination angle on this X-axis. This chapter will show how Helmholtz coils can be replaced by permanent magnets in order to generate a magnetic field for activating a conventional Hall Effect sensor in order to design a new sensor module for the measurement of angular displacement based on sensing mode of magnetic Null-point sensing. Activating of a Hall Effect sensor using the magnetic field density which was generated from permanent magnet can enhance the performance of a sensor device. Because some benefit is obtained this does cause the heat to accumulate while operating a Hall generator, as well as creating the ability to measure the variables in all ranges of measurement without deadband, and with a simplicity of installation which is reasonable for limited space. Due to it being a small device it can also be designed for use with sensor module in a portable compact. Its density of magnetic flux is high this could be used for non-contact measurement in remote sensing. The magnetic flux generated would be smooth and consistently, as well as the range of measurement including width, etc. Moreover, it would also be possible to measure the angular displacement then transmit this to a computer for real time monitoring while maintaining the appropriate position in order to maintain the machines in the industrial sector.

4.3.2.2 Design of the Two Flat-Curve Permanent Magnets

Design of new sensor module in this study was performed by using the fundamental of null-point sensing mode. The advantage of this methodology would be provided by an

output signal for measuring positive and negative aspects in both directions by sliding a permanent magnet through a Hall generator. Figure 4.19 shows magnetic null point which was developing from the slide-by sensing mode. The null-point sensing would be a combination with a single magnet to an operation with a sensitive axis direction which is perpendicular to the moving of a permanent magnet.

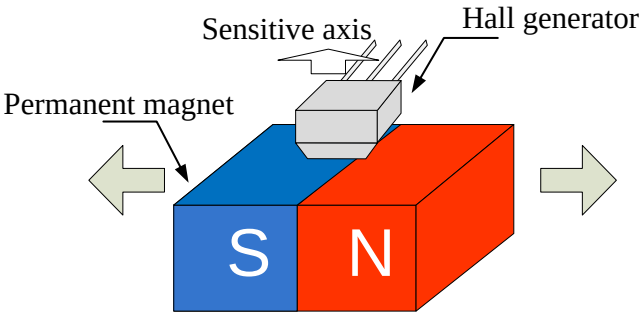

(a)

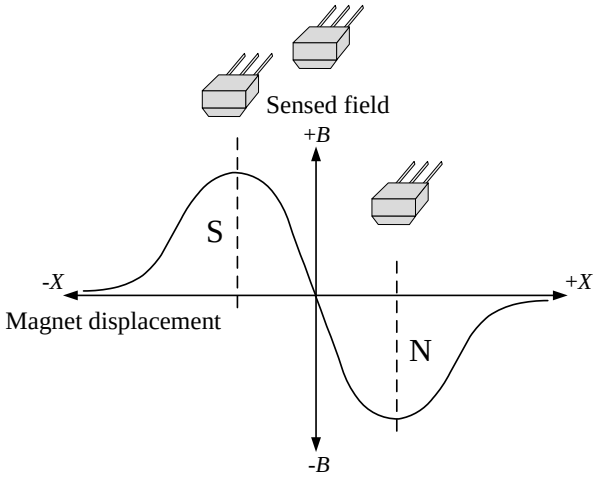

(b)

Figure 4.19: The Null-point sensing mode;
(a) Placement of a Hall generator between of S and N poles magnet;
(b) The position of a Hall generator for developing a magnetic null-point.

The configurations in the operation of the null-point sensing method will begin by placing a Hall generator at the centre and also between N-pole and S-pole of a permanent bar magnet. This position initially operates perpendicular to a magnetic flux with a flux density which was equal to zero, as shown in Figure 4.19 (a). If we slide a magnetic bar magnet in the direction of the S-pole of a magnet which is parallel to a Hall generator, it was found that, when a Hall generator was placed on the centre of S-pole of a permanent magnet, the magnetic field would be more intense than the maximum values in the positive

direction. On the other hand, the magnetic field density will decrease until maximum values of negative direction when a Hall generator placed at the centre of the N-pole of a permanent magnet, as shown in Figure 4.19 (b). (*Original by Edward Ramsden: Hall-Effect Sensor Theory and Applications; Elsevier Inc. 2006*) [1].

In this study, the design of a sensor module can be divided into three steps: the first involves studying the direction of magnetic flux distribution, the second selecting the kind and also the shape of magnet, the last step involves creating the structure of a sensor module. A diagram of process is shown in Figure 4.20. The first step involved a study of the direction of magnetic flux distribution being appropriate for the shape and the number of magnets by a calculation using COMSOL multiphysics. The second step involved selecting the kind and also the shape of the magnet as being suitable for measuring the various angles within the range of measurement by comparing the properties of the magnets in the shape of rectangular permanent magnets, permanent bar magnet or permanent curve magnets. Finally, the third step would involve creating a sensor module for measuring the variation of the angle in the range of -40 deg to 40 deg.

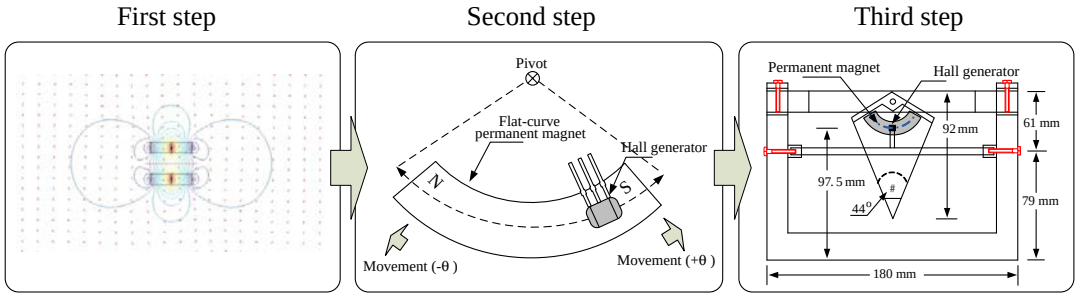

Figure 4.20: Diagram of designing a sensor module in three steps.

4.3.2.3 The Basic Idea for the Measurement of Angular Displacement Using Two Flat-Curve Permanent Magnets

The basic idea of creating a sensor module for measuring the angle in the case of angular displacement involves selections of the kind and also the shape of magnet including the placement of Hall generator, which was appropriate for the testing angle. The shape of the magnet and the kind of curve in this study was done on the basis of the provision of the widest linear range of magnetic density field rather than the permanent magnet in the shape of rectangle by comparing from the results of an empirical experiment. A sensor module used for angular displacement was used to examine the placing of a Hall generator in relation to the space between of both flat magnets, in order to provide the best readability and increase the resolution of measurement, as shown in Figure 4.21. Therefore, a permanent magnet, of a ferromagnetic material type, and with a maximum magnetic density

of 0.25 T, was selected for used in this study. The two flat-curve permanent magnets were 10 mm wide, 1.5 mm thick, and 41.5 mm long. The outer and inner radius measured 24 mm and 19 mm, respectively and the plate curve was 120 deg with a distance of 12 mm. The permanent magnet was mounted in parallel and the magnetic poles were placed in a position that can generate magnetic tension and provide the widest linearity range of the magnetic density field, as shown in Figure 4.22.

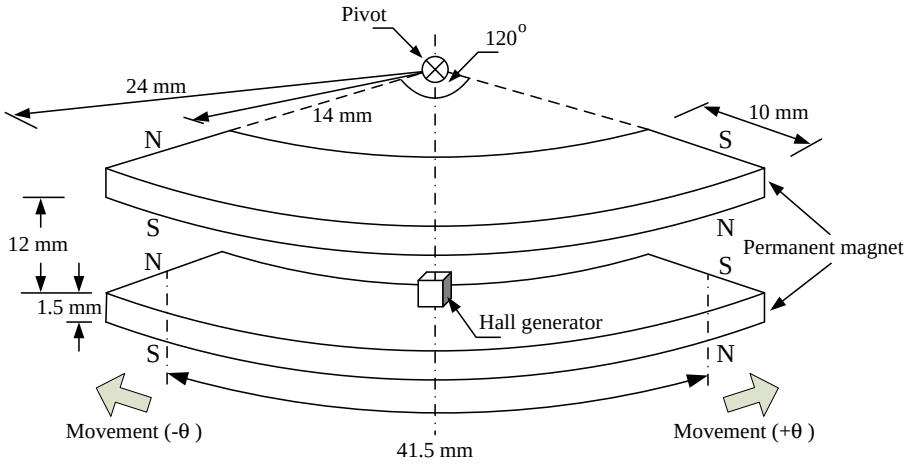

Figure 4.21: The Basic structure of permanent magnetic and the conventional Hall generator placement.

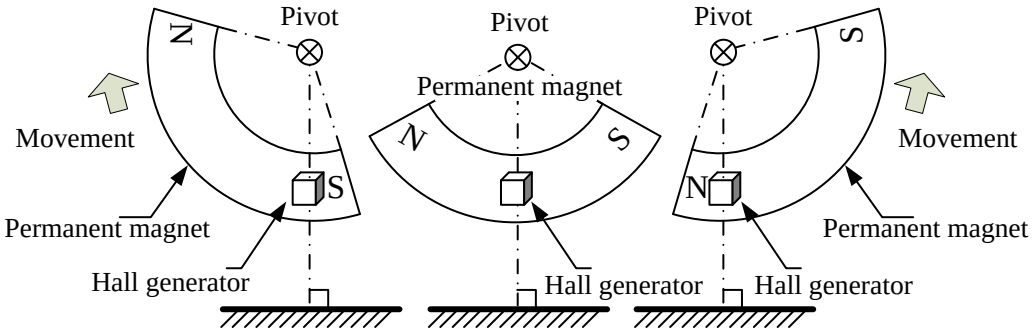

Figure 4.22: Direction of flat-curve permanent magnet movement.

4.3.2.4 The Performance of Stimulation by Flat-Curve Permanent Magnet

The advantages of activating a Hall Effect sensor using a magnetic field which is generated by a permanent magnet:

a) It does not cause heat to accumulate during the operation.

b) It has the ability to measure the variables of all ranges of measurement without a deadband.

c) The simplicity of installation is reasonable for a limited space due to it being a small device. It can also be designed with a new sensor module in a portable compact.

d) The density of magnetic flux has a high intensity and can be used for non-contact measurement in remote sensing.
e) The magnetic flux density which is generated would be smooth and consistent.
f) The range of measurement includes width.

The disadvantages of activating a Hall Effect sensor using a magnetic field which is generated by permanent magnet:

a) It does not make it easier to determine the direction of flow of a magnetic flux after installing a Hall generator and a permanent magnet combination.
b) It cannot be adjusted to compensate for the intensity of the magnetic flux.
c) It can be difficult to find a permanent magnet with a density which matches that of a Hall generator for measuring the variables.

4.4 Typical New Sensor Module for Detecting Material Imperfection

This section discusses the design of a sensor module for detecting material imperfection by using the conventional Hall Effect sensor as a sensor device. It can be divided into three types of new sensor module: the 4-array Hall sensor, the 5-array Hall sensor, and the 4-crossing Hall sensor, in order to compare the performance of each new sensor module from measurement the material imperfection in the same conditions. The design of a new sensor module in this study was performed by considering the placement of a Hall generator together with a permanent of magnet based on the principles of head-on sensing mode, which is similar to that of the sensor module, namely the single Hall sensor that was used to measure the lubricant viscosity and the level of lubricant contamination. However, in this study the number of Hall generators and number of permanent magnets will be increased in order to enhance the performance of the sensor module for a wider detection area. This means that if we use only one Hall generator to measure the width of a hole an error may be made due to the sensor module not being placed at the centre of hole. Therefore, we improved the new sensor module by increasing the number of Hall generators and number of permanent magnets, and compared the output voltage in each Hall generator in order to select the best signal to analyze.

4.4.1 Objectives of Design the New Sensor Module for Detecting Material Imperfection

The objectives in this section are to propose an alternative sensing system, in terms of size, system components, ease of installation, and cost, for detecting material imperfections. Then a conventional Hall Effect sensor will be improved as a sensor module by considering the placement of a Hall generator together with a permanent magnet. The next step is to design the new sensor module for detecting material imperfections based on the principles of elements of a conventional Hall Effect sensor. Finally, the performance of the sensor module will be enhanced by increasing the number of Hall generators and number of permanent magnets in order to widen the detected area.

4.4.2 Design of the New Sensor Module for Detecting Material Imperfection

4.4.2.1 The 4-Array Hall Sensor

The new sensor module namely the 4-array Hall sensor [21-23], the poles of four Neodymium permanent magnets (5 mm × 5 mm × 2 mm, 292 mT) were placed alternatively, as shown in Figure 4.23 and 4.24. The Hall generators namely x_3 and x_4 can operate with sensors x_1 and x_2. Therefore, the displacement of each Hall generator can be estimated by Equations 4-7 and 4-8 where Δx is the distance from the centre of x_3 and x_4 to the centre of x_1 and x_2.

$$x_1 = x_4 + \Delta x \tag{4-7}$$

$$x_2 = x_3 + \Delta x \tag{4-8}$$

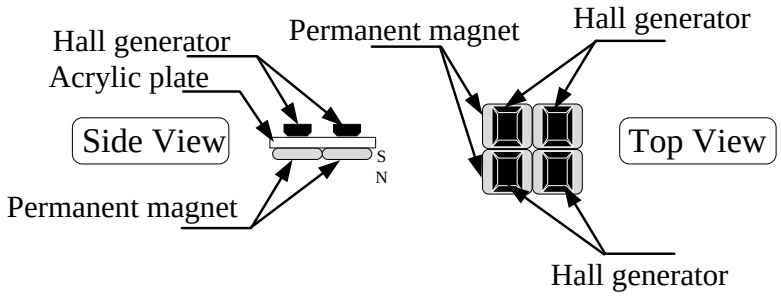

Figure 4.23: Placement of the 4-array Hall sensor.

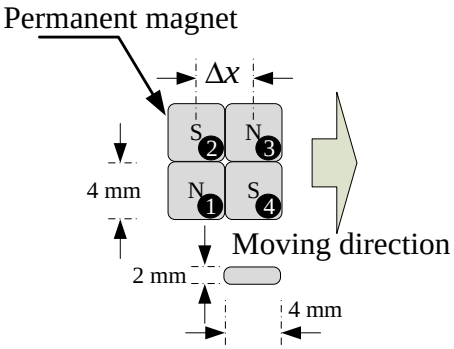

Figure 4.24: Alternative pole placement of permanent magnet in the 4-array Hall sensor.

4.4.2.2 The 5-Array Hall Sensor

The 5-array Hall sensor [24, 25] was placed in each Hall generator with the gap of 4 mm (same as sensor size). Only one Neodymium permanent magnet (15 mm x 15 mm x 2 mm, 135 mT) was used and was installed 3 mm away from the Hall generator, as illustrated in Figure 4.25.

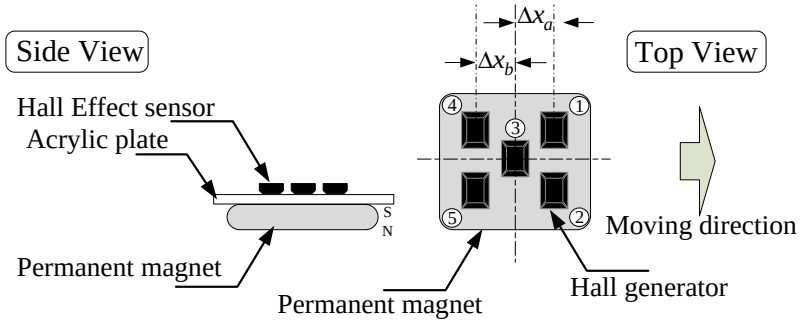

Figure 4.25: Placement of the 5-array Hall sensor.

The Hall generators, namely x_1 and x_2, could operate before the Hall generators, namely x_3, x_4, and x_5. Therefore, the displacement of each Hall generator can be expressed by Equations 4-9 to 4-11 where x_1, x_2, x_3, x_4, and x_5 are the positions of each Hall generator, Δx_a is the distance from the centre of x_1 and x_2 to the centre of x_3, Δx_b is the distance from the centre of x_3 to the centre of x_4 and x_5.

$$x_3 = x_2 + \Delta x_a \tag{4-9}$$

$$x_4 = x_1 + \Delta x_a + \Delta x_b \tag{4-10}$$

$$x_5 = x_2 + \Delta x_a + \Delta x_b \tag{4-11}$$

4.4.2.3 The 4-Crossing Hall Sensor

The 4-crossing Hall sensor consist of the Hall generators and four Samarium cobalt permanent magnets with a magnetic field density of 281 mT each, as shown in Figure 4.26. The Hall generators, namely x_4 could operate before the Hall generators, namely x_1, x_3, and x_2. Therefore, the displacement of each Hall generator can be expressed by Equations 4-12 and 4-13 where x_1, x_2, x_3, and x_4 are the positions of each Hall generator, Δx_a is the distance from the centre of x_1 and x_3 to the centre of x_4, Δx_b is the distance from the centre of x_2 to the centre of x_1 and x_3.

$$x_1 = x_3 \tag{4-12}$$

$$x_2 = x_4 + \Delta x_a + \Delta x_b \tag{4-13}$$

Figure 4.27 shows the dimension and the placement position of four permanent magnets with reference to the Hall generator. Hall generator was placed at the centre of permanent magnets by maintaining the space between each Hall generator equally their width. Also, an acrylic plate the 3 mm of thickness was installed between the Hall generator and permanent magnets in order to control the saturated point of output voltage of the sensor module similarly to a case of the 4-array Hall sensor.

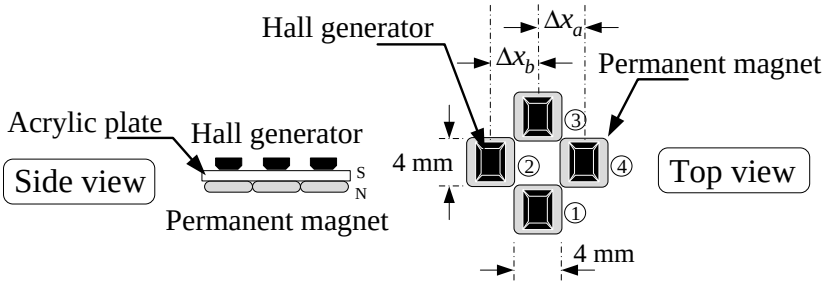

Figure 4.26: Shape and the placement position of 4-crossing Hall generator with permanent magnets.

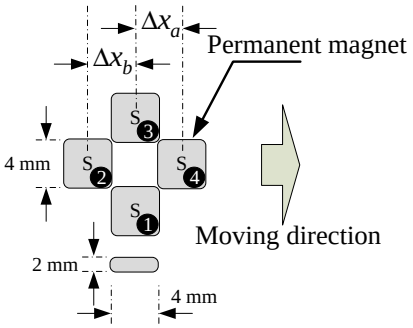

Figure 4.27: Dimension and the placement position of four permanent magnets with Hall generator.

4.5 Conclusion

Stimulation of the Hall Effect sensor is important in activating a Hall generator. The selection of a magnetic field in a different format could not be stereotyped to define the performance of a sensor module. The stimulation from each methodology would create advantages and disadvantages in different conditions of measurement depending on the requirements of consumer and the reasonable variables for measurement. In addition, there was an enhancement to the performance of the convention Hall Effect sensor in the case of measuring material imperfection such as detecting the drilled hole in terms of diameter and depth or cracks in the metal material surface using non-destructive inspection method. The measurement system was considered by studying the influences of sensor placement and by using a permanent magnet as a stimulator. This study has chosen Hall Effect sensor as a sensor device due to its high reliability and reasonable cost compared to other methodologies. Moreover, this sensor can simply connect to other electronic devices as output voltage is generated.

Chapter 5

Experiment of Lubricant Viscosity and Contamination in Lubricant

5.1 Introduction

The conditions of lubricant are vital for industrial machine efficiency as they are related to machine damage caused by lubricant deterioration. From previous studies [26, 27], it can be noted that machine failures would be influenced by the lubricant with low quality. Theoretically, the lubricant for each type of machine should be used in specific period. However, the lubricant conditions would be gradually deteriorated earlier than expected due to metal particles caused by machine wear itself or exterior contamination and also the maintenance period would not be appropriate for a given machine. At present, there are several studies proposing the experiments on lubricant conditions by using several methods such as ultrasonic measurement of viscosity of liquids, photoacoustic measurement of liquid viscosity, measurement of magnetic viscosity in NdFeB, a viscosity and density meter with a magnetically suspended rotor, capacitive sensor, IR-absorption and optical fiber sensing [28-33]. Previous studies will be complicated in terms of the composition of measurement systems and it also is difficult to set up or calibration of the instruments. Moreover, some techniques might require expensive equipment, and are also inconvenient to use practically. This chapter presents an alternative measurement by using a magnetic field together with the conventional Hall Effect sensor which can be applied to examining the lubricant contamination of metal particles. The new sensor module was designed by the assembling of the conventional Hall Effect sensor as a sensor device, so the results from measurements in the form of output voltage will be analysed in a relative way with the lubricant degradation and the saturation time.

5.2 Characteristic of Metal Particles

Contamination can be influenced by several causes such as machine wear and corrosion or exterior contamination from exposed surrounding. As a result, wear particles could be non-ferrous and ferrous metal that lead to the lower efficiency of the machine and also

machinery damages. Normally, the size of particles would range from 1 µm to 40 µm. The particles with 20 µm to 30 µm of size can directly cause the machine wear while those with less than 1 µm of size would insignificantly affect. Therefore, this study presents the measurement of ferrous metal contamination in machine lubricant, which essentially influences the variation of magnetic field depending on the metal contamination level.

The reference metal particles used for the experiments was analyzed by SEM (Scanning Electron Microscope) with a scan speed = 2, Extra high tension (EHT) = 10 kV, Work distance (WD) = 12 mm, and Magnification (Mag) = 50 X, 100 X, and 2 kX. The size of metal particle varied from 1 µm to 100 µm as shown in Figure 5.1 - 5.3, respectively.

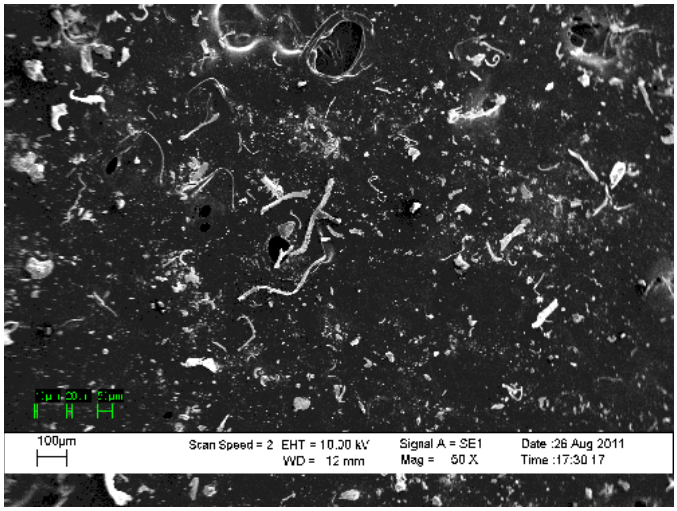

Figure 5.1: Reference metal particles size by SEM at 50X.

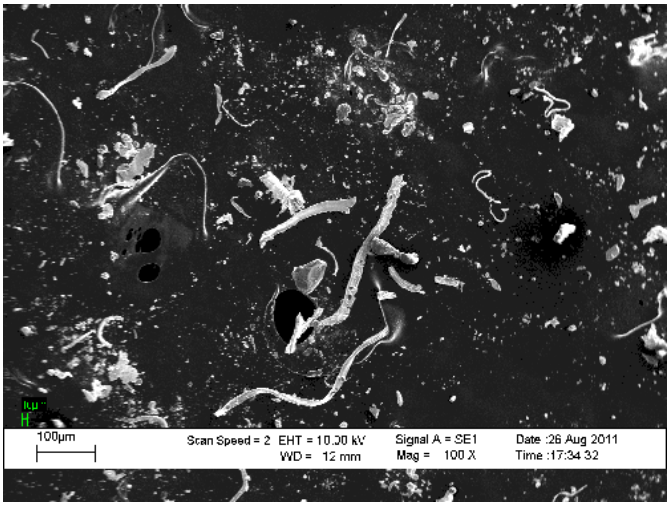

Figure 5.2: Reference metal particles size by SEM at 100 X.

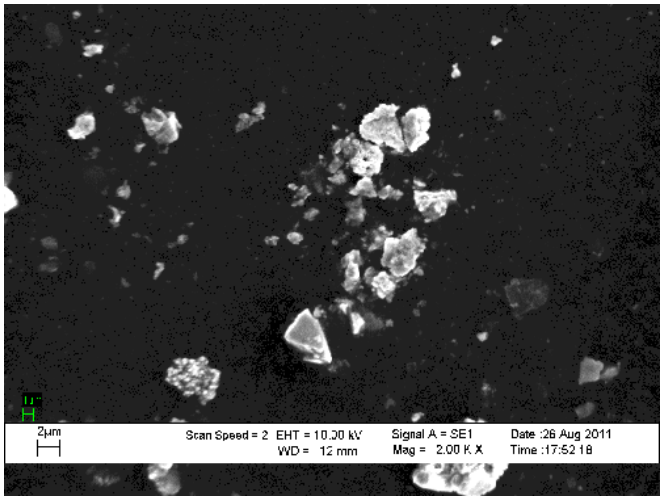

Figure 5.3: Reference metal particles size by SEM at 2 kX.

There three lubricants were tested in this study. About 25 ml of each sample was filled in 10 sets of 50 ml oil containers size is 0.3 mm of thickness, 20 mm of width, 40 mm of length and 70 mm of height. The reference metal particles was added in 0.1 g, 0.2 g, 0.3 g, 0.4 g, 0.5 g, 0.6 g, 0.7 g, 0.8 g, 0.9 g and 1 g increment, respectively as shown in Figure 5.4.

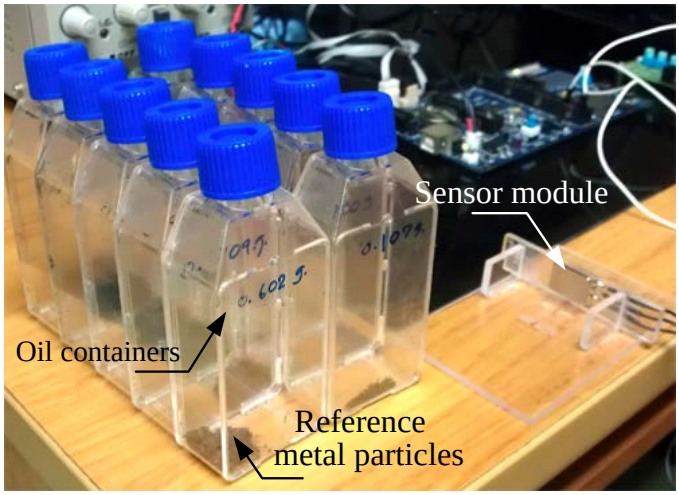

Figure 5.4: Oil containers for lubricant testing.

The details of the metal particles were to be used for the test on three sample lubricants which were filled in the oil container are presented in Table 5.1. It was also observed that the ISO VG 100 lubricant (most commonly used for industrial machines) could be initially measured from 0.001 g of contamination onward, while the remainder of two lubricant samples will be starting from 0.1 g until achieving 1 g of metal particles in weight.

Table 5.1: Weight of metal particles used for measurement.

Lubricant types	Quantity of metal particles in oil containers (mg)																
ISO VG 100	1	2	5	10	20	40	80	100	200	300	400	500	600	700	800	900	1000
15W-40	-	-	-	-	-	-	-	100	200	300	400	500	600	700	800	900	1000
20W-50	-	-	-	-	-	-	-	100	200	300	400	500	600	700	800	900	1000

New sensor module and each oil container filled with test the lubricant were placed in the designed positions during the experiments for accurate and precise results. In Figure 5.5, placement of the oil containers and movement of the reference metal particles to the permanent magnet are illustrated. As a result, the velocity of the reference metal particles can be varied by the lubricant viscosity as the velocity would be low for a high viscosity lubricant and on the other hand, the velocity would be high for a low viscosity lubricant. Therefore, the velocity of the metal particles is a function of the lubricant viscosity.

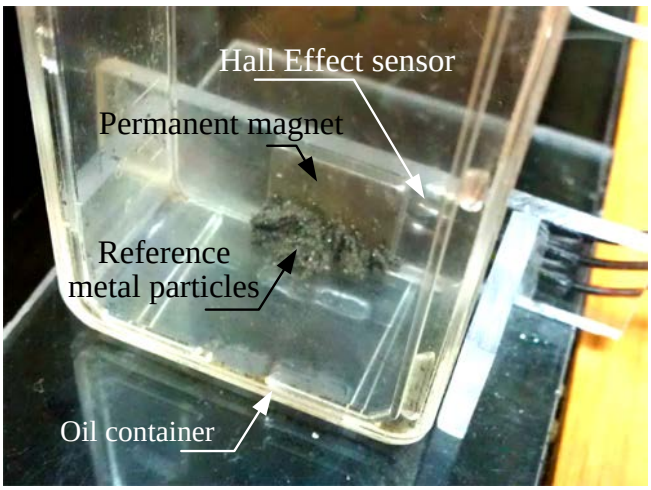

Figure 5.5: Movement of metal particles to the permanent magnet.

Figure 5.6 shows the degree of contamination of metal particles in lubricants by varying the weight from 0.1 g to 1 g being after stirred for about 3 sec in order to measure them dynamically. All the metal particles were settled in the bottom of the oil container for static measurement, as shown in Figure 5.7.

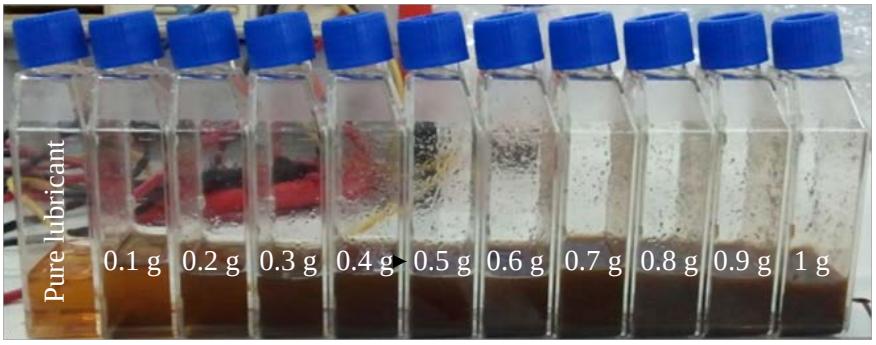

Figure 5.6: Quantity of metal particles with weights ranging from 0.1 g to 1 g in the oil containers.

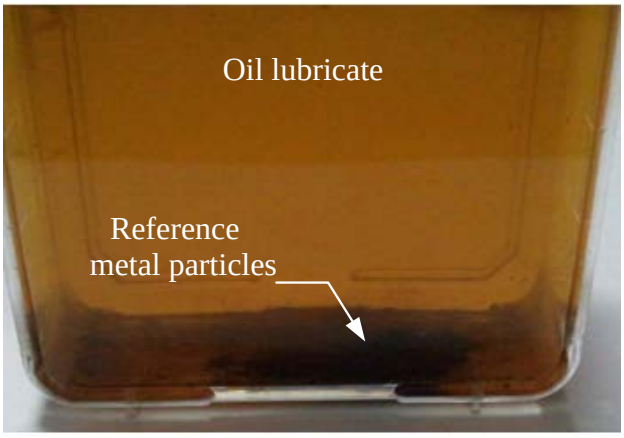

Figure 5.7: Lubricant and reference metal particles.

5.3 Experimental Conditions of a New Sensor Module for Viscosity and Contamination

A number of lubricants, namely SAE 15W-40, SAE 20W-50 and ISO VG 100, were selected for experiments in this study. A lubricant can gradually change its properties in the process of operation. In this study, the measurement of a lubricant was therefore divided into two parts: the contamination of metal particles and the viscosity of a lubricant. In this method, metal particles were added to 25 ml of lubricant oil containers by varying the weight from 0.1 g to 1 g and then stirring for about 3 seconds before testing as shown in Figure 5.8. The average values of output voltage from Hall Effect sensor started from 3.736 V and then increased continuously when metal particles moved close to a permanent magnet. The relationships between the moving metal particles, lubricant viscosity and output voltage of the Hall Effect sensor were determined are shown in the Figure 5.9. When the relationship is $T_A > T_B > T_C$ then $\eta_A > \eta_B > \eta_C$ where T_A, T_B, and T_C are the variation

from the starting point to a stable point of output from a new sensor module, η_A, η_B, and η_C are the viscosity of each lubricant.

From the empirical study, it can be determined using Equation 5-1.

$$t_{moving} = m \times V_H + c \tag{5-1}$$

Changing the mass of reference metal particles for measuring lubricant viscosity characteristics was performed in order to determine the appropriate mass of reference metal particles for 25 ml of lubricant in the oil containers and further use as mass of reference. The relationships between the factors depending on the viscosity can be determined by Equations 5-2 and 5-3.

$$\eta = M \times t_{moving} \tag{5-2}$$

$$M = \rho \times d \times a \tag{5-3}$$

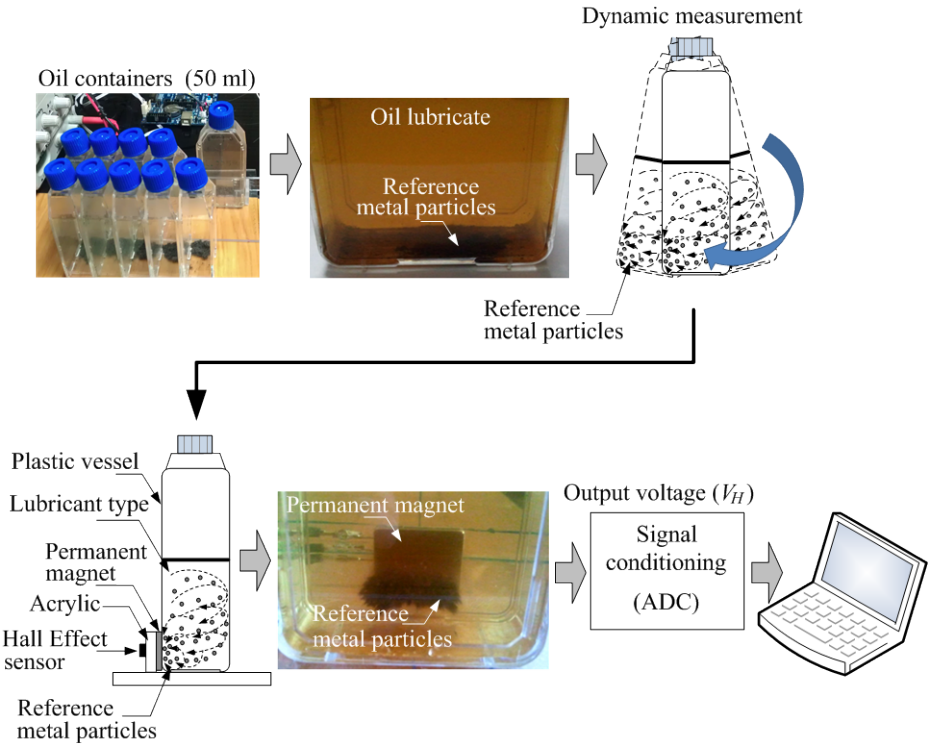

Figure 5.8: Illustration of all turbulent metal particles.

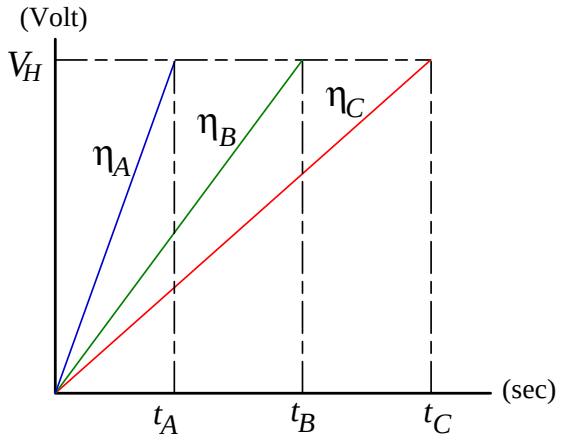

Figure 5.9: The relationships between viscosity and output voltage of Hall Effect sensor.

5.3.1 Static Experiment

A static experiment was carried out by adding reference metal particles to the tested lubricant with mass values ranging from 0.1 g to 1 g, waiting until all the metal particles were settled, and then testing as shown in Figure 5.10. Table 5.2 shows the average output voltages of Hall Effect sensor staring from 3.736 V (10 measurements for 1 mass of metal particles) and then increasing when reference metal particles moved to a permanent magnet [34].

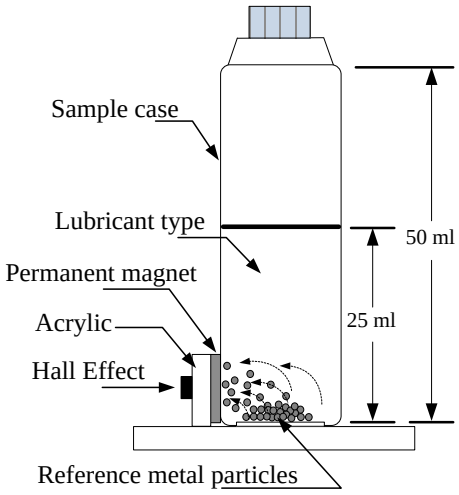

Figure 5.10: Illustration of all settled reference metal particles.

Table 5.2: Average output voltages of Hall Effect Sensor from static experiment.

Mass (g)	SAE 15W-40 (V)	SAE 20W-50 (V)	ISO VG 100 (V)
0.1	3.574	3.574	3.574
0.2	3.767	3.769	3.764
0.3	3.774	3.775	3.77
0.4	3.778	3.777	3.774
0.5	3.784	3.778	3.779
0.6	3.784	3.777	3.785
0.7	3.787	3.78	3.783
0.8	3.787	3.781	3.787
0.9	3.787	3.787	3.784
1	3.792	3.784	3.787

Considering the displacement time to the permanent magnet for each mass of reference metal particles used to analyze the lubricant viscosity, it can be noted that the output voltage from the Hall Effect sensor was non-linear, not-constant, and not-consistent. It should be noted that some residue in reference metal particles, which cannot move to the permanent magnet, and were possibly left on the bottom of the oil container. Therefore, the efficiency of the output voltage could be affected in each measurement illustrated in Figure 5.11. Therefore, the static experiment would not be effective and appropriate for the viscosity measurement using the magnetic field method.

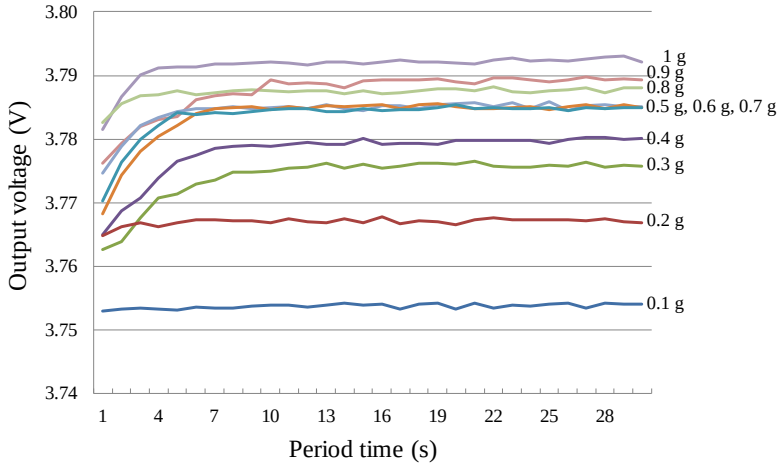

Figure 5.11: Output voltage from displacement of reference metal particles in SAE 15W-40 lubricant.

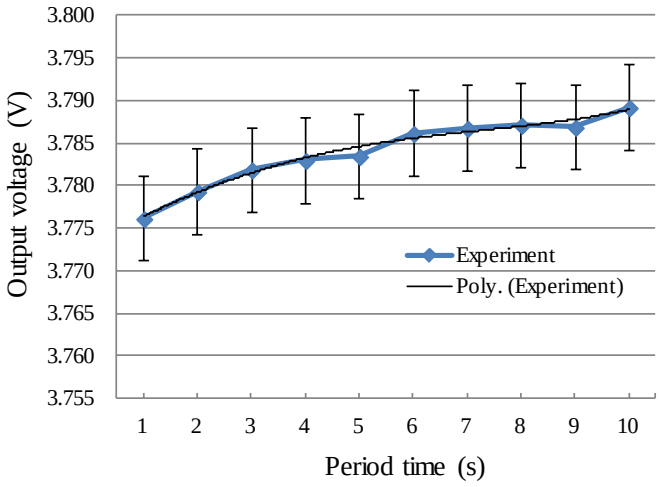

Figure 5.12: Relationship between output voltage and viscosity based on time period of reference metal particles moving to permanent magnet, SAE 15W-40 (0.8 g).

The experiment was conducted to observe the relationships between output voltage and viscosity tested. It can be divided the experiment into two sections which were based on time period of reference metal particles moving to permanent magnet as shown in Figure 5.12 and time to reach the stable point illustrated in Figure 5.13. The relationship between electrical voltage and viscosity which was tested from a starting point to a stable point of output from a sensing module, as shown in Figure 5.14.

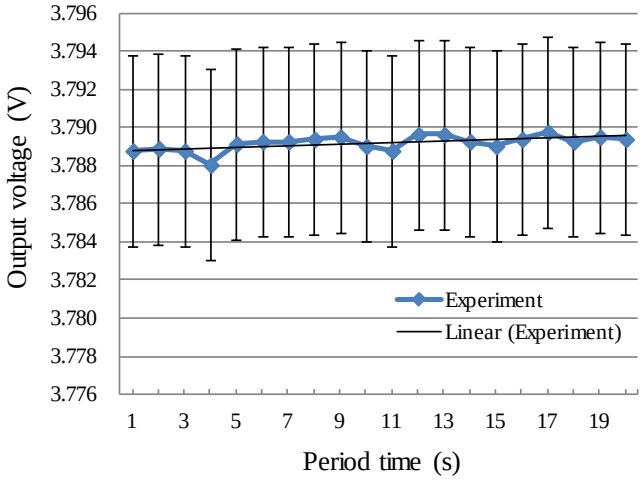

Figure 5.13: Relationship between output voltage and viscosity based on time reaching to the stable point, SAE 15W-40 (0.8 g).

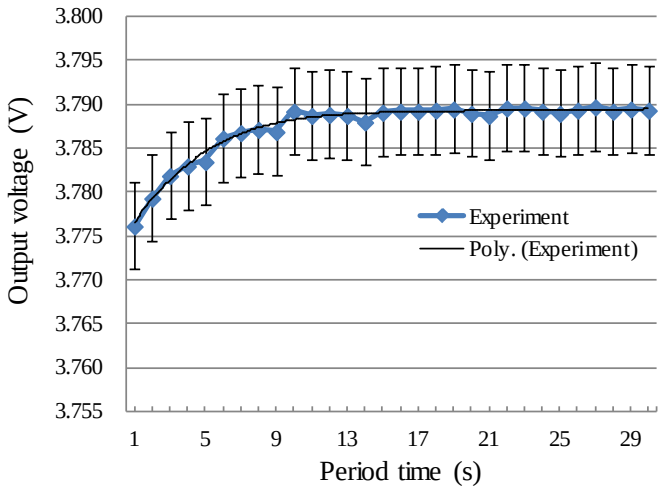

Figure 5.14: Relationship between output voltage and viscosity testing from starting point to stable point, SAE 15W-40 (0.8 g).

5.3.2 Dynamic Experiment

A dynamic experiment, the reference metal particles were added to 25 ml of lubricant in oil containers by varying the mass from 0.1 g to 1 g and then stirring for about 3 seconds before testing, as shown in Figure 5.15. Table 5.3 illustrates the average values of output voltage from a Hall Effect starting from 3.736 V. Them, the output voltage will increase continuously when iron scrap moves close to a permanent magnet. The time consumed when the reference metal particles moved to the permanent magnet for each experimental mass was considered. It was observed that the output voltage from the Hall Effect sensor was smoothly and consistently varied, as shown in Figure 5.16. Therefore, a dynamic experiment based on the magnetic field method was chosen for this study. It can also be noted that the appropriate mass for the experiments would range from 0.5 g to 0.9 g due to being on a sharp slope before reaching a stable point. Detailed analysis revealed that the appropriate reference mass values would be 0.6 g and 0.8 g. Therefore, these two mass values were used as a reference for other lubricant types [34].

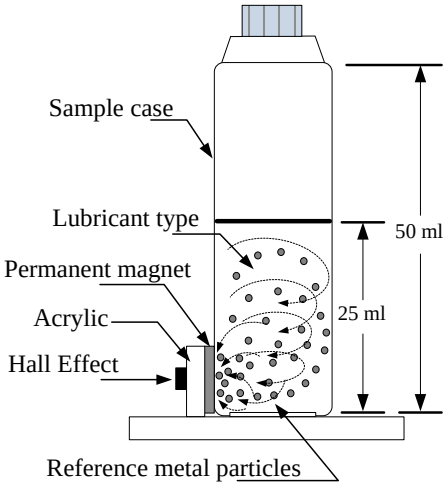

Figure 5.15: Illustration of all turbulent reference metal particles.

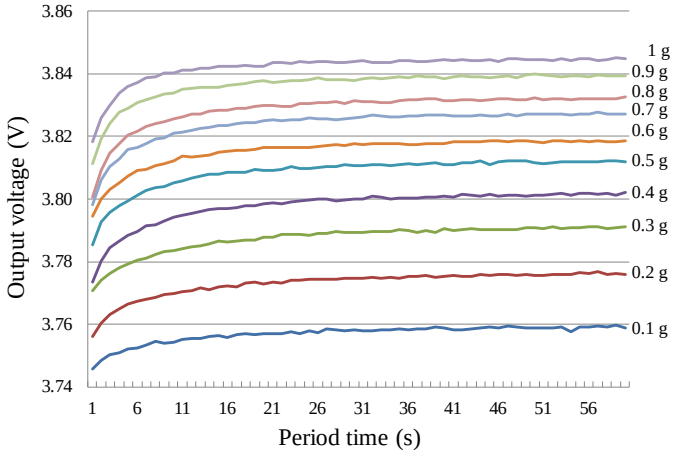

Figure 5.16: Output voltage from displacement of reference metal particles in case of dynamic experiment, SAE 15W-40.

The relationship between output voltage and viscosity in the dynamic experiment was performed similar to the static experiment. It can be divided into two sections which were based on the time period of the reference metal particles moving to the permanent magnet as shown in Figure 5.17, and the time to reach the stable point illustrated in Figure 5.18. Moreover the relationship between electrical voltage and viscosity testing from a starting point to a stable point of output from sensing module as shown in Figure 5.19. The developed system can be expressed by the variation in the output voltage using a third degree polynomial, as expressed by Equation 5-4.

$$y = 6E\text{-}05x^3 - 0.0014x^2 + 0.0115x + 3.7909 \quad (5\text{-}4)$$

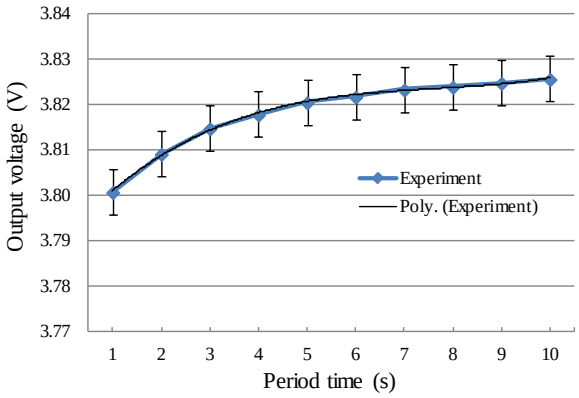

Figure 5.17: Relationship between output voltage and viscosity based on time period of reference metal particles moving to permanent magnet in case of dynamic experiment, SAE 15W-40 (0.8 g).

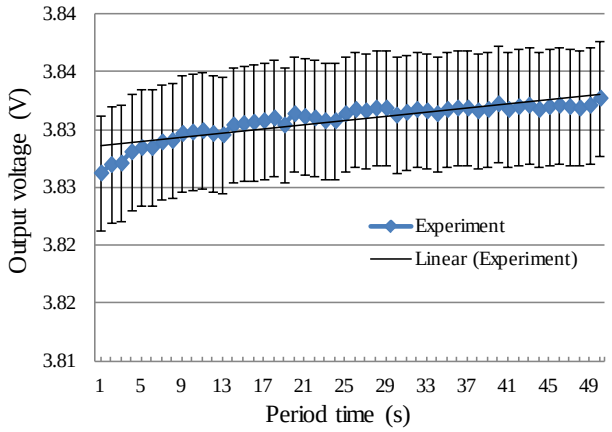

Figure 5.18: Relationship between output voltage and viscosity based on time reaching to the stable point in case of dynamic experiment, SAE 15W-40 (0.8 g).

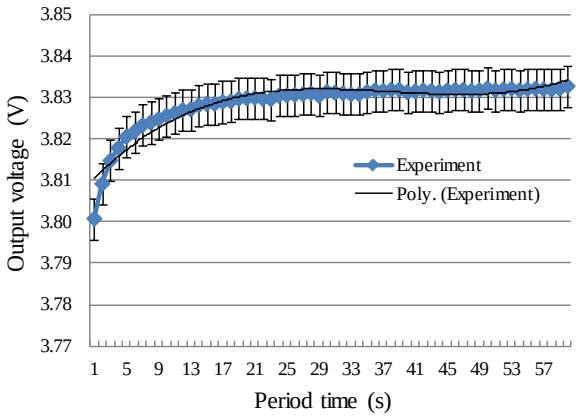

Figure 5.19: Relationship between output voltage and viscosity testing from starting point to stable point in case of dynamic experiment, SAE 15W-40 (0.8 g).

From the time period of the reference to metal particles moving to the permanent magnet, the linear relationship between the output voltage from the Hall Effect sensor on the Y axis and viscosity testing on the X axis as a function of the magnetic field variation is given in Equation 5-5. However, the relationship between the electrical voltage in a third degree polynomial and viscosity testing from a starting point to a stable output point from the sensing module, which is provided by Equation 5-6.

$$y = 9\text{E-}05x + 3.8285 \tag{5-5}$$

$$y = 5\text{E-}07x^3 - 6\text{E-}05x^2 + 0.002x + 3.8085 \tag{5-6}$$

Table 5.3: Average output voltage of Hall Effect sensor from dynamic experiment.

Mass (g)	SAE 15W-40 (V)	SAE 20W-50 (V)	ISO VG 100 (V)
0.1	3.757	3.759	3.758
0.2	3.773	3.774	3.774
0.3	3.787	3.784	3.788
0.4	3.798	3.797	3.799
0.5	3.809	3.806	3.809
0.6	3.815	3.815	3.818
0.7	3.824	3.82	3.825
0.8	3.829	3.828	3.831
0.9	3.836	3.836	3.836
1	3.842	3.838	3.842

5.3.3 Measurement of Lubricant Viscosity

The important causes of industrial machine damages are lubricant deterioration as well as low viscosity based on previous studies [26, 27]. Normally, the lubricant of each machine type should be used in specific period. However, in practice, the lubricant can deteriorate earlier than specific time or the lubricant replacement would be performed improperly for each machine. From previous studies [13, 14], it can be noted that more than 50 percent of lubricant replacement would be performed although the lubricant is still in good conditions that leads to significant business waste. By the way, viscosity characteristics of each lubricant are as shown in Table 5.4 and Table 5.5 [35].

Table 5.4: Lubricant characteristics of SAE 15W-40 and SAE 20W-50.

SAE Viscosity Grade	Low temperature viscosities Cranking (mPa.s) max at temp °C	Pumping (mPa.s) max at temp °C	High temperature viscosities Kinematic (mm^2/s) at 100°C min	max
SAE 15W-40	7000 at -20	60,000 at -25	5.6	-
SAE 20W-50	9500 at -15	60,000 at -20	5.6	-

Table 5.5: Lubricant characteristics of ISO VG 100.

ISO 3348 Viscosity class	Kinematic viscosity at 40 °C [mm^2/s = cSt] Mid-point	Minimum	Maximum
ISO VG 100	100	90	110

5.3.4 Measurement of Contamination in Lubricant

The measurement of contamination was based on the NAS 1638 standard and was performed by counting the number of particles and dividing the level of contamination into 14 degrees starting from NAS 00 to NAS 12. The incremental number of particles in each step of degree was doubled. The level of contamination exceeding level 12 can be determined by using extrapolation 11. Experimental results from the measurement of quantity of metal particles that are contaminated in lubricant will be used for comparison to the NAS 1638 standard in order to guarantee the performance of a sensor module also the reliability of the results from measurement. However, the standard value of NAS 1638 can be determined by measuring cleanliness of the lubricant using particle counter methodology of contaminated in lubricant. It can be divided the size of particles into five levels are 5 µm to 15 µm, 15 µm to 25 µm, 25 µm to 50 µm, 50 µm to 100 µm, and rather than 100 µm per volume for 100 ml of lubricant as shown in Table 5.6.

Table 5.6: Level of contamination in lubricant based on NAS 1638 standard.

Particle size range (µm)	NAS 1638 Classes													
	00	0	1	2	3	4	5	6	7	8	9	10	11	12
5 - 15	125	250	500	1,000	2,000	4,000	8,000	16,000	32,000	64,000	128,000	256,000	512,000	1,024,000
15 - 25	22	44	89	178	356	712	1,425	2,850	5,700	11,400	22,800	45,600	91,200	182,400
25 - 50	4	8	16	32	63	126	253	506	1,012	2,025	4,050	8,100	16,200	32,400
50 - 100	1	2	3	6	11	22	45	90	180	360	720	1,440	2,880	5,760
> 100	0	0	1	1	2	4	8	16	32	64	128	256	512	1,024

Conceptually, an experiment in this study used the methodology of metal particles' weight, which is different from the particle counter method of Zhengduo Pang methodologies

(Zhengduo Pang, 2009) [33]. An experiment of Zhengduo Pang measured the contamination level of metal particles in lubricant of 1,000 ml, as shown in Table 5.7.

Table 5.7: Weight of contamination in lubricant in a case study by Zhengduo Pang, 2009.

Contamination degree (NAS 1638)	12	13	14	15	16	17	18	19	20	21
mg/1,000 ml	50	100	200	400	800	1,600	3,200	6,400	12,820	256,000

Therefore, in order to be comparable to the experiment results of this study, 25 ml of lubricant volume was used. This was calculated by the rule of three in arithmetic function and was presented in Table 5.8.

Table 5.8: Weight of contamination used for measurement.

Contamination degree (NAS 1638)	12	13	14	15	16	17	18	19	20	21
mg/25 ml	1.25	2.5	5	10	20	40	80	160	320	640

However, in this study, it presents the methodology to experiment the ISO VG100 lubricant due to widespread use of this lubricant in industry such as gearbox and also refers to the metal particles contamination when the number of particles exceeds the maximum allowance of L-CKC [35] industrial closed gear oil standard as provided in Table 5.9. Typically, the maximum value for lubricant to be replaced should be 0.5 % or equivalent NAS 18 standard. Therefore, a sensor module used in this study was calibrated by using the weight of contamination starting from NAS 12 onward until the weight of metal particles reaching 1 g.

Table 5.9: L-CKC exchanging standard of industrial closed gear oil (method: SH/T0586).

Item	Exchanging oil Standard
Appearance	Abnormity
Movement viscosity (40°C) rate of change / % >	+15 or -20
Moisture / %	0.5
Mechanical impurities /% ≥	0.5
Copper corrosion (100°C), 3h/degree ≥	3b
Timken OK value /N ≤	133.4

5.4 Lubricant Viscosity and Contamination in Lubricant Analysis

Changing the weight of metal particles for measuring the characteristic of lubricant viscosity was performed in order to determine the weight of appropriate reference metal particles for 25 ml of lubricant in the oil containers and further use the reference weight. Therefore, an experiment in this study will separate the variables for measurement into two cases: the first is the result of an experimental result of lubricant viscosity, and the second is an experiment in contamination in the lubricant.

5.4.1 The Experiment Results of Lubricant Viscosity

An experiment considered in terms of time consumed when the metal particles moved to the permanent magnet of each experimental weight. It was observed that the output voltage from the Hall Effect sensor was smoothly and consistently varied, as shown in Figure 5.20 and 5.21. It can also be noted that the appropriate weights for the experiments ranged from 0.1 g to 1 g due to sharp slope before reaching a stable point. From the detailed analysis, the appropriate reference weights would be 0.6 g and 0.8 g. Therefore, these 2 weight values were further used as a reference for the other lubricant types.

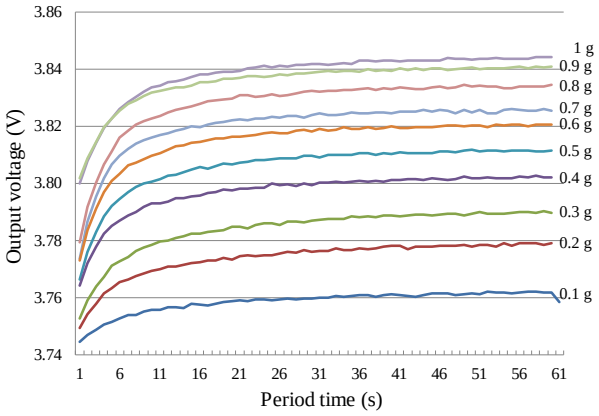

Figure 5.20: Output voltage variation and period time (SAE 20W-50).

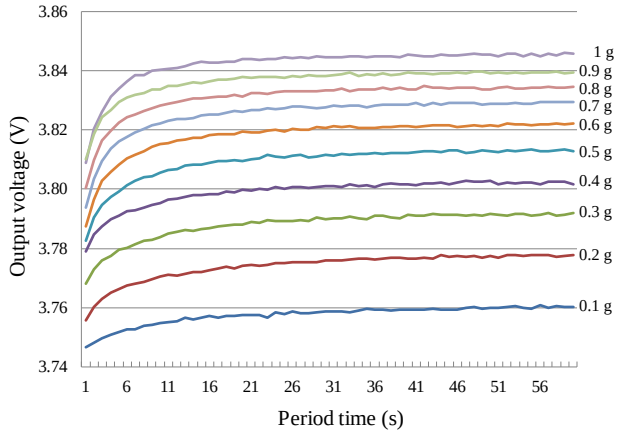

Figure 5.21: Output voltage variation and period time (ISO VG 100).

5.4.2 The Experiment Results of Contamination in Lubricant

In an experimental study of ISO VG 100 lubricant shown in Table 5.10, it can be noted that the variation of output voltage from a Hall Effect sensor can initially be measured as 0.01 g of contamination onward with ± 1 mV of the maximum error, as shown in Figure 5.22. Compared to NAS 15, the system can effectively measure the contamination level for replacement of the lubricant based on the specific standard. However, for NAS 14 downwards, an insignificant variation of output voltage from the Hall Effect sensor was observed or this system could not distinguish the contamination of metal particles lower than NAS 14. A standard variation of the experimental results is presented in Figure 5.23, and it can be noted that a greater number of metal particles would lead to a higher standard deviation. It is because the quantity of particles is greater than the area of the permanent magnet that causes a saturated magnetic field.

Table 5.10: Output voltage of the Hall Effect sensor.

Particles (g)	Output (V)	Particles (g)	Output (V)
0.001	3.737	0.3	3.788
0.002	3.737	0.4	3.799
0.005	3.737	0.5	3.809
0.01	3.739	0.6	3.818
0.02	3.741	0.7	3.825
0.04	3.745	0.8	3.831
0.08	3.752	0.9	3.836
0.1	3.758	1	3.842
0.2	3.774		

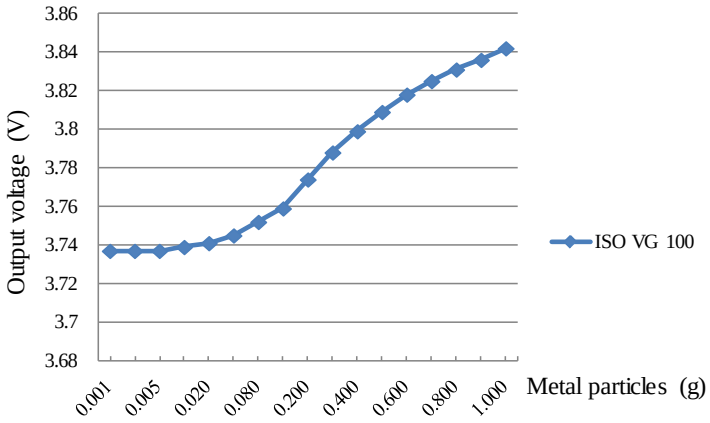

Figure 5.22: Output voltage of Hall Effect sensor corresponding to weigh level.

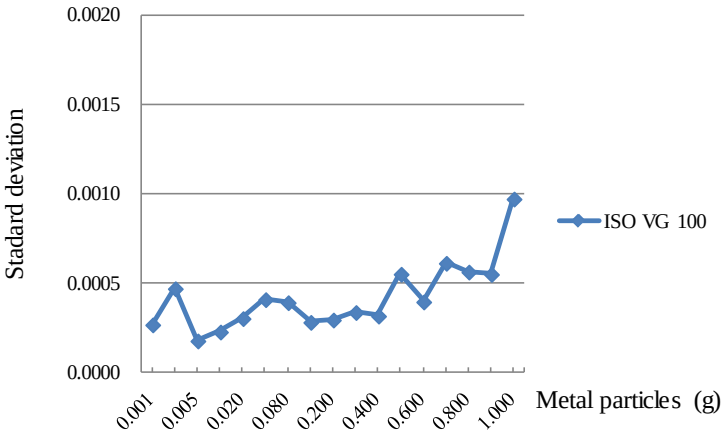

Figure 5.23: Standard deviation of contamination in ISO VG 100.

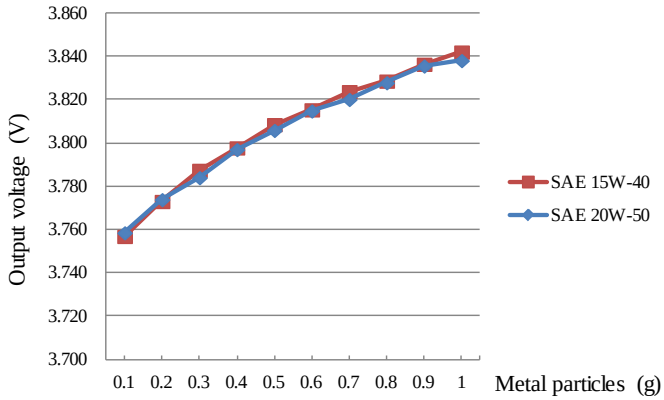

Figure 5.24: Effect of metal particle in contamination standard tests in the case of measuring motor oil SAE 15W-40 and SAE 20W-50.

The same experimental methodology was applied to testing other different lubricant types which are used for engines based on the standards of SAE 15W-40 and SAE 20W-50, as shown in Figure 5.24. From the experiments, it was observed that the conventional Hall Effect sensor could measure the variation of metal particle contamination without limitations on types of lubricant.

5.5 Error Analysis of Lubricant Viscosity and Contamination in Lubricant

In this section, it presents only a case of ISO VG 100 (0.6 g and 0.8 g of weight). The experiment was conducted to observe the relationship of output voltage and viscosity tested. It can be divided the experiment into two sections which were based on the time period of the metal particles moving to the permanent magnet and the time to reach the stable point as shown in Figure 5.25 and 5.26. The developed system can be expressed by the variation in the output voltage using a third degree polynomial as expressed by Equation 5-7 and second degree polynomial as expressed by Equation 5-8, respectively.

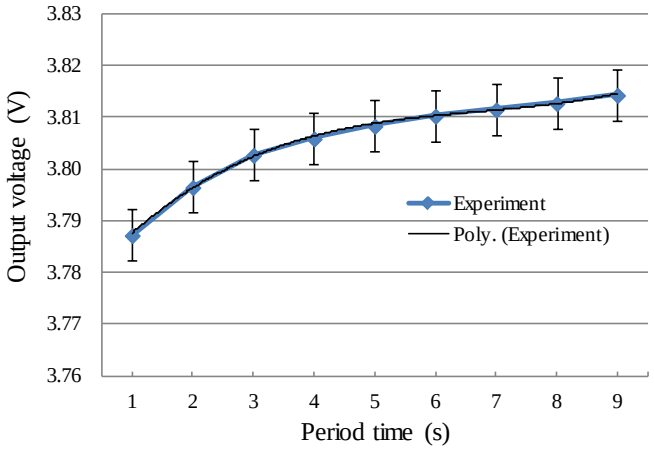

Figure 5.25: Relationship of output voltage and viscosity tested in a third degree polynomial of ISO VG 100 (0.6 g).

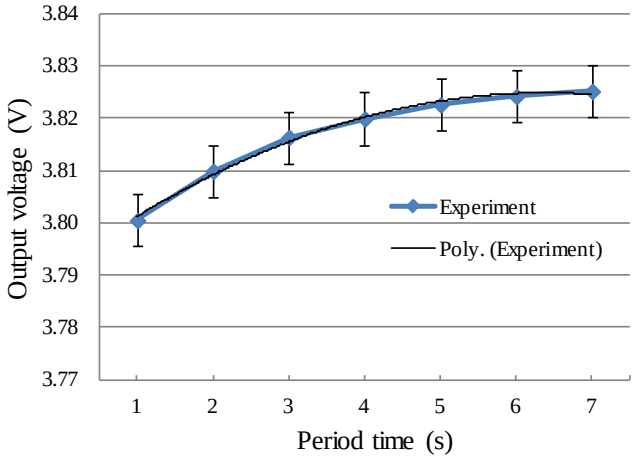

Figure 5.26: Relationship of output voltage and viscosity tested in a second degree polynomial of ISO VG 100 (0.8 g).

$$y = 5E\text{-}05x^3 - 0.0019x^2 + 0.0138x + 3.7755 \quad (5\text{-}7)$$

$$y = -0.0008x^2 + 0.0104x + 3.7916 \quad (5\text{-}8)$$

The linear relationship of the output voltage from the Hall Effect sensor on the Y axis and viscosity testing on the X axis as a function of the magnetic field variation in case of 0.6 g as shown in Figure 5.27 and that in case of 0.8 g as shown in Figure 5.28. The relationship between an electrical voltage in a third degree polynomial and viscosity tested from starting point to stable point generated by a sensor module (0.6 g of metal particles) as shown in Figure 5.29 and that in case of 0.8 of metal particles as shown in Figure 5.30.

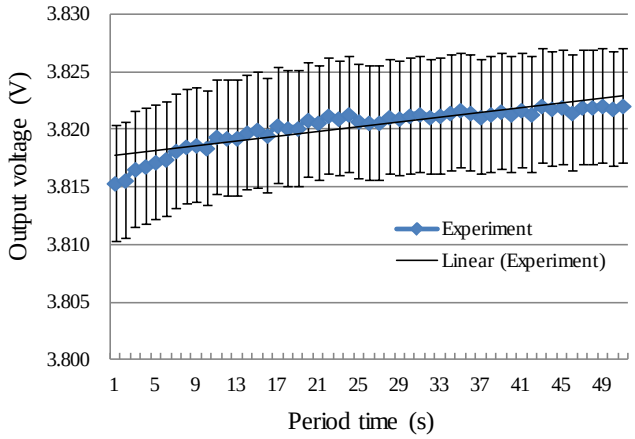

Figure 5.27: Linear relationship of output voltage and viscosity tested at the stable point (0.6 g of metal particles).

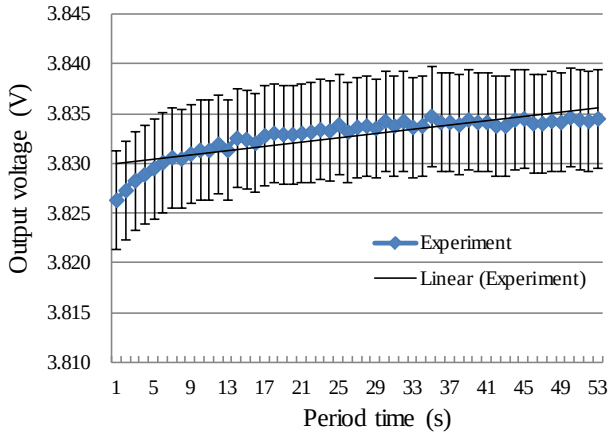

Figure 5.28: Linear relationship of output voltage and viscosity tested at the stable point (0.8 g of metal particles).

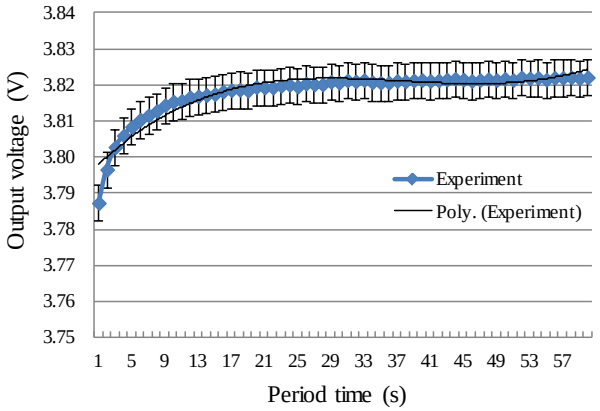

Figure 5.29: Relationship of electrical voltage and viscosity tested in a third degree polynomial (0.6 g of metal particles).

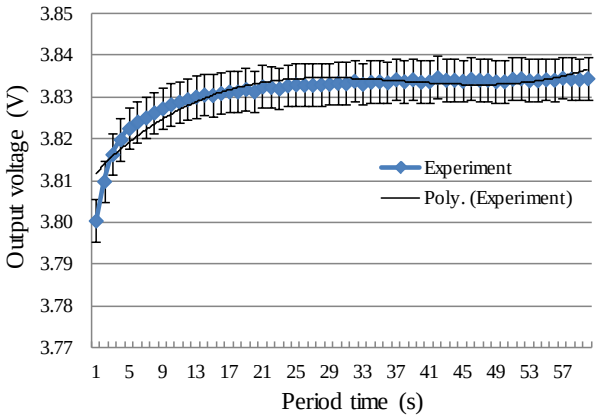

Figure 5.30: Relationship of electrical voltage and viscosity tested in a third degree polynomial (0.8 g of metal particles).

Details of time to stable point, Mean, and Standard deviation [34] at the stable point of those 3 selected lubricant using 0.6 g and 0.8 g of metal particles weight are presented in Table 5.11 and 5.12.

Table 5.11: Mean and standard deviation at the stable point of 0.6 g reference metal particles.

Lubricates grade	Moving time (s)	Mean (V)	Standard deviation
ISO VG 100	10	3.81	0.008
SAE 15W-40	15	3.81	0.007
SAE 20W-50	17	3.8	0.013

Table 5.12: Mean and standard deviation at the stable point of 0.8 g reference metal particles.

Lubricates grade	Moving time (s)	Mean (V)	Standard deviation
ISO VG 100	7	3.817	0.009
SAE 15W-40	10	3.818	0.008
SAE 20W-50	13	3.813	0.014

However, if the reference metal particles weight is higher than 0.9 g, the output voltage from Hall Effect sensor would be not constant. A significant influence on the lowest viscosity of the lubricant is as shown in Figure 5.31. It was found that SAE 15 W-40 exhibited least time consumed to stable point (5 s) followed by ISO VG 100 (6 s) and SAE 20W-50 (12 s), respectively.

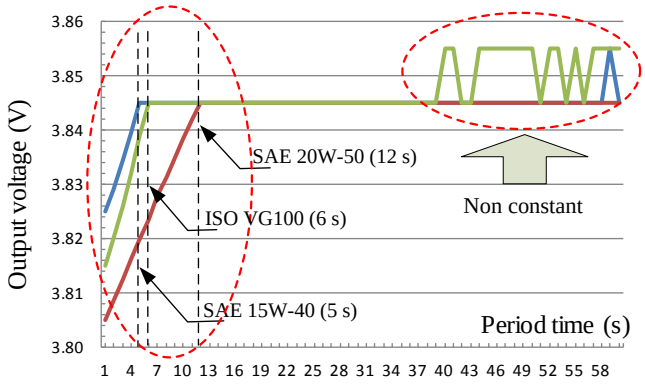

Figure 5.31: Time consumed to stable point for 1 g reference metal particles.

5.6 Conclusion

Lubricant degradation testing based on the magnetic field method using the conventional Hall Effect sensor can be effective and reliable and can be applied to measuring the viscosity of several industrial lubricants and engines. The major benefit of this methodology is the reasonable cost of the sensor as well as the ease of use and installation. Moreover, the output voltage from the developed system was simply managed due to the electrical signal generated. However, in this study, lubricant degradation by considering the contamination in lubricant and viscosity test was performed using a dynamic experiment. Based on the experiments, it was observed that the results were accurate and reliable due to consistent variation from the starting point to a stable output point in the sensing module. The reference metal particles of various mass values were added to the lubricant (25 ml) and then evaluated in order to determine the appropriate mass values to be used for testing. Also, the use of greater reference metal particles was found to exhibit a shorter testing time under the same conditions. As the greater volume of metal particles can cause a greater attractive force, the higher mass of metal particles would exhibit the faster movement of metal particles, which leads to a high tendency for errors in the experiments. However, applying this methodology to other lubricants should be evaluated as well as collecting data for a reliable output voltage conversion, which would then used to analyze the lubricant's viscosity.

Chapter 6

Experiment of Angular Displacement Using A Hall Effect Sensor with Helmholtz Coil

6.1 Introduction

Normally, a Hall Effect sensor can be applied as a sensor to detect and control several variables in the industrial sector. Considering in application of a Hall Effect sensor of each variable would be divided into four sections starting from the design and the development of a sensor module, a design for a signal conditioning circuit for processing, experiments and analysis of the output signal from a Hall Effect sensor, and finally, error analysis caused by measuring. Moreover, this study proposes to enhance the performance of the sensor module by means of appropriate stimulation methodologies of a Hall Effect sensor and also to consider the placement of the Hall generator with Helmholtz coil. The design of a sensor module for applying to measure the angular displacement will proposes in this study. Angular displacement is one of the important variables in industrial processes such as industrial machine alignment and installation and also in civil engineering studies.

6.2 Design the Waveform of Electromagnetic Field

6.2.1 Principle of COMSOL Multiphysics

COMSOL multiphysics is a software environment for simulation and modelling in engineering based on the finite element method (FEM). The finite element method is a method of numerical calculation which is designed to solve differential equations. The finite element method involves separated into sub-parts called ‘elements’, each of which can be connected by nodes, which will then use system control equations to build components of the finite element equation. The optional modules of software were added for the purpose of mechanical, fluid, electromagnetic, and chemical simulations, as well as CAD interoperability [36]. COMSOL multiphysics software version 4.1 was selected, the features of which are shown in Figure 6.1.

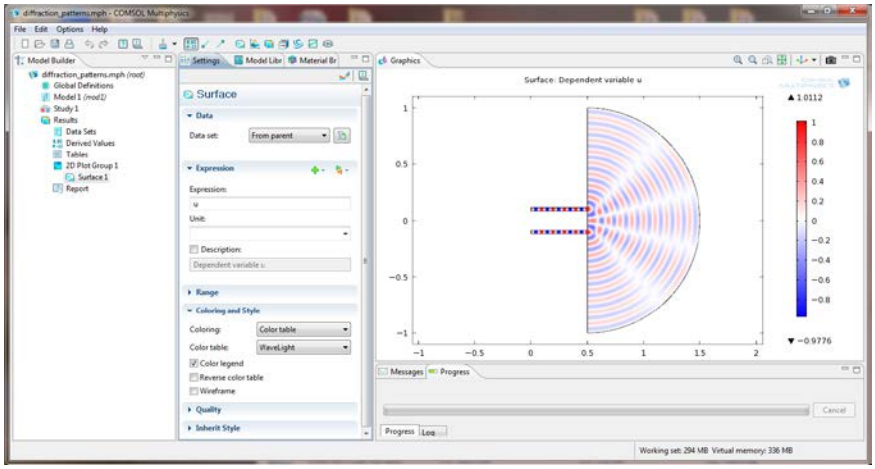

Figure 6.1: Example of wave propagation in diffraction patterns which was calculating by the COMSOL multiphysics.

6.2.2 The Electromagnetic Field Density Calculated by COMSOL Multiphysics

In this study, the waveform of an electromagnetic field was analyzed from the gap of two Helmholtz coils using COMSOL software simulation. The gap of two coils was fixed by 0.8*R* space, *R* space and 1.2*R* of coil space. The results obtained from simulation are as shown in Figure 6.2, 6.3 and 6.4 where Y-axis is the density of the electromagnetic field and X-axis is declination of the shaft within the Helmholtz coil radius.

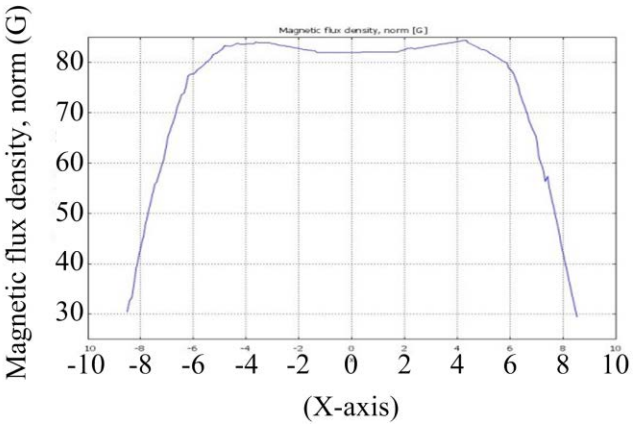

Figure 6.2: The space of two coils was 0.8*R*.

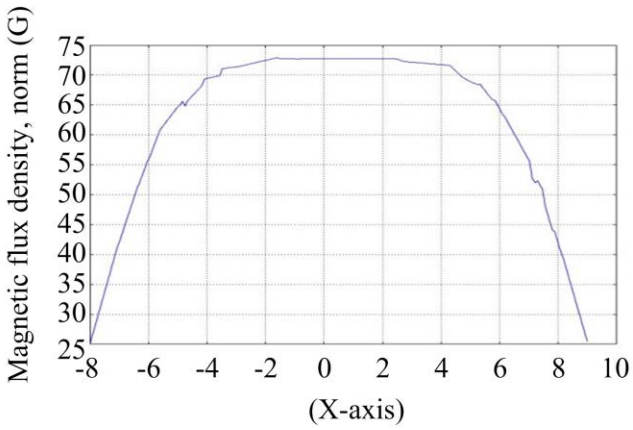

Figure 6.3: The space of two coils was *R*.

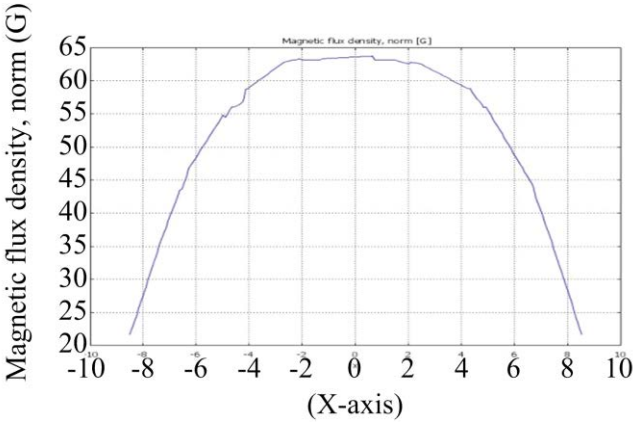

Figure 6.4: The space of two coils was 1.2*R*.

The results from COMSOL simulation at any distance position of the Helmholtz coil under the same condition indicated that coils mounted in parallel at 0.8*R* of space would exhibit the large graph as well as the slope and the width being greater than the deadband. In the case of 1.2*R* space of coils, the graph would be small and the slope would have declined less than the deadband. Considering the *R* space of coils, it can be noted that the relationship between angle and electromagnetic field is well balanced. Therefore, the space of the Helmholtz coils in this study was fixed at *R*.

6.3 Structure of a New Sensor Module

Considering the measurement of angular displacement in this study uses coils, namely Helmholtz coils, for generation into an electromagnetic flux for stimulation of Hall generator. The Helmholtz coil was selected for this study for several reasons. It is standard equipment and the electromagnetic field generated at the centre of two Helmholtz coils was found to be stable as the magnetic flux was distributed from the centre of coil. Furthermore, it was easy to control the density of the magnetic flux and the direction of the magnetic

field. Design principle of Helmholtz coil in this study was considered with reference to the ratio of the wire-turn thickness and radius of Helmholtz coil by 1:5. The cross-sectional area of coil should be square shaped if possible and is similar to the standard Helmholtz coil [37] as shown in Figure 6.5. Therefore, the thickness was 2 cm with a radius of 9.75 cm from 500 turns of 0.9803 mm copper wire (AWG 19 standard), which with this spec can be constructed as a square shape at the cross-sectional area of coil, as shown in Figure 6.6. Figure 6.6 (a) shows completed set of Helmholtz coils, which is available for experiment, and Figure 6.6 (b) shows the installation and alignment of a Helmholtz coil.

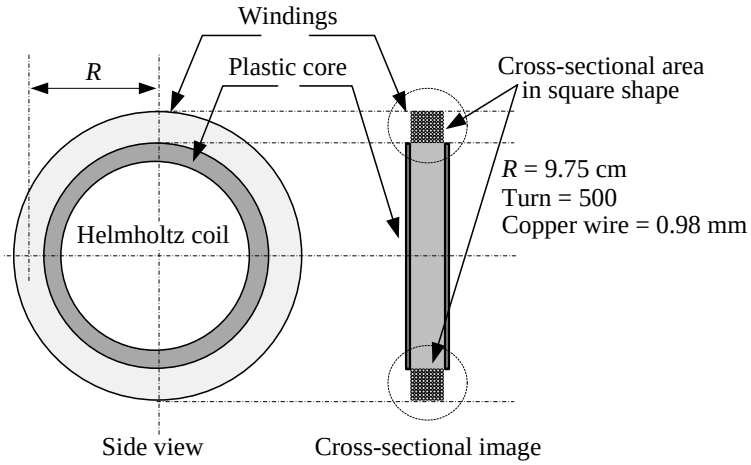

Figure 6.5: The cross-sectional area of coil.

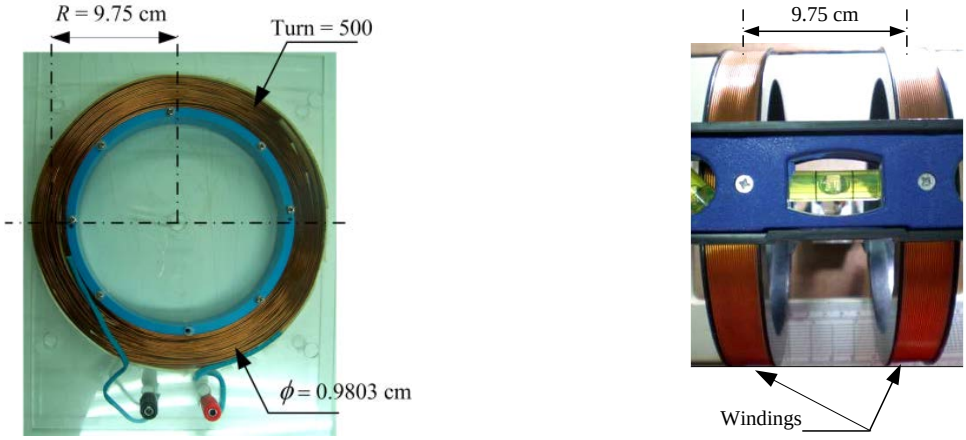

(a) (b)

Figure 6.6: Structure of the Helmholtz coils used for generated electromagnetic field;
(a) Completed set of Helmholtz coils;
(b) Installation and alignment of Helmholtz coil.

The system developed for analysis of shaft declination consists of two Helmholtz coils with radius of 9.75 cm, placed at the structure of 8 mm-thick acrylic plates with the shaft length of 30 cm. The reference scale perpendicularly placed on the 5 cm-thick acrylic rod for adjusting the declined angle in experiment, and the reference scale used for measuring an accuracy of angular displacement in each degree of shaft. To detect the electromagnetic field density in any position within Helmholtz coil radius, the sensor namely Hall generator was placed at the center between two Helmholtz coils as shown in Figure 6.7.

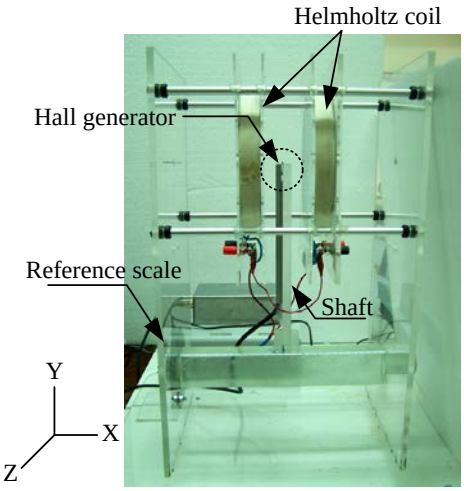

Figure 6.7: Hall generator position at the center between two Helmholtz coils.

6.4 Experimental Conditions of New Sensor Module in Angular Displacement

An experiment was conducted on a new sensor module in order to consider the performance of the system was divided in two parts: the first involved measuring every angle by shaft declination on an X-axis. The Hall generator was placed at the top of shaft between two Helmholtz coils. The second part involved testing the sensor module, the signal conditioning and overall system, as shown in Figure 6.8. The performance testing of measurement system was conducted in order to analyze the output signal from sensor module when the angle of shaft starts declination away from the centre of the Helmholtz coils on X-axis in the range of -15 to 15 deg, with 1 deg of resolution per step as shown in Figure 6.9.

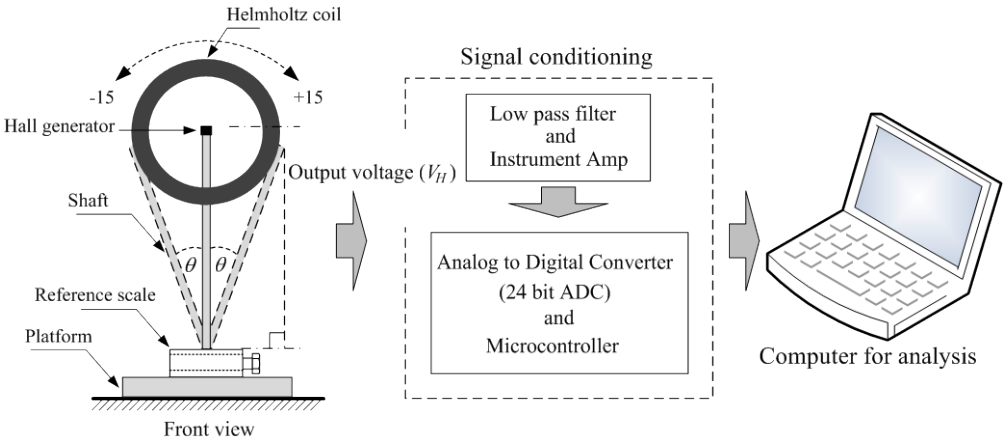

Figure 6.8: Diagram of overall system.

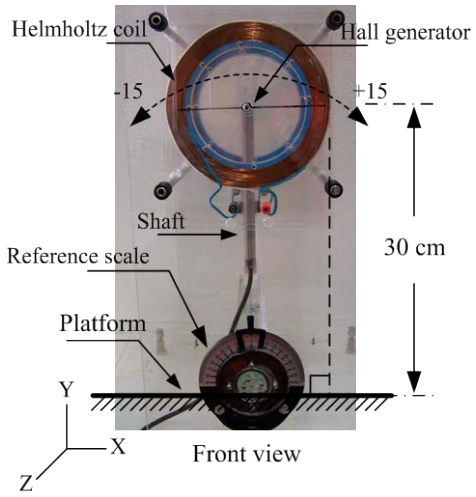

Figure 6.9: Shaft declination on X-axis.

Therefore, the components of system needed to be tested in order to obtain the high performance and reliability as follows:

6.4.1 Current Supplied Constant

The electromagnetic field was generated by applying a 1 A constant current to the Helmholtz coil, while the testing of the measurement system was performed by varying the resistance (load) between 10 Ω, 15 Ω, and 20 Ω in order to test the ability of power supply to supply a constant current.

6.4.2 Sensitivity of Hall Generator

Sensitivity testing of the Hall generator was performed by changing the value of the input power supply of the generator at different levels of voltage according to values specified as 4.5 V, 5 V, and 5.5 V. The angle of shaft declination away from the X-axis direction varied

by 1 degree per step in order to consider the response of the output signal from Hall generator.

6.4.3 Database System in a Digital Signal Pattern

A test on the database system in a digital signal pattern was performed by five point test methodologies in a measured range using reference voltage which also had different levels from 0 V to 5 V, and which was then converted to percentages between 0 % and 100 % in order to determine the accuracy and reliability of the conversion process between analog and digital signals, the details of which are shown in Table 6.1.

Table 6.1: Data conversion process to determine the accurate and reliability of a database system.

Data converting	Range of measurement				
Reference voltage (V)	0	1.25	2.5	3.75	5
Percentage (%)	0	25	50	75	100

6.4.4 Testing of a Helmholtz coil

The testing considered the density of electromagnetic field at the centre of coils using a Tesla meter (PHYWE) with the resolution of 1 mT. The measured results were then being taken to be compared with the results from calculated using Equation 4-6.

Variability of the output voltage from the sensor module was then considered. There is a relation between a density of electromagnetic field generated by applying 1 A current into the Helmholtz coil and the output voltage from the sensor module.

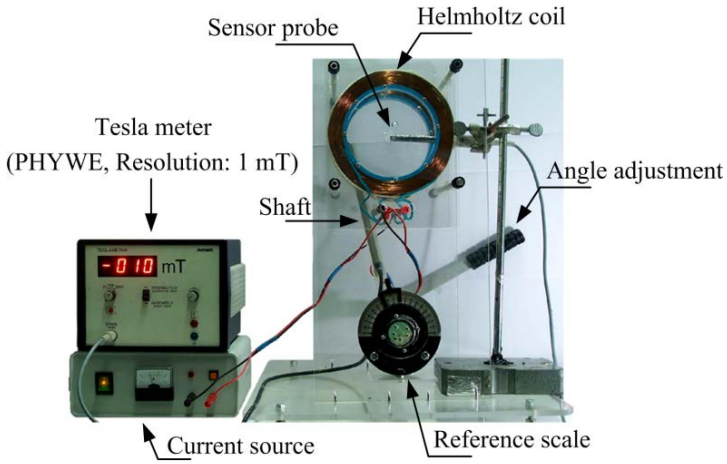

Figure 6.10: Reference point for installation of the Hall generator.

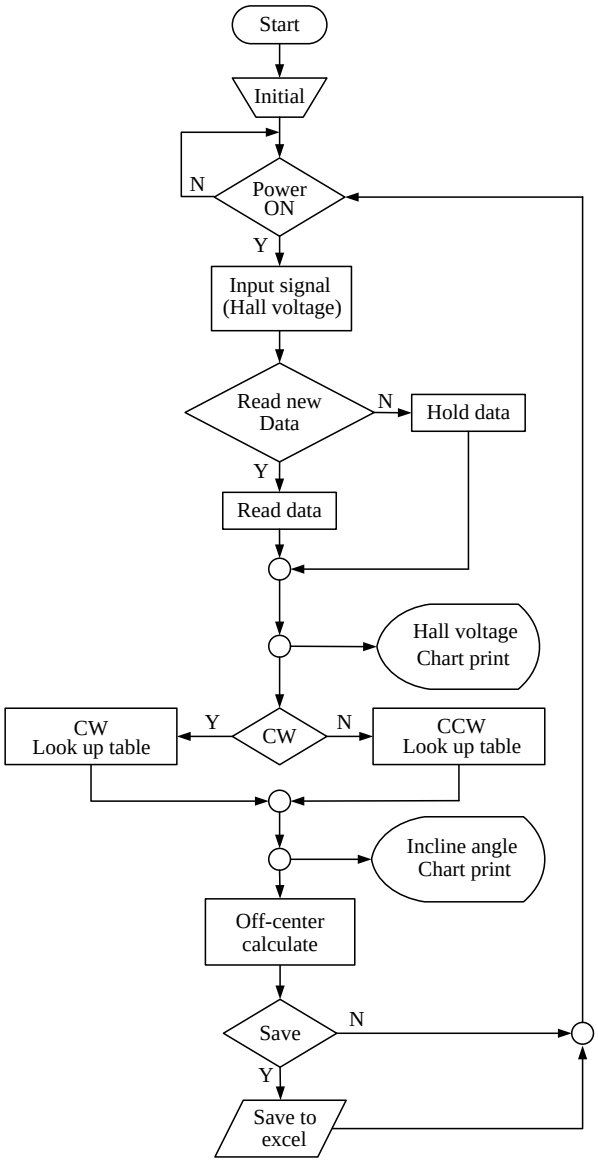

Figure 6.11: Flowchart of processing in shaft declination analysis.

The density of the electromagnetic field generated by the Helmholtz coil can be measured using Tesla meter (PHYWE) with the resolution of 1 mT at the reference position (0 deg). A probe was installed at the center of Helmholtz coil and the constant current of 1 A was provided for generating electromagnetic field with the density of 4.624 mT (from calculation). From experiment, the density of electromagnetic field measured at the center of the Helmholtz coil was 5 mT after compensating an error. The discrepancy from analysis was 0.376 mT (7.52 %) that would be caused by the resolution of the Tesla meter used as shown in Figure 6.10. Output voltages from the sensor module were also available for real time collection and display via the computer. Data were sent to a computer for analysis and processing through LabVIEW software, as shown the flowchart in Figure 6.11.

6.5 Angular Analysis

Analysis of the shaft declination angle was based on trigonometric functions. The system developed was designed for the shaft to be declined on an X-axis in both (+) and (-) directions, ranging from 0 to ±15 deg (normal to Y-axis) with 1 deg resolution per step. To analyze the density of the electromagnetic field at any position within the Helmholtz coil radius, the shaft was angularly moved on the X-axis, starting from the reference point (0 deg) clockwise (CW) until it reached 15 deg, as shown in Figure 6.12. The results were presented in output voltage which varied in terms of the current flowing through the Hall generator, depending on electromagnetic field density. However, the output voltage of the sensor module was also dependent on the density and direction of the magnetic field which varied from 0 deg to 15 deg, as well as the relationship between the output voltage from a sensor module, the angular positions of the shaft with a declination on the X-axis, and magnetic field density in a clockwise condition as illustrated in Table 6.2.

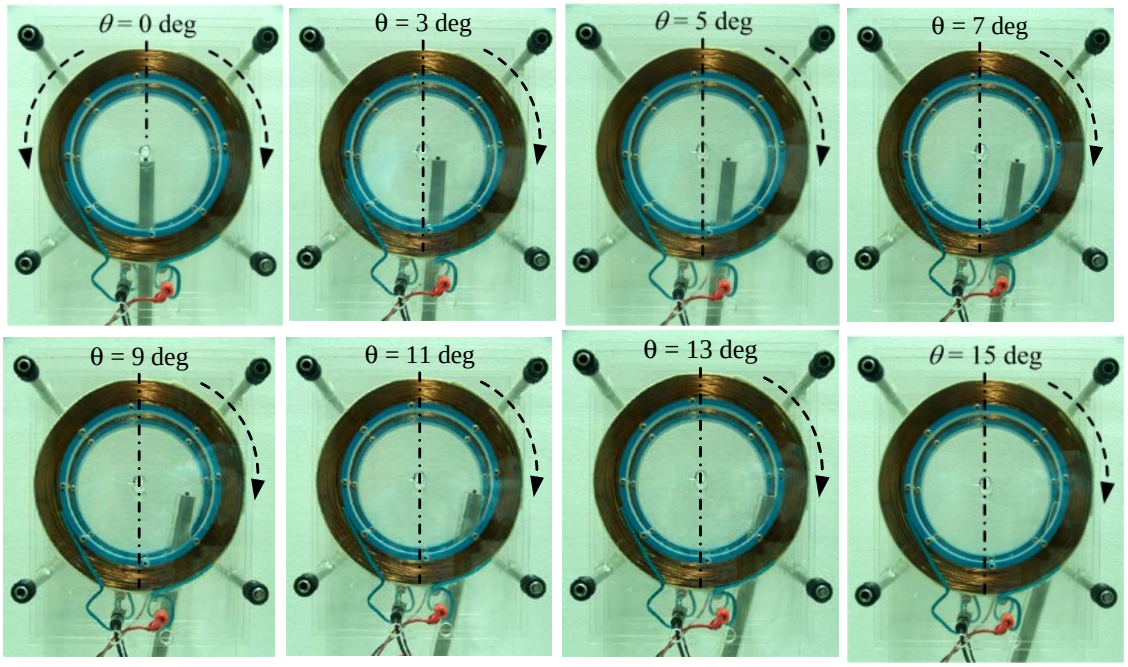

Figure 6.12: Shaft declination by step varying from 0 to +15 deg in clockwise.

Table 6.2: The relationship between the output voltage, the angular positions of shaft with declination on X-axis, and magnetic field density in condition of clockwise.

Angle (deg)	Output voltage (V)	Magnetic fields density (mT)	Angle (deg)	Output voltage (V)	Magnetic field density (mT)
0	2.77	4.99	8	2.759	4.594
1	2.77	4.988	9	2.753	4.351
2	2.769	4.978	10	2.746	4.084
3	2.769	4.963	11	2.732	3.522
4	2.769	4.945	12	2.717	2.956
5	2.768	4.911	13	2.699	2.276
6	2.766	4.838	14	2.67	1.156
7	2.763	4.738	15	2.646	0.240

Figure 6.13 shows the shaft declination on X-axis from the centre of a Helmholtz coil in a counter clockwise (CCW) direction. The output voltage of the sensor module was also dependent on the density and direction of magnetic field which varied from 0 deg to -15 deg similar to that of clockwise direction. Therefore the relationship between the output voltages from a sensor module, the angular positions of shaft with declination on X-axis, and magnetic field density in condition of counter clockwise as illustrated in Table 6.3.

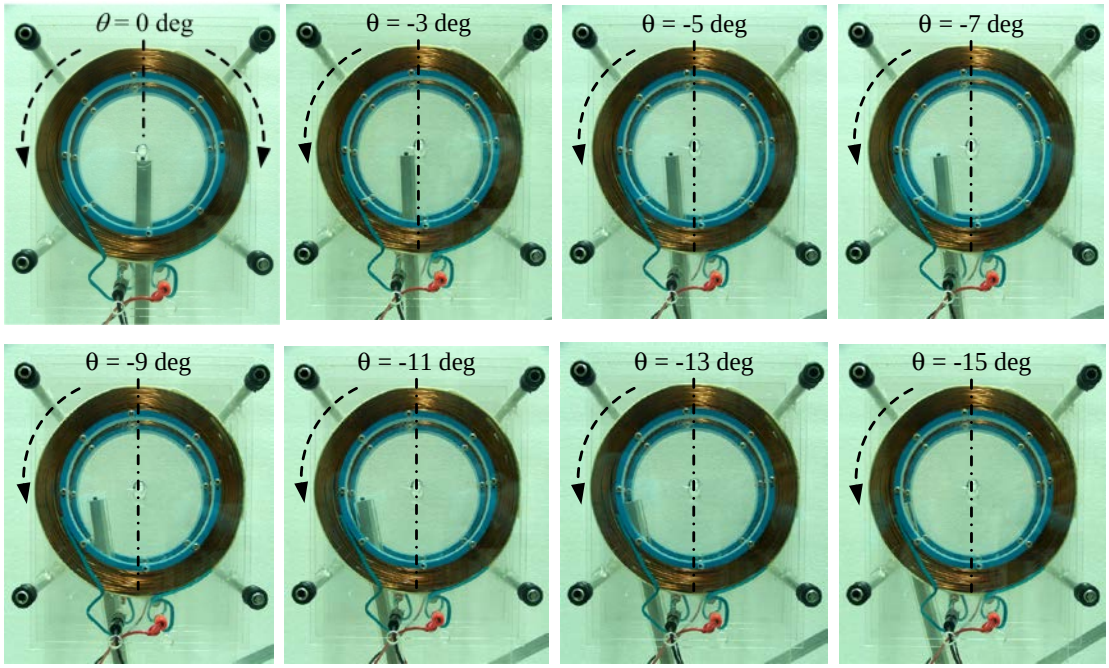

Figure 6.13: Shaft declination by step varying from 0 to -15 deg in counterclockwise.

Table 6.3: The relationship between the output voltage, the angular positions of shaft with declination on X-axis, and magnetic field density in condition of counterclockwise.

Angle (deg)	Output voltage (V)	Magnetic fields density (mT)	Angle (deg)	Output voltage (V)	Magnetic field density (mT)
0	2.77	4.99	-8	2.763	4.719
-1	2.77	4.998	-9	2.758	4.53
-2	2.77	4.998	-10	2.75	4.225
-3	2.77	4.996	-11	2.74	3.838
-4	2.77	4.986	-12	2.727	3.345
-5	2.769	4.964	-13	2.707	2.585
-6	2.768	4.919	-14	2.688	1.851
-7	2.766	4.859	-15	2.65	0.388

Moreover, when considering the relationship between magnetic field density and the angular declination of shaft by comparing clockwise and counter clockwise directions, it can be observed that the results from measurement would be agreeable in both directions, as illustrated in Figure 6.14. When considering the relationship between the output voltage from a sensor module and the magnetic field density by comparing between the direction of clockwise and counter clockwise of shaft declination on X-axis, it can be noted that the results of measurement can also provide the best linearity of both directions, as shown in Figure 6.15.

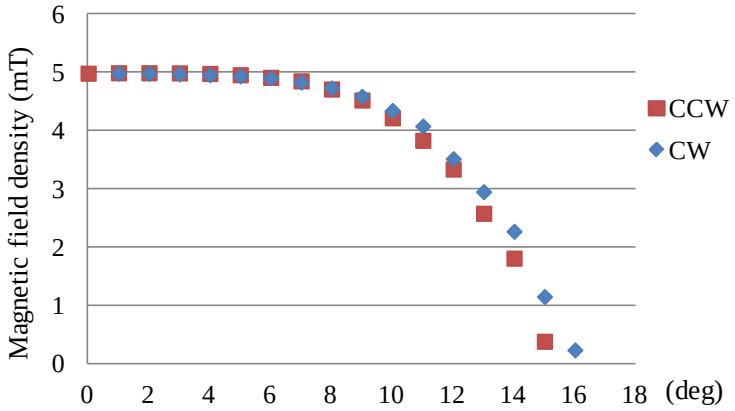

Figure 6.14: Relationship between the magnetic field density and the angular declination of shaft by comparing between the direction of clockwise and counter clockwise.

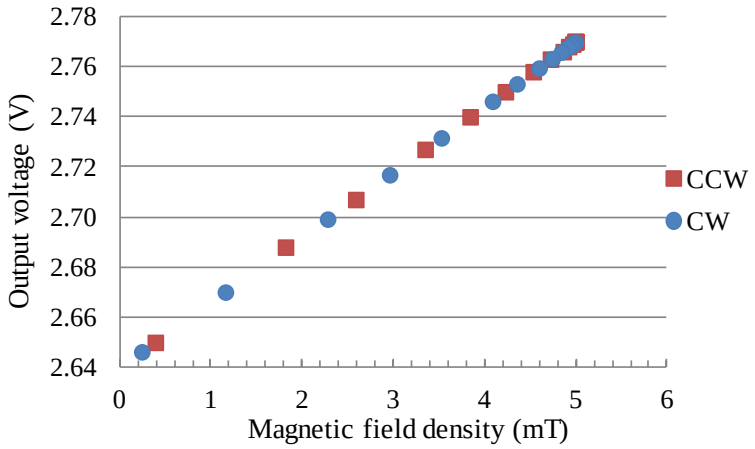

Figure 6.15: Relationship between the output voltage from a sensor module and magnetic field density by comparing between the direction of clockwise and counter clockwise.

Experimental results can be used for analysis of the relationship of output voltage from sensor module and electromagnetic field density within the Helmholtz coil radius on X-axis as showing the graph in Figure 6.16. The results agree well to the results from calculation using COMSOL software simulation. The gap between two coils of Helmholtz coils was equal to *R*.

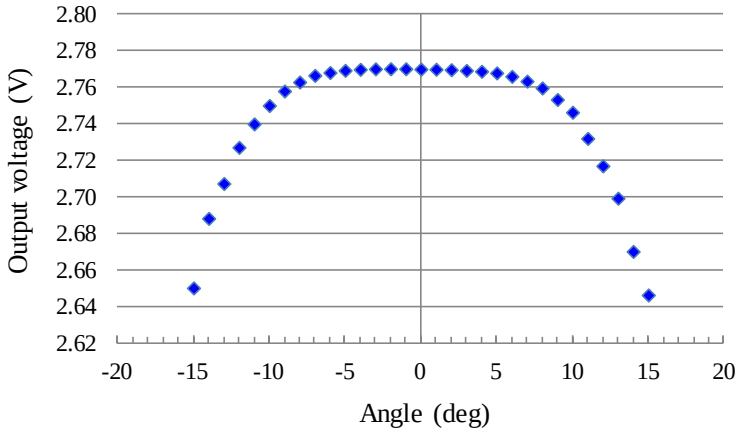

Figure 6.16: Relationship between output voltage from the sensor module and electromagnetic field density.

Furthermore, the performance testing of the Hall generator which is a component of sensor module, in order to enhance the reliability of the conventional Hall Effect sensor and the signal conditioning system would be performed by measuring the variation of angle when the shaft was angularly moved on the X-axis, starting from the reference point (0 deg, at the

centre of Helmholtz coil) in a clockwise direction until it is +15 deg and from the reference point in a counter clockwise direction until it reaches -15 deg with 1 deg resolution per step under the same conditions. Then the output voltage of sensor module would be converted to a digital signal before being transferring to a microcontroller for processing and comparison to the standard values, as shown in Table 6.4. It can be noted that using the Helmholtz coils for generating an electromagnetic field for sensor module exhibited the results with high accuracy and reliability at every angle in the range between - 15 deg to 15 deg, except the range of -3 deg to 2 deg at the centre area of Helmholtz coils.

Table 6.4: Comparison of experiment results and reference standard on inclined angle in the range of -15 to 15 deg.

Angle (deg)		Angle (deg)	
Actual	Measurement	Actual	Measurement
-15	-15	1	0
-14	-14	2	1
-13	-13	3	3
-12	-12	4	4
-11	-11	5	5
-10	-10	6	6
-9	-9	7	7
-8	-8	8	8
-7	-7	9	9
-6	-6	10	10
-5	-5	11	11
-4	-4	12	12
-3	0	13	13
-2	-3	14	14
-1	0	15	15
0	0		

Table 6.5: Analysis of experiment results compared to standard value from calculation based on trigonometric functions.

Angle	Calculation value			Measurement value		
(deg)	$\sin\theta$	D	X	$\sin\theta$	D	X
-15	0.259	7.932	-7.864	0.259	7.932	-7.864
-14	0.242	7.406	-7.35	0.242	7.406	-7.35
-13	0.225	6.879	-6.835	0.225	6.879	-6.835
-12	0.208	6.352	-6.317	0.208	6.352	-6.317
-11	0.191	5.824	-5.797	0.191	5.824	-5.797
-10	0.174	5.296	-5.276	0.174	5.296	-5.276
-9	0.156	4.768	-4.753	0.156	4.768	-4.753
-8	0.139	4.239	-4.228	0.139	4.239	-4.228
-7	0.122	3.71	-3.703	0.122	3.71	-3.703
-6	0.105	3.18	-3.176	0.105	3.18	-3.176
-5	0.087	2.651	-2.648	0.087	2.651	-2.648
-4	0.07	2.121	-2.119	0.07	2.121	-2.119
-3	0.052	1.591	-1.59	0.052	1.591	-1.59
-2	0.035	1.061	-1.06	0.035	1.061	-1.06
-1	0.017	0.53	-0.53	0.017	0.53	-0.53
0	0	0	0	0	0	0
1	0.017	0.530	0.53	0.017	0.53	0.53
2	0.035	1.061	1.06	0.035	1.06	1.06
3	0.052	1.591	1.59	0.052	1.591	1.59
4	0.07	2.121	2.119	0.07	2.121	2.119
5	0.087	2.651	2.648	0.087	2.651	2.648
6	0.105	3.18	3.176	0.105	3.18	3.176
7	0.122	3.71	3.703	0.122	3.71	3.703
8	0.139	4.239	4.228	0.139	4.239	4.228
9	0.156	4.768	4.753	0.156	4.768	4.753
10	0.174	5.296	5.276	0.174	5.296	5.276
11	0.191	5.824	5.797	0.191	5.824	5.797
12	0.208	6.352	6.317	0.208	6.352	6.317
13	0.225	6.879	6.835	0.225	6.879	6.835
14	0.242	7.406	7.35	0.242	7.406	7.35
15	0.259	7.932	7.864	0.259	7.932	7.864

The analysis of the experiment results by considering the relationship between of output voltage from sensor module used the Hall generator as a sensor device and the Helmholtz coil was used to generated the electromagnetic field to stimulate of the conventional Hall Effect sensor based on principle of trigonometric functions in order to determine the variation of angle when the shaft declination on X-axis within the Helmholtz coil radius consisted of $\sin\theta$, D distance, and X distance, as shown in Table 6.5.

Conclusively, the output voltage of the sensor module can be used for analyzing the angles of sine, cosine, and tangent of the trigonometric functions as well as the length of triangle. The results from experiment and also the range of deadband agreed well to those from calculation. Angular positions of shaft with declination on X-axis are as shown in Figure 6.17 - 6.19.

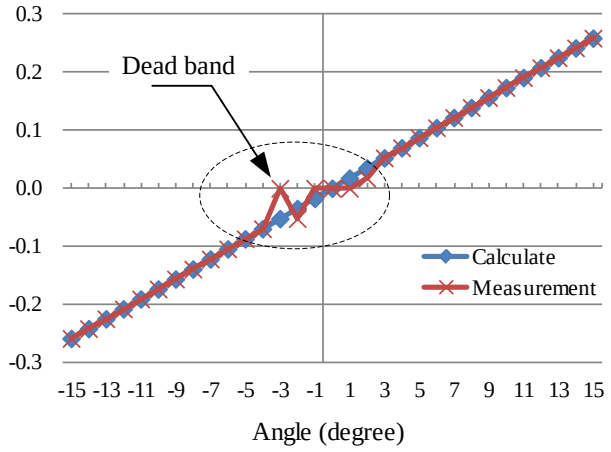

Figure 6.17: Comparison of sine from experiment and calculation.

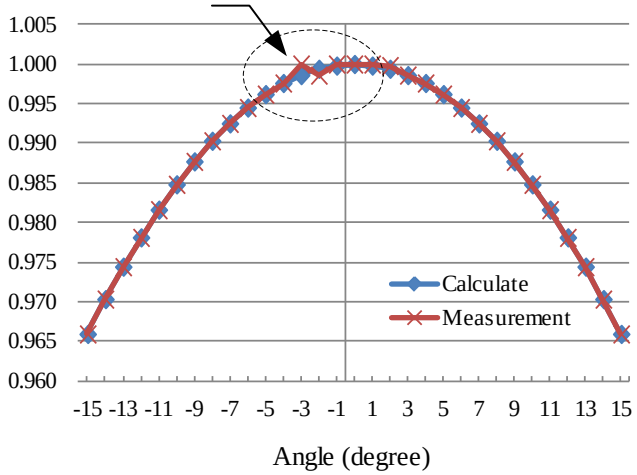

Figure 6.18: Comparison of cosine from experiment and calculation.

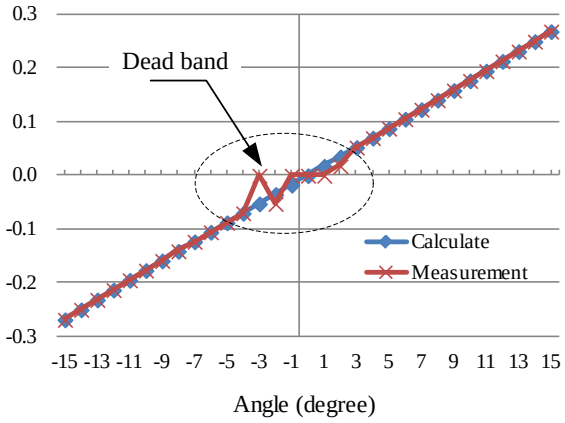

Figure 6.19: Comparison of tangent from experiment and calculation.

6.6 Error Analysis of Angular Measurement

Error analysis of results from measurement is important and necessary to establish the reliability of a measurement system and how successfully sensor module has been designed and developed. Error analysis was performed by repeatedly measuring in order to consider the repeatability of sensor module, and then the results from measurement were analyzed for accuracy, standard deviation, and the uncertainty of the system. The performance of the conventional Hall Effect sensor as a sensor device for measurement of angular declination was analysed by using data in a digital signal pattern, through a five point test which took 15 measurements times in order to test the repeatability of the measurement system. This means that the measurements of the voltage signal which was generated from the power supply in different levels were 0 %, 25 %, 50 %, 75 % and 100 % of 5 V. From these results, it was found that the maximum value of the voltage signal at 100 % was about 4.997 V, as shown in Table 6.6.

Table 6.6: Test of repeatability of measurement system by measuring the electrical voltage using a five point test.

Times	Range of measurement (%)				
number	0	25	50	75	100
1	0	1.256	2.487	3.734	4.997
2	0	1.256	2.487	3.734	4.997
3	0	1.256	2.487	3.734	4.997
4	0	1.256	2.487	3.734	4.997
5	0	1.256	2.487	3.734	4.997
6	0	1.256	2.487	3.734	4.997

Table 6.6: (cont'd)

Times number	Range of measurement (%)				
	0	25	50	75	100
7	0	1.256	2.487	3.734	4.997
8	0	1.256	2.487	3.734	4.997
9	0	1.256	2.487	3.734	4.997
10	0	1.256	2.487	3.734	4.997

The repeatability of sensor module was uncertain after measuring. Therefore, the results are obtained from test for repeated measurement could be calculated in order to consider the reliability of the measurement system's accuracy while standard deviations [34] were all within range, as shown in Table 6.7.

Table 6.7: Mean, standard deviation, and accuracy for five point test.

Characteristics	Range of measurement (%)				
	0	25	50	75	100
Voltage average (V)	0	1.256	2.487	3.734	4.997
Actual voltage (V)	0	1.256	2.487	3.735	4.997
Standard deviation	0	0	0	0	0
Accuracy (%)	0.008	0	0.002	0.011	0.007

Previous five point tests found that the percentage of maximum error was about 0.01123 % in the level of 75 % of the range, and the results were then compared to standard deviation from sensor module and signal conditioning system. It can be noted that the output voltage of the sensor was given the maximum deviation of about 0.000561 V at the level of 75 % of range, as shown in Figure 6.20. Therefore, this would guarantee the ability of the conventional Hall Effect sensor and signal conditioning system, which could be applied as a sensor to detect several variables in the industrial sector due to its accuracy and reliability.

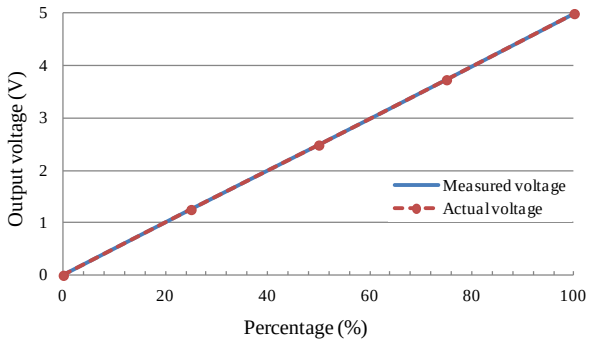

Figure 6.20: Error analysis in comparison of real voltage and measurement.

In experimental study, accuracy, precision, and reliability were analyzed by considering the average value, standard deviation and experimental uncertainty. In analysis of the Hall Effect sensor output voltage, it can be observed that the declination of the shaft at any position within the Helmholtz coil radius would exhibit the best accuracy and reliability of 95 %. The maximum error was at -3 deg or equal to 0.735 as shown in Table 6.8.

Table 6.8: Error analysis in the range of -15 to 15 deg with 1 degree of resolution per step.

Angle (deg)						Characteristics		
Actual	Measurement					Average value	Standard deviation	Uncertainty
	1	2	3	4	5			
-15	-15	-15	-15	-15	-15	-15	0	0
-14	-14	-14	-14	-14	-14	-14	0	0
-13	-13	-13	-13	-13	-13	-13	0	0
-12	-12	-12	-12	-12	-12	-12	0	0
-11	-11	-11	-11	-11	-11	-11	0	0
-10	-10	-10	-10	-10	-10	-10	0	0
-9	-9	-9	-9	-9	-9	-9	0	0
-8	-8	-8	-8	-8	-8	-8	0	0
-7	-7	-7	-7	-7	-7	-7	0	0
-6	-6	-6	-6	-6	-6	-6	0	0
-5	-5	-5	-5	-5	-5	-5	0	0
-4	-4	-4	-4	-4	-4	-4	0	0
-3	-3	-4	-3	-4	0	-2.8	1.643	0.735
-2	0	-2	-4	-3	-3	-2.4	1.517	0.678
-1	-3	-3	-4	-3	0	-2.6	1.517	0.678
0	0	0	0	0	0	0	0	0
1	0	0	0	0	0	0	0	0
2	0	1	1	1	1	0.8	0.447	0.2
3	3	3	3	3	3	3	0	0
4	4	4	4	4	4	4	0	0
5	5	5	5	5	5	5	0	0
6	6	6	6	6	6	6	0	0
7	7	7	7	7	7	7	0	0
8	8	8	8	8	8	8	0	0
9	9	9	9	9	9	9	0	0
10	10	10	10	10	10	10	0	0
11	11	11	11	11	11	11	0	0

Table 6.8: (cont'd)

Angle (deg)						Characteristics		
Actual	Measurement					Average value	Standard deviation	Uncertainty
	1	2	3	4	5			
12	12	12	12	12	12	12	0	0
13	13	13	13	13	13	13	0	0
14	14	14	14	14	14	14	0	0
15	15	15	15	15	15	15	0	0

6.7 Conclusion

This study proposed that as conventional Hall Effect sensor with Helmholtz coils could be used as a sensor module for analyzing the relationship between trigonometric functions in terms of angle and the remaining length of a triangle. Stimulation of the conventional Hall Effect sensor in this case used an electromagnetic field generated by Helmholtz coil. An electromagnetic field generated at the centre of coil was found to be stable and magnetic flux was distributed from the centre of Helmholtz coil. Therefore, in this position the maximum value of output voltage from a sensor module was exhibited. On the other hand, when the angle of the shaft declined away from the centre of Helmholtz coils, then the output voltage of a sensor module also decreased. Thus, the distance and angular movement of a shaft can be calculated with reference to the output voltage of sensor module, using this algorithm. Moreover, it can be observed that the sensor module can distinguish the resolution of an angle in the range of -4 deg to -15 deg in a counter clockwise direction and the range of 3 deg to 15 deg in a clockwise direction with 1 deg of resolution per step. In case of the range between -3 deg to 2 deg, the measurement system could not exhibit the measured stability due to the small difference of output voltage at any angle from sensor module in this area. Instability in this range was caused by the hysteresis of magnetic flux having a high density at the centre area of Helmholtz coils. This zone is the deadband of measurement.

Chapter 7

Experiment of Angular Displacement Using The Two Flat-Curve Permanent Magnets

7.1 Introduction

An industrial production line is one of the most important processes as it is dependent on the quality of products from the manufacturing process. Therefore, the machines used in this process should provide good performance. Proper alignment of the industrial machines and building construction to prevent ground subsidence needs to be prepared. However, the most common problem would be an error in machine operation caused by the level of land subsidence in the areas where a number of large and heavy-load machines had been used. Generally, the angle can be measured by using several methodologies [16-18]. Angular measurement based on a magnetic field method using the conventional Hall Effect sensor was the alternative methodology used to measure and monitor land subsidence. The measured results were obtained in electrical voltage form from the conventional Hall Effect sensor and then transmitted to a computer for real time monitoring and in order to maintain the appropriate position of the machines.

7.2 The Magnetic Field Density Calculated by COMSOL Multiphysics

Improvement of a sensor module using a flat-curve permanent magnet as a stimulator device of the conventional Hall Effect sensor began with the analysis of magnetic flux density and also the direction of magnetic flux distribution by calculation using COMSOL multiphysics simulation [36]. From the empirical experiment, the direction of magnetic flux distribution of two rectangular permanent magnets and direction of magnetic flux in Y-axis was selected to making a sensor module in this study.

To define the permanent magnet shape for generating the magnetic field, COMSOL software simulation was adopted. The permanent magnets were then positioned to generate a magnetic flux in the direction of the Y-axis. Two sets of four magnetic domains (one set

consists of two domains) were placed alternately in poles as shown in Figure 7.1. The appropriate gap of two permanent magnets was fixed at 12 mm, which was half the length of the outer radius of permanent magnet (24 mm). The results obtained from simulation are as shown in Figure 7.2 where Y-axis is the density of the magnetic field and X-axis is the inclination angle within the permanent magnet radius.

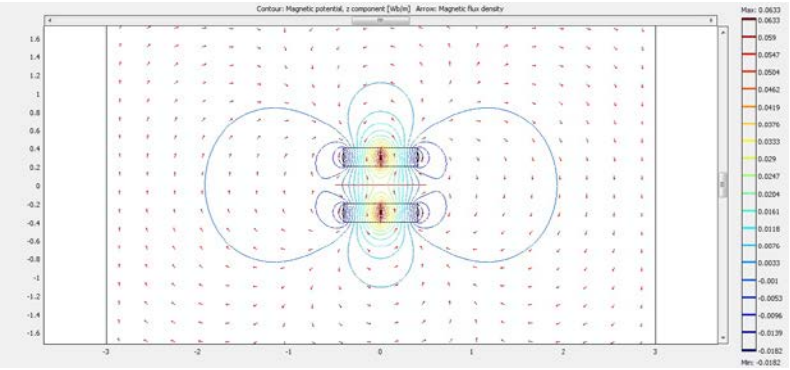

Figure 7.1: Magnetic flux in Y-axis of two rectangular permanent magnets using COMSOL multiphysics simulation.

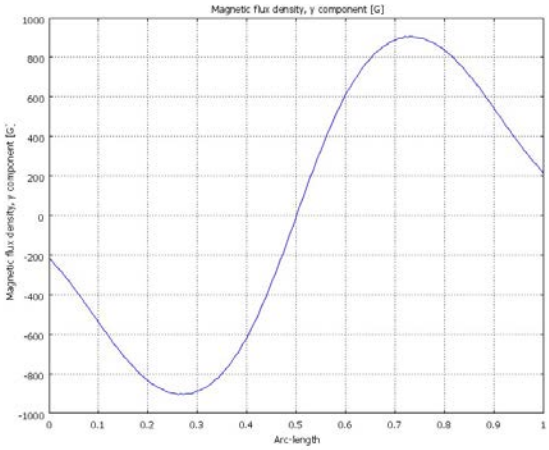

Figure 7.2: Waveform of magnetic field density in Y-axis of two rectangular permanent magnets calculated by COMSOL multiphysics.

However, the usability of two permanent magnets to enhance the density of magnetic flux for doubling intensity would not be side-effects of the variation of measuring range. Therefore, two flat-curve permanent magnets were selected for this study. The magnets were then positioned to generate a magnetic flux in the direction of the Y-axis as components of a sensor module for experimental purposes so that a reasonable cost could be maintained and so that it would still be readily available.

7.3 Shape and Dimension of Permanent Magnet

This section describes selecting the shape and dimension of a magnet so it would be suitable assembling as a sensor module in order to measure the variables in various angular patterns. Testing the performance of magnets would involve considering the properties by making comparisons between the rectangular permanent magnet and the curve permanent magnet. From the empirical experiment, it was found that the permanent magnet in kind of curve can be provided the widest range of measurement better than the magnet in kind of rectangle. However, the permanent magnet in the curve, known as a flat-curve permanent magnet, was selected to assembling as a sensor module in this study.

7.3.1 Performance of Rectangular Permanent Magnet

An experiment to consider the response of the output voltage of the conventional Hall Effect sensor consists of the Hall generator and a rectangular permanent magnet which were installed together. The Hall generator was placed at the centre between the S pole and N pole of a rectangular permanent magnet and was perpendicular to the X-axis with a radius of curve of 19 mm, as shown in Figure 7.3.

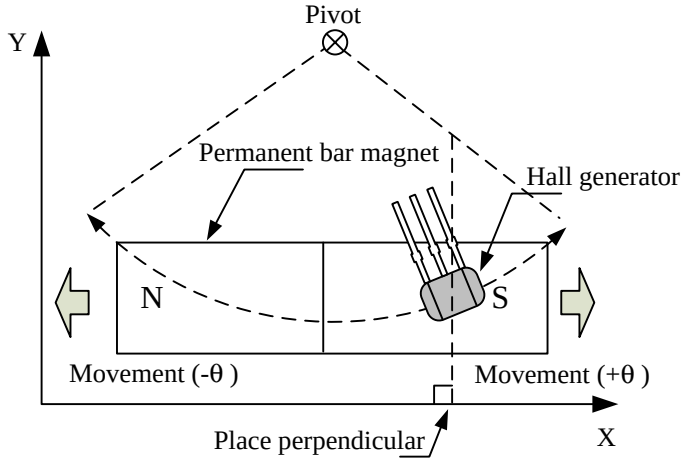

Figure 7.3: Installation of Hall generator for testing a rectangular permanent magnet.

When analyzing the output voltage from the Hall Effect sensor at every angle within the range of measurement, it was found that the movement of Hall generator can provide the narrow linearity range of measurement as shown in Figure 7.4.

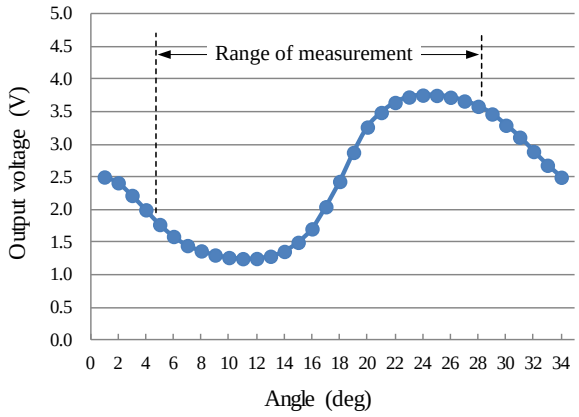

Figure 7.4: Characteristics of output voltage from tested of rectangular permanent magnet.

Therefore, the relationship between the output voltage from a sensor module, the angular positions, and the magnetic field density in the condition of a rectangular permanent magnet is illustrated in Table 7.1.

Table 7.1: The relationship between the output voltage, the angular positions, and magnetic field density in the condition of a rectangular permanent magnet.

Angle (deg)	Output voltage (V)	Magnetic field density (mT)	Angle (deg)	Output voltage (V)	Magnetic field density (mT)
1	2.5	187.967	18	2.432	182.821
2	2.412	181.325	19	2.877	216.307
3	2.217	166.707	20	3.266	245.532
4	1.997	150.117	21	3.489	262.306
5	1.771	133.174	22	3.643	273.878
6	1.588	119.387	23	3.726	280.152
7	1.448	108.908	24	3.755	282.35
8	1.367	102.753	25	3.751	282.004
9	1.304	98.012	26	3.722	279.885
10	1.265	95.107	27	3.665	275.552
11	1.248	93.831	28	3.583	269.427
12	1.25	93.982	29	3.466	260.608
13	1.284	96.576	30	3.293	247.614
14	1.358	102.141	31	3.11	233.832
15	1.498	112.622	32	2.891	217.335
16	1.705	128.182	33	2.68	201.479
17	2.044	153.683	34	2.496	187.664

7.3.2 Performance of Flat-Curve Permanent Magnet

Figure 7.5 shows the direction of a flat-curve permanent magnet movement. The Hall generator was placed at the centre of a permanent magnet and perpendicular to an X-axis similar to that of a rectangular permanent magnet.

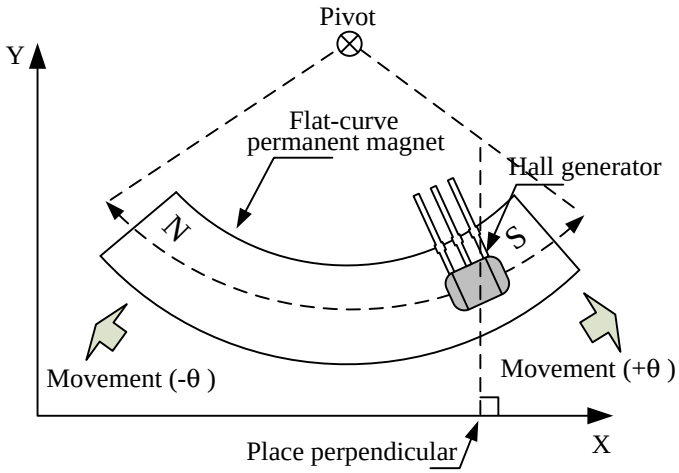

Figure 7.5: Measured range of flat-curve permanent magnet.

In this experiment, the relationship between output voltage from a Hall Effect sensor and the magnetic field density generated by flat-curve permanent magnet was observed. The results agreed with the results from calculation using COMSOL software simulation, as shown in Figure 7.6. It can be noted that when the permanent magnet was moved, the output voltage from a Hall Effect sensor varied significantly in the middle range of the permanent magnet. The relationship between the output voltage from a sensor module, the angular positions, and magnetic field density in condition of flat-curve permanent magnet is illustrated in Table 7.2.

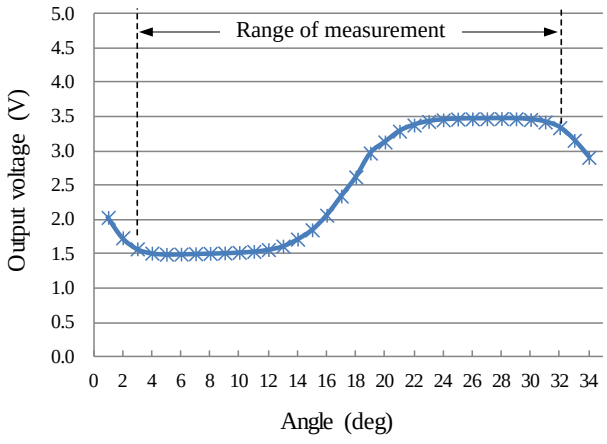

Figure 7.6: Characteristics of output voltage from tested of flat-curve permanent magnet.

Table 7.2: The relationship between the output voltage, the angular positions, and magnetic field density in condition of flat-curve permanent magnet.

Angle (deg)	Output voltage (V)	Magnetic field density (mT)	Angle (deg)	Output voltage (V)	Magnetic field density (mT)
1	2.033	152.841	18	2.621	197.071
2	1.737	130.588	19	2.97	223.287
3	1.575	118.44	20	3.132	235.493
4	1.513	113.739	21	3.289	247.329
5	1.496	112.498	22	3.379	254.04
6	1.498	112.665	23	3.431	257.969
7	1.504	113.1	24	3.454	259.72
8	1.509	113.469	25	3.466	260.584
9	1.515	113.93	26	3.469	260.839
10	1.524	114.562	27	3.47	260.915
11	1.538	115.631	28	3.473	261.106
12	1.564	117.597	29	3.47	260.907
13	1.615	121.432	30	3.459	260.039
14	1.716	129.051	31	3.423	257.377
15	1.853	139.293	32	3.34	251.154
16	2.065	155.292	33	3.156	237.271
17	2.345	176.291	34	2.908	218.66

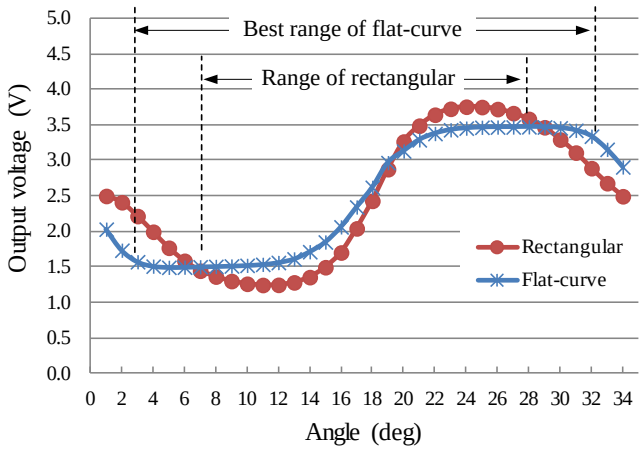

Figure 7.7: Comparison of measurement range between rectangular permanent magnet and flat-curve permanent magnet.

Experimental results can be used for an analysis of the performance of both magnets in terms of measured range. It was found that a flat-curve permanent magnet can provide a wider range of measurement than the magnet in terms of the kind of rectangle, as shown in Figure 7.7. Therefore, a flat-curve permanent magnet was selected for assembly as a sensor module in this study.

7.4 Structure of a New Sensor Module

The basic structure of a sensor module should consist of low level permeable material in order to protect the interference error from the magnetic field.

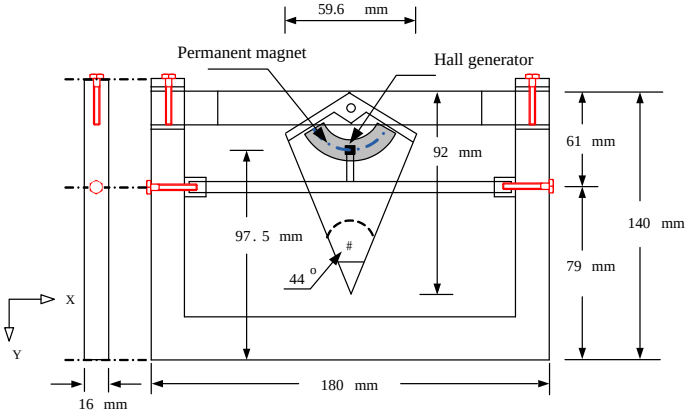

Figure 7.8: Profile of the sensor module at set point position (0 deg).

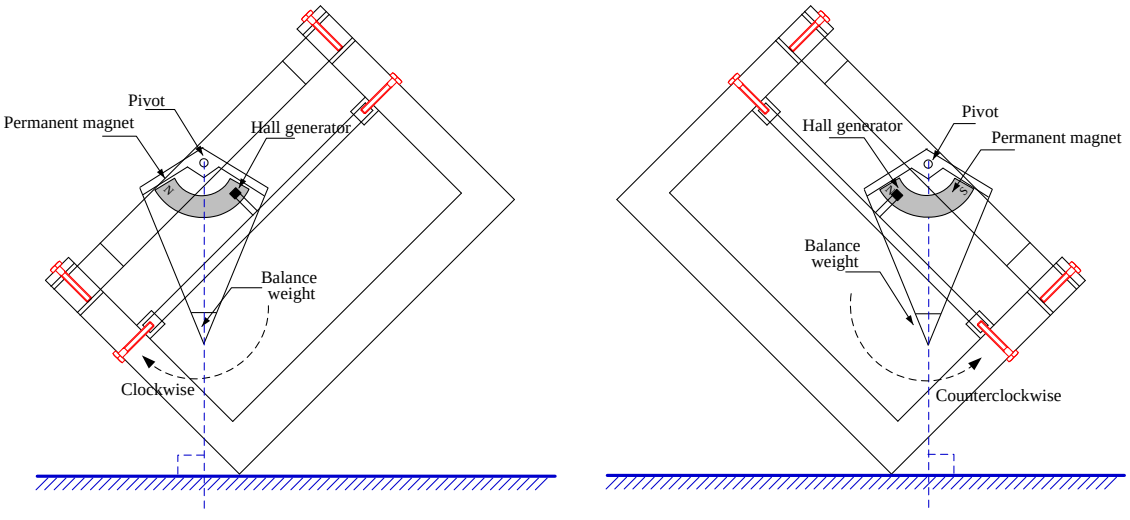

(a) (b)

Figure 7.9: Movement of a sensor module;
(a) Clockwise direction;
(b) Counter clockwise direction.

The acrylic material type was selected in this study. The profile of the measuring system consists of a sensor, namely a Hall generator, which was placed at the centre between two flat-curve permanent magnetic plates with the distance of 12 mm. The set point of 0 deg is shown in Figure 7.8. Determining the movement direction of a sensor module involved designed it to be inclined away from the X-axis in both clockwise and counter clockwise directions, ranging from -40 to 40 deg, as shown in Figure 7.9.

7.5 Experimental Conditions of New Sensor Module and Monitoring System

This section was divided into two parts: the first is a calibration of a sensor module in order to guarantee its accuracy and reliability, the second refers to the electrical system and the monitoring system.

7.5.1 Calibration of a Sensor Module

An experiment with a sensor module in this section was conducted under conditions similar to the application of angular declination using a Helmholtz coil in order to enhance the performance of the sensor as follows:

7.5.1.1 Sensitivity of Hall Generator

Sensitivity testing of the Hall generator was performed by changing the value of the input power supply of the generator at different levels of voltage according to the values specified at 5 V, 5.5 V, and 6 V. While the inclined angle was tilting away on an X-axis, the direction was varied by 1 deg per step in order to consider the response of the output signal of the Hall generator, which is related to the magnetic density generated by the permanent magnet.

7.5.1.2 Database System in a Digital Signal Pattern

Testing of the database system of a digital signal pattern was performed by five point test methodologies in the measured range using reference voltage, which used different levels from 0 V to 5 V, and then converted them to percentages in order to determine the accuracy and reliability of the conversion process between analog and digital signals. The details are shown in Table 7.3.

Table 7.3: Data conversion process to determine the accurate and reliability of database system.

Data converting	Range of measurement				
Reference voltage (V)	0	1.25	2.5	3.75	5
Percentage (%)	0	25	50	75	100

7.5.1.3 Linearity of Measuring Range

The linearity of a sensor device would be exhibited with regard to the performance of a sensor module. The test for linearity used a standard instrument with 5 arc min or about 0.0833 deg of resolution per step as a calibrated instrument.

From experiment, the sensing module exhibited high accuracy and reliability. The output voltage from inclination of angle experimented was calibrated using high accurate and precious instruments to setup the system developed as shown in Figure 7.10.

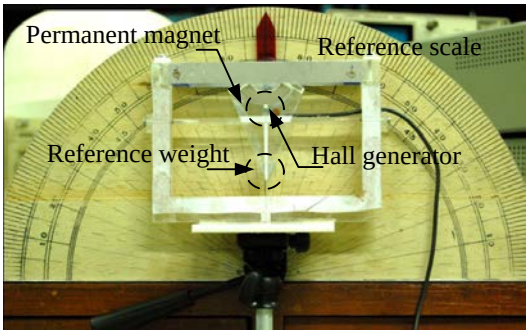

Figure 7.10: Calibration of a sensor module.

Figure 7.11 illustrates the angle calibration due to magnetic field movement. The high accurate and precious instrument (reference scale) for inclined angle adjustment was installed and defines the position of set point at 0 deg.

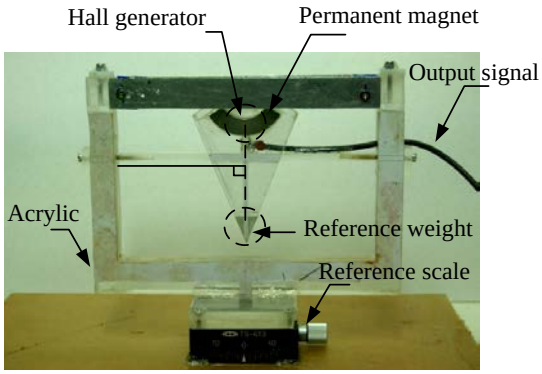

Figure 7.11: Angle calibration and reference angle measurement.

7.5.2 Monitoring System

The electrical signal system was developed by considering the voltage output of a Hall Effect sensor which is related to the magnetic density. The variation of output voltage is a function of the displacement of permanent magnets moving away from the center on X-axis that causes the distortion of magnetic fields interacting with a Hall Effect sensor. Therefore, the output voltage was varied by the density and direction of magnetic field. This voltage was compared to the constant reference signal (5 V) provided to the circuit by IC (REF02) and then converted to digital signal by 24-bit ADC before transferring to microcontroller (AT89S52) for processing. Digital signal was finally transmitted to computer for collecting and analyzing data at a specified time interval by using database program developed. Block diagram of the system in overall is as shown in Figure 7.12.

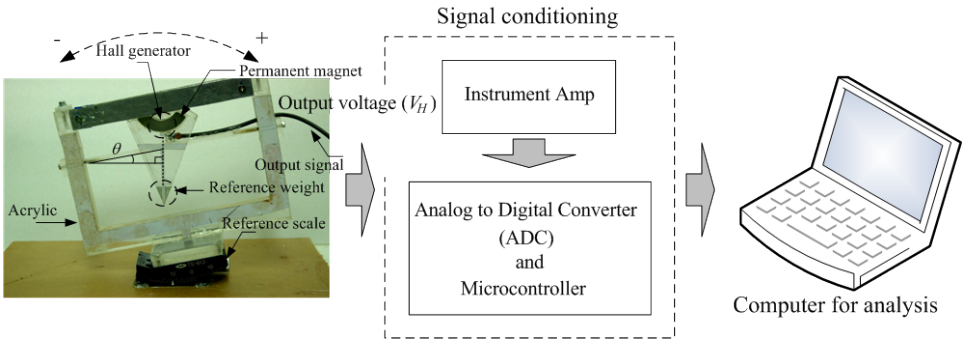

Figure 7.12: Block diagram of overall system.

The inclined angel was examined using the conventional Hall Effect sensor based on magnetic field. Monitoring and displaying modules has been design and developed to show the results of the measurement of angular displacement. The measured results were in electrical voltage form obtained from output of a Hall Effect sensor. Data were sent to a computer for analyzing and processing through LabVIEW software as shown in Figure 7.13.

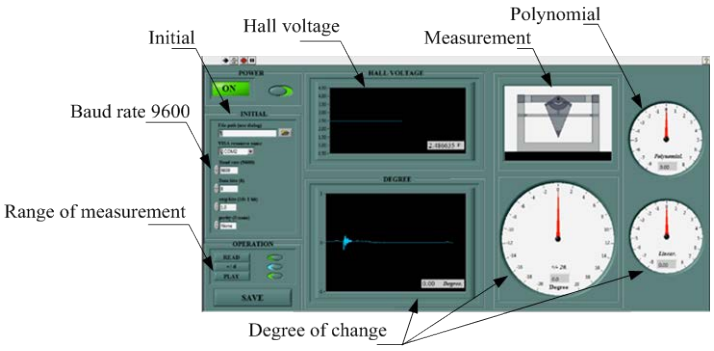

Figure 7.13: Angular displacement monitoring system.

7.6 Angular Displacement Analysis

Analysis of the output signal from a sensor module involving a range of measurement was divided into three ranges depending on the resolution of angular displacement, consisting of normal range (-40 to 40 deg), linearity and high accuracy (-20 to 20 deg), best linearity and the highest accuracy (-6 to 6 deg).

7.6.1 Analysis of -40 to 40 Degree

The system developed was designed to be inclined on X-axis in both (+) and (-) directions ranging from -40 to 40 deg. The measured results were agreed well to the results from calculation as shown in Table 7.4 and 7.5, while the angle at 0 deg as equal to 2.573 V with 13.574 mT. Considering the output voltage variation from a Hall Effect sensor and magnetic field density when a sensor module displacing and tilting away from floor level, it was found that the maximum variation of output voltage from a Hall Effect sensor with the linearity and high accuracy was in the ranges of -20 to 20 deg as shown Figure 7.14. However, the relationship of output voltage and inclined angle can provide the best linearity and the most accuracy of the results in the range of -6 to 6 deg.

Table 7.4: Output voltage is depending on inclined angle in the range of 0 to -40 deg.

Angle (deg)	Output voltage (V)	Magnetic field density (mT)	Angle (deg)	Output voltage (V)	Magnetic field density (mT)
-1	2.462	7.072	-21	1.146	250.872
-2	2.354	27.129	-22	1.131	253.657
-3	2.232	49.631	-23	1.118	255.981
-4	2.118	70.716	-24	1.108	257.839
-5	2.009	90.893	-25	1.099	259.425
-6	1.916	108.261	-26	1.092	260.803
-7	1.822	125.651	-27	1.086	261.894
-8	1.726	143.395	-28	1.081	262.842
-9	1.649	157.729	-29	1.077	263.509
-10	1.573	171.799	-30	1.075	263.994
-11	1.503	184.73	-31	1.073	264.234
-12	1.439	196.55	-32	1.073	264.332
-13	1.39	205.588	-33	1.073	264.264
-14	1.341	214.712	-34	1.075	264
-15	1.305	221.448	-35	1.077	263.654

Table 7.4: (cont'd)

Angle (deg)	Output voltage (V)	Magnetic field density (mT)	Angle (deg)	Output voltage (V)	Magnetic field density (mT)
-16	1.266	228.639	-36	1.08	262.946
-17	1.237	233.971	-37	1.084	262.218
-18	1.209	239.093	-38	1.09	261.235
-19	1.183	243.98	-39	1.097	259.933
-20	1.162	247.859	-40	1.104	258.542

Table 7.5: Output voltage is depending on inclined angle in the range of 0 to 40 deg.

Angle (deg)	Output voltage (V)	Magnetic field density (mT)	Angle (deg)	Output voltage (V)	Magnetic field density (mT)
1	2.697	36.563	21	3.851	250.279
2	2.819	58.987	22	3.865	252.782
3	2.918	77.496	23	3.874	254.576
4	3.018	96.029	24	3.883	256.189
5	3.122	115.252	25	3.89	257.495
6	3.214	132.277	26	3.896	258.595
7	3.306	149.292	27	3.9	259.401
8	3.385	163.92	28	3.904	260.067
9	3.449	175.691	29	3.906	260.477
10	3.514	187.893	30	3.907	260.597
11	3.571	198.38	31	3.907	260.611
12	3.63	209.314	32	3.906	260.417
13	3.669	216.484	33	3.904	259.996
14	3.706	223.288	34	3.901	259.43
15	3.74	229.594	35	3.896	258.638
16	3.769	234.962	36	3.889	257.368
17	3.775	236.151	37	3.882	255.966
18	3.8	240.733	38	3.873	254.288
19	3.82	244.514	39	3.86	251.863
20	3.836	247.484	40	3.849	249.926

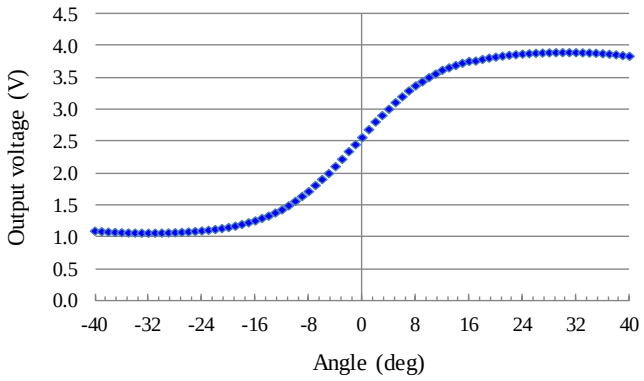

Figure 7.14: Relationship of output voltage from a Hall Effect sensor and magnetic field density in the range of -40 to 40 deg.

7.6.2 Analysis of -20 to 20 Degree

Analysis of inclined angle using the conventional Hall Effect sensor which tilting away on X-axis in both (+) and (-) direction was considered in the range of 0 to ±20 deg (normal to Y-axis) with 1 deg of resolution per step as shown in Figure 7.15. To analyze the density of magnetic field at any position within the flat-curve permanent magnetic plate radius, the module system was angularly moved on the X-axis starting from the reference point (0 deg). The measured results were presented in output voltage which varied by the current flowing through the Hall Effect sensor and dependent on magnetic field density. Moreover, the output voltage of a Hall Effect sensor was also dependent on the density and direction of magnetic field which varied from -20 deg to 20 deg.

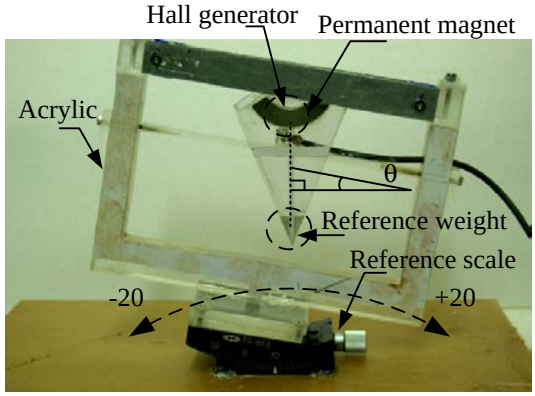

Figure 7.15: Sensor module inclination on X-axis in range of -20 to 20 deg.

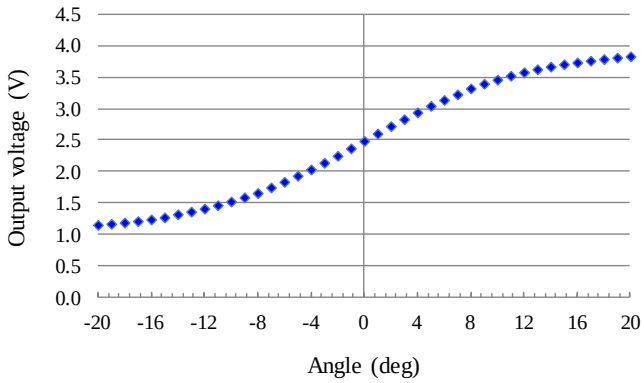

Figure 7.16: Relationship of output voltage from a Hall Effect sensor and magnetic field density in range of -20 to 20 deg.

Experimental results can be used for analysis of the relationship of output voltage from a Hall Effect sensor and magnetic field density at the tilted position of sensing module on X-axis as showing in Figure 7.16. The results agreed well to the results from calculation using COMSOL software simulation. The space between two flat-curve permanent magnets was equal to 12 mm.

Considering the angle of a sensor module inclination by repeatedly measuring 15 times and then comparing to actual values, it can be noted that the measured inclination angle exhibited the results with high accuracy and reliability at every angle in the range between -20 to 20 deg. From the experiment result, it can be observed that the range with the best linearity was -10 to 10 deg because the position of a Hall Effect sensor was mostly close to permanent magnets and the magnetic density can reach the maximum at this position. Therefore, the range of -10 to 10 deg was practically used. The output voltage as a function of inclined angle change for every single degree can be provided as shown in Table 7.6 and 7.7, while the angle at 0 deg as equal to 2.487 V with 2.401 mT.

Table 7.6: Output voltage is depending on inclined angle in the range of 0 to -20 deg.

Angle (deg)	Output voltage (V)	Magnetic field density (mT)	Angle (deg)	Output voltage (V)	Magnetic field density (mT)
-1	2.37	24.163	-11	1.468	191.125
-2	2.252	45.925	-12	1.414	201.144
-3	2.142	66.285	-13	1.367	209.829
-4	2.035	86.05	-14	1.324	217.768
-5	1.936	104.545	-15	1.275	226.837
-6	1.839	122.363	-16	1.243	232.786

Table 7.6: (cont'd)

Angle (deg)	Output voltage (V)	Magnetic field density (mT)	Angle (deg)	Output voltage (V)	Magnetic field density (mT)
-7	1.75	138.888	-17	1.216	237.79
-8	1.662	155.314	-18	1.194	241.923
-9	1.592	168.121	-19	1.174	245.677
-10	1.528	180.096	-20	1.157	248.707

Table 7.7: Output voltage is depending on inclined angle in the range of 0 to 20 deg.

Angle (deg)	Output voltage (V)	Magnetic field density (mT)	Angle (deg)	Output voltage (V)	Magnetic field density (mT)
1	2.604	19.28	11	3.521	189.136
2	2.722	41.163	12	3.576	199.378
3	2.832	61.406	13	3.624	208.148
4	2.94	81.495	14	3.666	215.931
5	3.043	100.59	15	3.703	222.806
6	3.137	118.028	16	3.732	228.138
7	3.225	134.332	17	3.759	233.291
8	3.32	151.961	18	3.785	238.025
9	3.395	165.704	19	3.809	242.382
10	3.459	177.643	20	3.829	246.085

Therefore, it can be noted that the relationship of output voltage and inclined angle can provide the best linearity of the results in the range of -6 to 6 deg for the resolution of 100 mV per 1 deg. Use of the monitoring system developed to observe ground level subsidence or to setup industrial machines would provide high accuracy and reliable in this range.

7.6.3 Analysis of -6 to 6 Degree

Considering angular analysis of the range of -6 to 6 deg by using the conventional Hall Effect sensor developed, it was found that the results were similar to the range of -20 to 20 deg with 0.01 deg of resolution per step as shown in Figure 7.17. In this case, the output voltage of a Hall Effect sensor was also dependent on the density and direction of magnetic field which varied from -6 deg (1.839 Volt) to 6 deg (3.137 Volt).

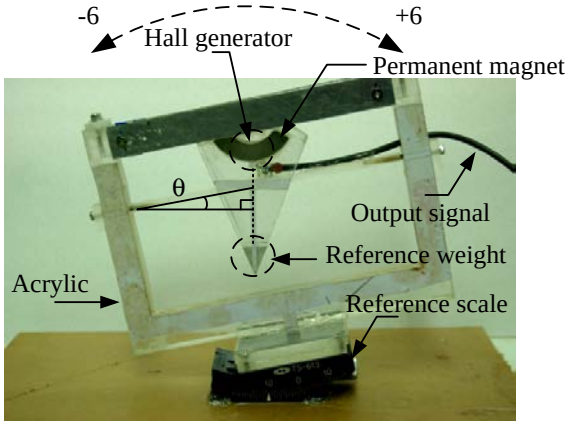

Figure 7.17: Sensor module inclination on X-axis (-6 to 6 deg).

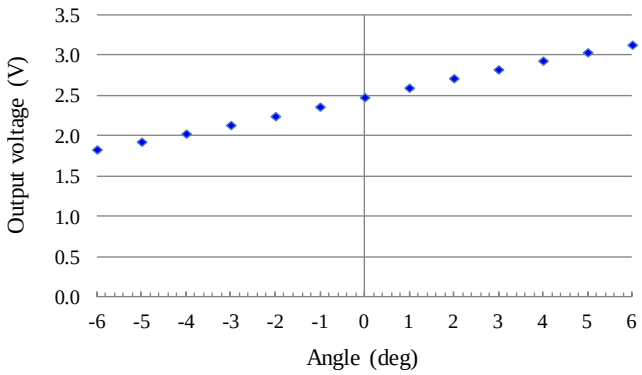

Figure 7.18: Relationship of output voltage from a Hall Effect sensor and magnetic field density in range of -6 to 6 deg.

The experimental results of the relationship between output voltage from a Hall Effect sensor and magnetic field density in any inclined position of Hall generator can be used analysis is as shown in Figure 7.18. The relationship of different angular in range of -6 to 6 deg of a sensor module declination on X-axis, which is perpendicular of ground surface and output voltage from a Hall Effect sensor as shown in Table 7.8, while the angle at 0 deg as equal to 2.487 V with 2.401 mT.

Table 7.8: Output voltage is depending on inclined angle in the range of -6 to 6 deg.

Angle (deg)	Output voltage (V)	Magnetic field density (mT)	Angle (deg)	Output voltage (V)	Magnetic field density (mT)
-6	1.839	122.363	1	2.604	19.28
-5	1.936	104.545	2	2.722	41.163
-4	2.035	86.05	3	2.832	61.406
-3	2.142	66.285	4	2.94	81.495
-2	2.252	45.925	5	3.043	100.59
-1	2.37	24.163	6	3.137	118.028

7.7 Error Analysis of Angular Measurement

Error analysis in this section was conducted under conditions similar to that of the experiment of angular displacement using a Hall Effect sensor with Helmholtz coil by repeated measurement in order to estimate the repeatability of a sensor module. The measured results will be taken to analyze the accuracy, standard deviation, and the uncertainty of the system.

7.7.1 Error Analysis of -20 to 20 Degree

Error analysis in range of -20 to 20 deg was performed by varying the inclined angle in an X-axis direction at 1 deg per step (0.1 deg of resolution of measured) by repeatedly measuring 10 times, as shown in Table 7.9. In this experimental study, accuracy, precision, average, and reliability were analyzed by considering the standard deviation, relative accuracy, and relative repeatability [34] as shown in Table 7.10. From the results of the experiment it can be observed that the most tilting level of the inclined angle at 1 deg accounted for about 10 % of the error. However, the error would appear to be caused by several reasons such as friction, angular adjustment, and readability errors on the reference scale.

Table 7.9: Repeated measurement of inclined angle in the range of -20 to 20 deg.

Angle	Times number									
(deg)	1	2	3	4	5	6	7	8	9	10
-20	-19.5	-19.4	-19.5	-19.5	-19.4	-19.5	-19.5	-19.5	-19.4	-19.5
-19	-18.9	-18.7	-18.8	-18.8	-18.8	-18.9	-18.8	-18.8	-18.7	-18.9
-18	-18.1	-17.9	-18.1	-18.1	-17.9	-18.1	-18.1	-18	-17.9	-18.1
-17	-17.2	-17.1	-17.2	-17.2	-17.1	-17.2	-17.2	-17.2	-17.1	-17.2

Table 7.9: (cont'd)

Angle	Times number									
(deg)	1	2	3	4	5	6	7	8	9	10
-16	-16.2	-16.1	-16.3	-16.3	-16.2	-16.2	-16.3	-16.3	-16.1	-16.1
-15	-15.2	-15.1	-15.3	-15.3	-15.2	-15.2	-15.2	-15.3	-15.1	-15.2
-14	-14.4	-14.3	-14.4	-14.3	-14.3	-14.4	-14.3	-14.4	-14.3	-14.4
-13	-13.3	-13.2	-13.3	-13.3	-13.2	-13.3	-13.3	-13.3	-13.2	-13.3
-12	-12.2	-12.2	-12.3	-12.2	-12.2	-12.2	-12.2	-12.3	-12.2	-12.2
-11	-11.1	-11	-11.2	-11.1	-11	-11.1	-11.1	-11.2	-11	-11
-10	-10.1	-10	-10.1	-10.1	-10	-10.1	-10.1	-10.1	-10	-10.1
-9	-9	-8.9	-9	-9	-9	-9	-9	-9	-8.9	-9
-8	-8	-7.9	-8	-8	-7.9	-8	-8	-8	-7.9	-8
-7	-7	-7	-7	-7.1	-7	-7	-7.1	-7	-7	-7
-6	-6.1	-6.1	-6.1	-6.1	-6.1	-6.1	-6.1	-6.1	-6.1	-6.1
-5	-5.2	-5.1	-5.2	-5.1	-5.1	-5.2	-5.1	-5.2	-5.1	-5.2
-4	-4.2	-4.2	-4.2	-4.2	-4.1	-4.2	-4.2	-4.2	-4.2	-4.2
-3	-3.2	-3.2	-3.2	-3.2	-3.1	-3.2	-3.1	-3.2	-3.2	-3.2
-2	-2.2	-2.2	-2.2	-2.2	-2.1	-2.2	-2.2	-2.2	-2.2	-2.2
-1	-1.1	-1.1	-1.1	-1.1	-1	-1.1	-1.1	-1.1	-1.1	-1.1
0	0	0	0	0	0	0	0	0	0	0
1	1.1	1.1	1.1	1.1	1.1	1.1	1.1	1.1	1.1	1.1
2	2.1	2.1	2.1	2.2	2.1	2.1	2.2	2.1	2.1	2.1
3	3.2	3.1	3.1	3.2	3.1	3.2	3.2	3.1	3.1	3.2
4	4.1	4.1	4.1	4.1	4.1	4.1	4.1	4.1	4.1	4.1
5	5	5	5	5.1	5	5	5.1	5	5	5
6	5.9	5.9	6	6	5.9	5.9	6	6	5.9	5.9
7	6.8	6.8	6.9	6.9	6.8	6.8	6.9	6.9	6.8	6.8
8	7.8	7.8	7.8	7.8	7.8	7.8	7.8	7.8	7.8	7.8
9	8.8	8.8	8.8	8.9	8.8	8.8	8.9	8.8	8.8	8.8
10	9.8	9.8	9.8	9.9	9.8	9.8	9.9	9.8	9.8	9.8
11	10.8	10.9	11	11	10.9	10.8	11	11	10.9	10.8
12	12	12	12	12.1	12.1	12	12.1	12	12	12
13	13.1	13.2	13.2	13.3	13.2	13.1	13.3	13.2	13.2	13.1
14	14.2	14.3	14.3	14.3	14.3	14.2	14.3	14.3	14.3	14.2
15	15.3	15.3	15.4	15.4	15.3	15.3	15.4	15.3	15.3	15.3
16	16.3	16.3	16.4	16.4	16.3	16.3	16.4	16.4	16.3	16.3
17	17.3	17.3	17.4	17.4	17.3	17.3	17.3	17.4	17.3	17.3

Table 7.9: (cont'd)

Angle	Times number									
(deg)	1	2	3	4	5	6	7	8	9	10
18	18.2	18.2	18.3	18.3	18.2	18.2	18.3	18.3	18.2	18.2
19	19	19	19.1	19.1	19	19	19.1	19.1	19	19.1
20	19.8	19.8	19.8	19.9	19.8	19.8	19.9	19.8	19.8	19.8

Table 7.10: Standard deviation, relative accuracy error, and relative repeatability error for within the range of -20 to 20 deg.

Angle (deg)	Min (deg)	Max (deg)	Average (deg)	Standard deviation	Relative accuracy error (%)	Relative repeatability error (%)
-20	-19.5	-19.4	-19.5	0.048	-2.65	-0.5
-19	-18.9	-18.7	-18.8	0.074	-1	-1.05
-18	-18.1	-17.9	-18	0.095	0.17	-1.11
-17	-17.2	-17.1	-17.2	0.048	1	-0.59
-16	-16.3	-16.1	-16.2	0.088	1.31	-1.25
-15	-15.3	-15.1	-15.2	0.074	1.4	-1.33
-14	-14.4	-14.3	-14.4	0.053	2.5	-0.71
-13	-13.3	-13.2	-13.3	0.048	2.08	-0.77
-12	-12.3	-12.2	-12.2	0.042	1.83	-0.83
-11	-11.2	-11	-11.1	0.079	0.73	-1.82
-10	-10.1	-10	-10.1	0.048	0.7	-1
-9	-9	-8.9	-9	0.042	-0.22	-1.11
-8	-8	-7.9	-8	0.048	-0.37	-1.25
-7	-7.1	-7	-7	0.042	0.29	-1.43
-6	-6.1	-6.1	-6.1	0	1.67	0
-5	-5.2	-5.1	-5.2	0.053	3	-2
-4	-4.2	-4.1	-4.2	0.032	4.75	-2.5
-3	-3.2	-3.1	-3.2	0.042	6	-3.33
-2	-2.2	-2.1	-2.2	0.032	9.5	-5
-1	-1.1	-1	-1.1	0.032	9	-10
0	0	0	0	0	N/A	N/A
1	1.1	1.1	1.1	0	10	0
2	2.1	2.2	2.1	0.042	6	5
3	3.1	3.2	3.2	0.053	5	3.33
4	4.1	4.1	4.1	0	2.5	0

Table 7.10: (cont'd)

Angle (deg)	Min (deg)	Max (deg)	Average (deg)	Standard deviation	Relative accuracy error (%)	Relative repeatability error (%)
5	5	5.1	5	0.042	0.4	2
6	5.9	6	5.9	0.052	-1	1.67
7	6.8	6.9	6.8	0.052	-2.29	1.43
8	7.8	7.8	7.8	0	-2.5	0
9	8.8	8.9	8.8	0.042	-2	1.11
10	9.8	9.9	9.8	0.042	-1.8	1
11	10.8	11	10.9	0.088	-0.82	1.82
12	12	12.1	12	0.048	0.25	0.83
13	13.1	13.3	13.2	0.074	1.46	1.54
14	14.2	14.3	14.3	0.048	1.93	0.71
15	15.3	15.4	15.3	0.048	2.2	0.67
16	16.3	16.4	16.3	0.052	2.13	0.62
17	17.3	17.4	17.3	0.048	1.94	0.59
18	18.2	18.3	18.2	0.052	1.33	0.56
19	19	19.1	19.1	0.053	0.26	0.53
20	19.8	19.9	19.8	0.042	-0.9	0.5

7.7.2 Error Analysis of -6 to 6 Degree

An error analysis in the range of -6 to 6 deg was conducted under conditions similar to the range of -20 to 20 deg under which variations of the inclined angle are tilting away on an X-axis with 1 deg per step (0.1 deg of resolution of measured), as shown in Table 7.11. When repeatedly measuring 10 times, it was observed that the range of -6 to 6 deg exhibited the results with high resolution, high accuracy, and high reliability throughout experiment. From experimental study, accuracy, precision, and reliability were analyzed by considering the standard deviation, relative accuracy error, and relative repeatability error as shown in Table 7.12. In analysis of the output voltage from a Hall Effect sensor, it can be observed that the inclination of a sensor module at any position within the flat-curve permanent magnets radius would exhibit the best accuracy of 99 %.

Table 7.11: Repeated measurement of inclined angle in the range of -6 to 6 deg.

Angle	Times number									
(deg)	1	2	3	4	5	6	7	8	9	10
-6	-6	-6.04	-6	-6.04	-6	-6.03	-6	-6.04	-6	-6.04
-5	-5.01	-5.05	-5.03	-5.04	-5	-5.05	-5.03	-5.04	-5.01	-5.05
-4	-4	-4.03	-4.02	-4.03	-4	-4.03	-4.02	-4.03	-4.00	-4.03
-3	-2.99	-3.01	-3.01	-3.01	-3	-3.01	-3.01	-3.01	-2.99	-3.01
-2	-2	-2.02	-1.98	-1.99	-1.99	-2	-1.98	-1.99	-2	-2.02
-1	-1	-1	-0.99	-0.99	-1	-1	-0.99	-0.99	-1	-1
0	0	-0.01	0	0.01	0	0	0	0.01	0	-0.01
1	1	0.99	1	1	1	1	1	1	1	0.99
2	2.02	1.99	2	2	2.01	2	2	2	2.02	1.99
3	2.99	2.99	3	2.99	2.99	2.99	3	2.99	2.99	2.99
4	4	4	4	4	4.01	4.01	4	4	4	4
5	5.04	4.99	5.02	5.02	5.02	5	5.02	5.02	5.04	4.99
6	6.02	5.99	6.04	6.01	6.03	6	6.04	6.01	6.02	5.99

Table 7.12: Standard deviation, relative accuracy error, and relative repeatability error for within the range of -6 to 6 deg.

Angle (deg)	Min (deg)	Max (deg)	Average (deg)	Standard deviation	Relative accuracy error (%)	Relative repeatability error (%)
-6	-6.04	-6	-6.02	0.02	0.32	-0.67
-5	-5.05	-5	-5.03	0.019	0.62	-1
-4	-4.03	-4	-4.02	0.014	0.48	-0.75
-3	-3.01	-2.99	-3.01	0.008	0.17	-0.67
-2	-2.02	-1.98	-2	0.014	-0.15	-2
-1	-1	-0.99	-1	0.005	-0.4	-1
0	-0.01	0.01	0	0.007	N/A	N/A
1	0.99	1	1	0.004	-0.2	1
2	1.99	2.02	2	0.011	0.15	1.5
3	2.99	3	2.99	0.004	-0.27	0.33
4	4	4.01	4	0.004	0.05	0.25
5	4.99	5.04	5.02	0.018	0.32	1
6	5.99	6.04	6.02	0.018	0.25	0.83

7.8 Conclusion

A two flat-curve permanent magnet was selected in this study for several reasons. The first reason was that the measuring of an inclined angle can provide the widest linearity range of a magnetic density field rather than using a rectangular permanent magnet. The second was performed in order to consider the variation of an inclined angle, which is related to the magnetic density which was generated by a permanent magnet. The last reason was to achieve the best readability and increase the resolution of measurement. From the experimental results of a sensor module, it can be noted that it stimulated the conventional Hall Effect sensor by two flat-curve permanent magnets, which are two sets of four magnetic domains (one set consists of two domains) as a stimulator of the conventional Hall Effect sensor can provide the results from the measurement of linearity in the range of -20 deg to 20 deg with 1 deg of resolution per step. This means a sensor module and signal conditioning system can be used for measuring the variation of the inclined angle with accuracy and reliability. Considering the resolution of measuring the variation of inclined angle from an output voltage of a sensor module, it was found that the best linearity and the most accurate of the results were in the range of -6 to 6 deg with 0.01 deg of resolution per step. Moreover, the results of measurement in the range of -6 deg to 6 deg was found the error caused by friction at pivot point of two flat-curve permanent magnets, despite as the small friction was appeared. If the measurement had occurred it would be very high resolution in this range. Therefore, a small friction would be significantly effective, which is related to the error. Furthermore, one reason is that the error caused by the standard instrument was used as calibration instrument of a sensor module, because the angle resolution of the standard instrument is 0.0833 deg, but would be taken to calibrate a sensor module with 0.01 deg of resolution.

Chapter 8

Experiment of Metal Material Imperfection Based on Time Domain

8.1 Introduction

Material imperfection can be detected by using several methodologies, but this study will propose a new methodology using the conventional Hall Effect sensor by considering the placement of a Hall generator together with a permanent magnet based on the principles of the head-on sensing mode as a new sensor module for detecting material imperfections. In this study, the appropriate position of the 4-array Hall sensor, the 5-array Hall sensor, and the 4-crossing Hall sensor were examined using drilled holes in a sample material at 3 mm, 10 mm, and 20 mm in diameter as well as 3 mm, 23 mm, 25 mm, and 26 mm of depth, respectively.

8.2 Experimental of a New Sensor Module for the Material Imperfection

8.2.1 Experiment of the 4-Array Hall Sensor

The 4-array Hall sensor, the process of measurement of using the sensor module was performed by placing the sample material on the moving table and then considering the moving time of the sample material passed through each Hall generator. The sensor module was experimented on by passing the sample materials through the sensor module with the speed of 0.311 mm/s, the overall moving time of the sample material through each Hall generator can be determined by Equation 8-1.

$$t_m = (x_3 / v_1) = (x_4 / v_1) = (x_1 + \Delta x) / v = (x_2 + \Delta x) / v \quad (8\text{-}1)$$

8.2.2 Experiment of the 5-Array Hall Sensor

In the experiment, the 5-array Hall sensor was used to detect the holes on the X-axis with the speed of 0.311 mm/s or a moving time of 4.21 s/mm. Therefore, the differential moving time of the sample materials can be estimated by using Equations 8-2 and 8-3.

$$\Delta t_{x3} = \Delta x_a / v_1 \tag{8-2}$$

$$\Delta t_{x4,x5} = (\Delta x_a + \Delta x_b) / v_1 \tag{8-3}$$

8.2.3 Experiment of the 4-Crossing Hall Sensor

An experiment was performed by passing the sample materials through the Hall generators with a stable speed of 0.33 mm/s under conditions which were similar to two previous cases. The overall moving time of the sample material through each hall generator can be expressed by Equations 8-4 and 8-5.

$$\Delta t_{x1,x3} = \Delta x_a / v_1 \tag{8-4}$$

$$\Delta t_{x2} = (\Delta x_a + \Delta x_b) / v_1 \tag{8-5}$$

8.3 Evaluating the Dimensions of a Drilled Hole

Analysis of material imperfections in this study will be performed by dividing the measurement into two conditions, the first being the depth of the drilled hole and the second being the width of the drilled hole.

8.3.1 Analysis of the Depth of Hole

The analysis of depth will be performed by considering the maximum difference between the maximum value and the minimum value of the output voltage from the measurement of each Hall generator, while the maximum difference between the maximum value and the minimum value of the output voltage can be calculated with Equation 8-6. However, this Equation can be derived from Equations 8-7 and 8-8.

$$Dp = V_{max} \{\Delta H_S\} ; S = 1, 2, \ldots, n \tag{8-6}$$

$$\Delta H_S = V_{S(max)} - V_{S(min)} \tag{8-7}$$

$$\left.\begin{aligned} V_{S(max)} &= \text{Max} \{V_{Si}\} \\ V_{S(min)} &= \text{Min} \{V_{Si}\} \end{aligned}\right\} i = 1, 2, \ldots, m \tag{8-8}$$

Figure 8.1 shows the analysis of the depth of hole by considering the output signal from the measurement using a new sensor module and calculated result, the blue line is the output voltage from the measurement and the red line is the signal from calculation.

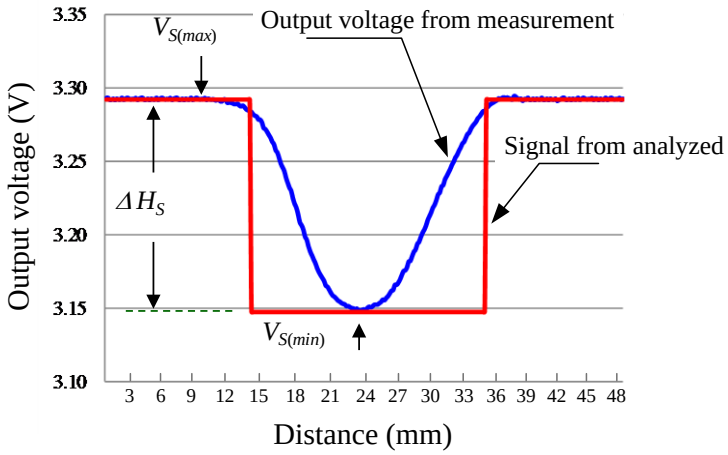

Figure 8.1: Analysis of the depth of hole.

8.3.2 Analysis of the Width of Hole

The analysis of the width of hole will be performed by considering the widest output voltage of each Hall generator, as shown in Figure 8.2, while the widest output voltage of each Hall generator can be estimated with Equation 8-9. However, this Equation can be derived from Equations 8-10 and 8-11. By the way, the value of the threshold, used to calculate in this study, is equal to 0.15 V. This means that the maximum value of the output voltage of each Hall generator will be set as logical high and if the signal from the measurements are lower than the set point, the signal will inverse into logical low. Therefore, we can use these data to multiply by the resolution of movement; in this study, the moving table used a stepping motor with a resolution of 0.5 μm per step.

$$Wd = Sum_S \times St \tag{8-9}$$

$$Sum_S = \sum_{i=1}^{m} \{D_{Si}\} \tag{8-10}$$

$$D_{Si} = \begin{cases} 0; V_{Si} > (V_{S(max)} - Th) \\ 1; V_{Si} \le (V_{S(max)} - Th) \end{cases} \tag{8-11}$$

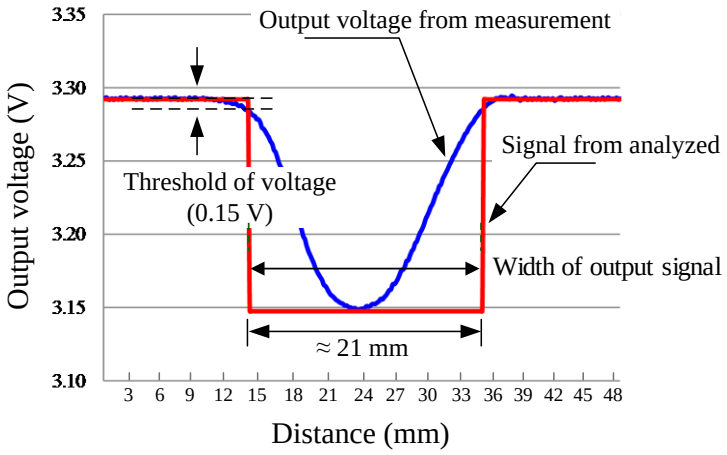

Figure 8.2: Analysis of the width of hole.

8.4 Experiment Result of Sensor System for Material Imperfection

The influences of the Hall generator and the permanent magnet placements under the same conditions were studied to enhance the efficiency of the Hall Effect sensor. The experiment of using the sensor module was performed by passing the sample materials through a Hall generator with the stable speed, using the moving table as shown in Figure 8.3.

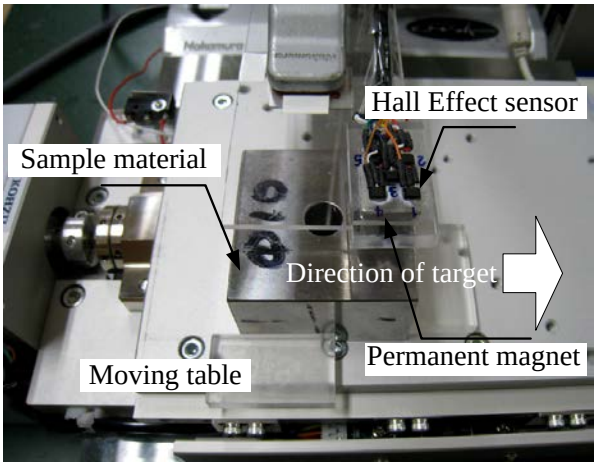

Figure 8.3: Installation of the sensor module and moving table used for experiment.

The specimens used in this study were made of metal material (48 mm of width and length, and 28 mm of thickness) with the density of 7.8 g/cm^3. The acoustic velocity of the transverse wave was 3.23 km/s and acoustic impedance was 450×10^4 g/cm^{2}s. The specimens were drilled at the centre with different diameters and depths of holes, as shown

in Figure 8.4 (a). Nine points at the centre of specimen surface with 5 mm of distance between each point were determined, as shown in Figure 8.4 (b).

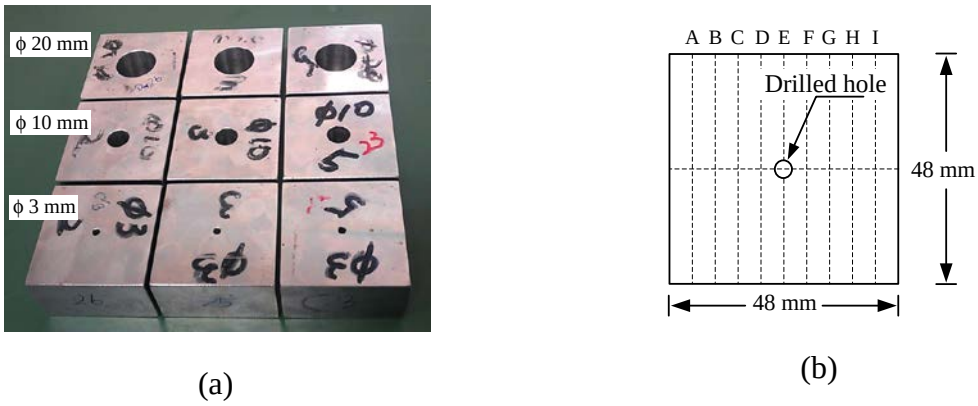

Figure 8.4: Test specimen;
(a) Samples in experiment;
(b) Test points.

The experiment was performed by placing the sample materials on the moving table and then passing the sensor module on X-Axis with slow and constant speed in order to uniform the initial point of each measurement. Moreover, the output voltage of the sensor module can be clearly observed, simply compared as well as analyzed due to simultaneous response of real time experiment. All experimental cases for testing the sensor module in this study were performed under the same conditions. The sample material was passed through the sensor module on the X-axis of the moving table with a specific distance (2 mm) between a permanent magnet and the sample material on Y-axis. The measurement was performed 5 times. The data transmitting speed of the ARM7 microcontroller to a computer was 300 ms. Therefore, the amounts of data transmitted in each case were 218 (4-array Hall sensor) and 204 (5-array Hall sensor and 4-crossing Hall sensor), starting from the initial point to the end point (48 mm of long).

An experiment using the 5-array Hall sensor used a Hall generator (x_3) as a reference. All output signals from other sensors were initially calibrated to be equal to the signal from S3. As the drilled hole on metal sample surface was smaller than the sensor, an experiment with the 4-array Hall sensor was performed by placing the Hall generator (x_2) and (x_3) at the centre of the holes. Therefore, the output signals would be obtained only from (x_2) and (x_3) and would be able to detect the 3 mm hole, as shown in Figure 8.5. Thus the error was about ±1.2 mm of radian.

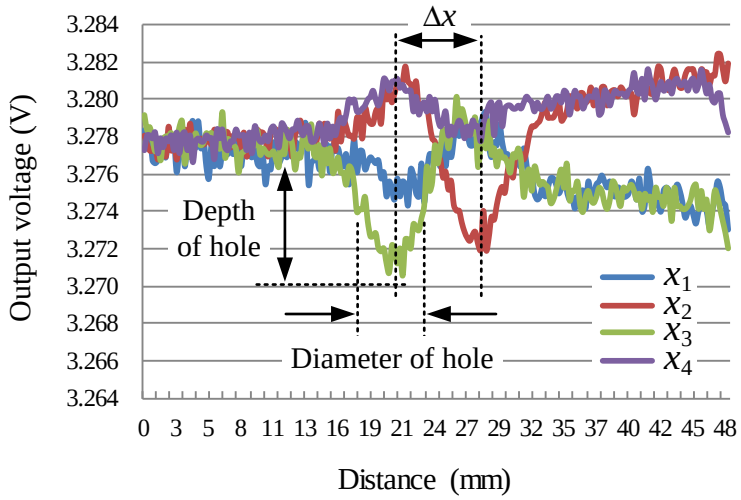

Figure 8.5: Output voltage from the 4-array Hall sensor (3 mm of diameter).

In the case of the 4-crossing Hall sensor, an experiment was performed similarly to a case of the 4-array Hall sensor by placing a Hall generator (x_2) and (x_4) at the centre of the holes. Therefore, the output signals would be obtained only from (x_2) and (x_3) with an error of ±1.2 mm of radian, as shown in Figure 8.6.

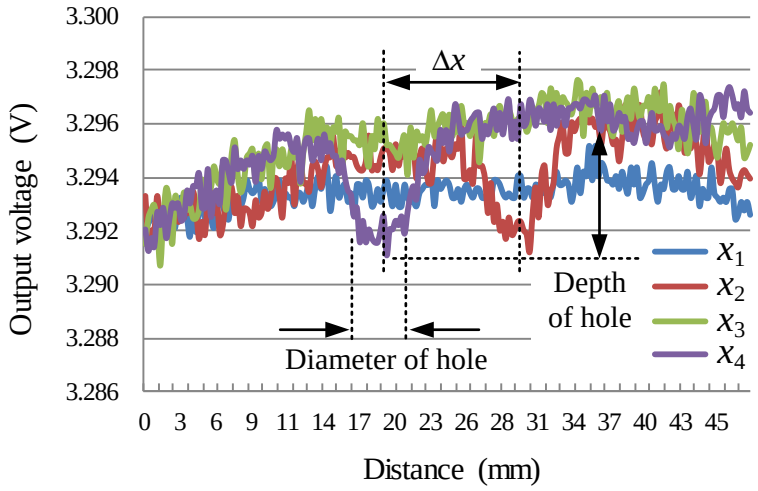

Figure 8.6: Output voltage from the 4-crossing Hall sensor (3 mm of diameter).

Figure 8.7 shows the results of the 4-array Hall sensor. An experiment with the 4-array Hall sensor was performed by placing Hall generator (x_2) and (x_3) at the centre of the holes. Therefore, the output signals would be obtained only from (x_2) and (x_3), which would be able to detect the 10-mm diameter hole at 25-mm depth. The error was about ±1.25 mm of radian. In the case of alternative magnetic pole placement, the disadvantages were due to flux reversal generation caused by instantaneous transition between the N and S poles of

the magnet during measurement. The output signal in this case thus disagreed with the theory used. This would be caused by a difference in the magnetic direction which resulted in a differing sensitivity for each Hall generator. In practical terms, the optimum performance of a Hall Effect sensor can be obtained when installing the S-poles of permanent magnet directed to the front size of the sensors. An error would be about ±1 mm of radian.

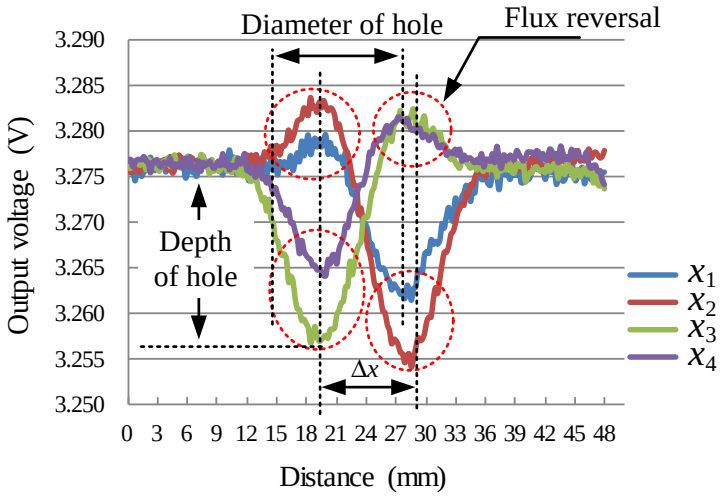

Figure 8.7: Output voltage from the 4-array Hall sensor.

For the 5-array Hall sensor, the sensors were placed at the centre of the large-diameter hole. The results were as shown in Figure 8.8 and the error was ±0.8 mm of radian.

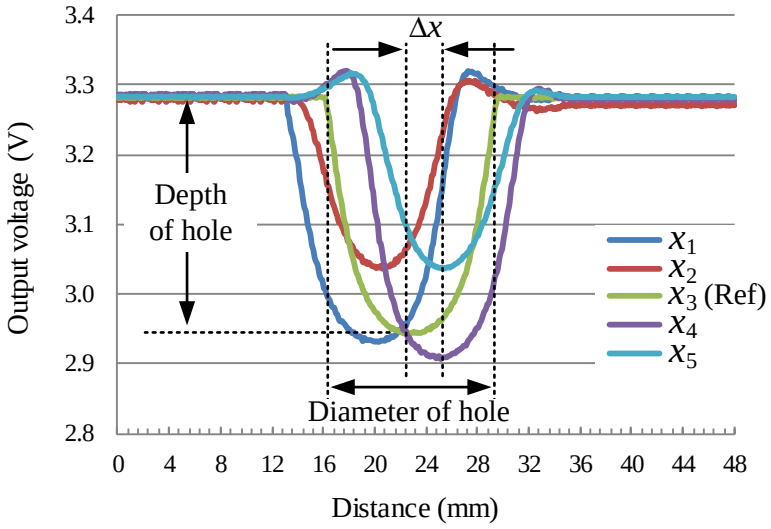

Figure 8.8: Output voltage from the 5-array Hall sensor (10 mm of diameter).

In case of the 4-crossing Hall sensor, an experiment was performed which was similar to a case of the 4-array Hall sensor by placing Hall generators (x_2) and (x_4) at the centres of

holes. The results from the experiment with the 4-crossing Hall sensor was mostly stable and continuous when the poles of permanent magnets moved in the same direction and the S-poles of permanent magnets were directed to the front size of the sensors, as shown in Figure 8.9. The sensitivity of each sensor was also consistent with an error of ±1.5 mm of radian.

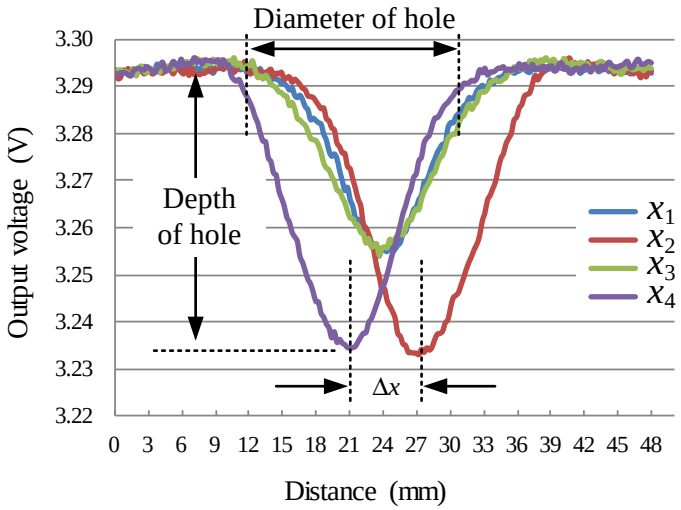

Figure 8.9: Output voltage from the 4-crossing Hall sensor.

Figure 8.10 shows the results from the analysis using the 4-crossing Hall sensor. The dimension of the drill hole was measured at 20 mm of diameter and at 25 mm depth for collecting and analysing data in order to display on them a computer.

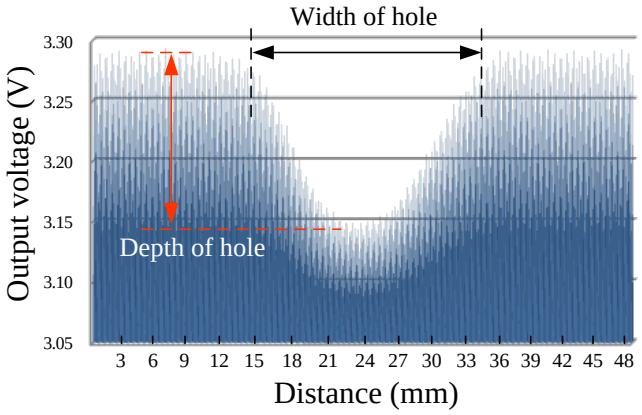

Figure 8.10: The results from the analysis of the width and the depth of the drilled hole.

8.5 Conclusion

The design of the new sensor module for non-destructive inspection for measuring material imperfections, the type of new sensor module can be divided into three types: the 4-array Hall sensor, the 5-array Hall sensor, and the 4-crossing Hall sensor. When compare the performance from the experiment of each sensor module under the same conditions, it found that the 4-array Hall sensor was unsuitable to be an alternative of magnetic pole placement; one of its disadvantages is the errors can be occurred due to flux reversal. The 5-array Hall sensor can provide high measurement resolution, but may make errors due to the fact that they only use one permanent magnet. Finally, the 4-crossing Hall sensor were the most appropriate, with optimum performance compared with the other sensors due to their smooth and stable output signal. Therefore, in this study we only used one type of sensor module, namely the 4-crosing Hall sensor, for the experiment, because this sensor module can provide results with the high accuracy and reliability.

Chapter 9

Experiment of Metal Material Imperfection Based on Frequency Domain

9.1 Introduction

Normally, the output of a Hall Effect sensor can be analyzed by using two methods: voltage analysis and current analysis [38]. However, this study presents an analysis based on frequency domain [39] by using MATLAB [40-42] to enhance the efficiency of a new sensor module. Hall Effect sensor is a semiconductor device which can be applied as a sensor to detect several variables in the industrial sector due to its accuracy and reliability. Moreover, its compact size is convenient for installation. In this study, the appropriate position of the 4-crossing Hall sensor was examined using the drilled holes in sample material at 10 mm and 20 mm in diameter as well as 0 mm, 1 mm, 2 mm, and 3 mm of depth, respectively.

9.2 The Objectives

The objectives in this chapter are to present an alternative measurement by using a magnetic field together with the conventional Hall Effect sensor which can be applied to the inspection of imperfection of metal materials by using the non-destructive inspection methodology. An analysis of the output signal was performed based on the principle of frequency domain by using the new sensor module as sensor equipment. Conceptually, an analysis in frequency domain can provide high resolution of reading the output signal from measurement. This is requires the benefit of the frequency domain to be readability in order to distinguish the signal with a small difference. Therefore, it can be noted that the output signal from measuring used a sensor module analyzed in frequency domain would provide high resolution compared to voltage analysis. An analysis of the output signal from the sensor module based on a frequency domain in this study considered only one type of the sensor modules, namely the 4-crossing Hall sensor. Each dimension of the drilled hole in a specimen was repeatedly measured and then evaluated for accuracy, standard deviation

(SD), reliability and repeatability of this sensor module [34].

9.3 The Basic Idea

The frequency domain is one of the methods used to control the signal processing unit due to long signal transmission and the high resolution of demodulation with less interference from other signals. The frequency change in this study was directly varied by the input of the voltage to frequency converter, which was derived from the conversion of the output voltage of Hall Effect sensor to a pulse. This output was then transformed to frequency domain [43] by using the Fourier transform [44] which could provide a high frequency by MATLAB. The measurement and analysis of this study was divided into three parts: a sensor module, signal conditioner, and frequency transform. Initially, the experiment was conducted with the electrical signal, a voltage form that can be transmitted to the signal conditioner, which consists of a comparator circuit for filtering the signal difference between measured and reference voltages. The signal was finally transformed for analysis, as shown in Figure 9.1.

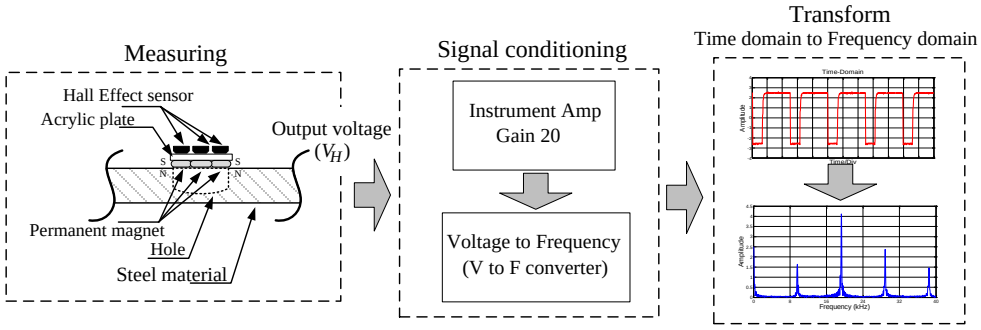

Figure 9.1: Block diagram of the measurement system.

In this case, the frequency variation from measuring using the 4-crossing Hall sensor and measurement system would be related to the variation of the voltage signal in the same direction. This means that the variation of the voltage was proportional to the frequency. However, the 4-crossing Hall sensor for measuring a drilled hole on the surface of the test specimen with a different diameter and depth found that the level of the output frequency was also proportional to the diameter and the depth of drill holes.

9.3.1 Instrumentation Amplifier

Since the output voltage of a Hall Effect sensor for measuring some variables in industrial fields have rather low values, some cases would be united as “mV” or less. The result from a small amount value affects an error from reading a voltmeter [45]. Therefore, an amplifying of the output voltage to enhance the intensity of the levels of the signal will

helpfully distinguish the signal with a small difference. This study has chosen the instrumentation amplifier (No. AD542) which was produced by the Analog Devices, Inc., to amplify the output voltage of a Hall Effect sensor. The characteristics of the instrumentation amplifier can provide a gain for adjustment from between 10 times to 10,000 times depending on the operating connections as illustrated in equivalent circuit and feature of IC used in Figure 9.2.

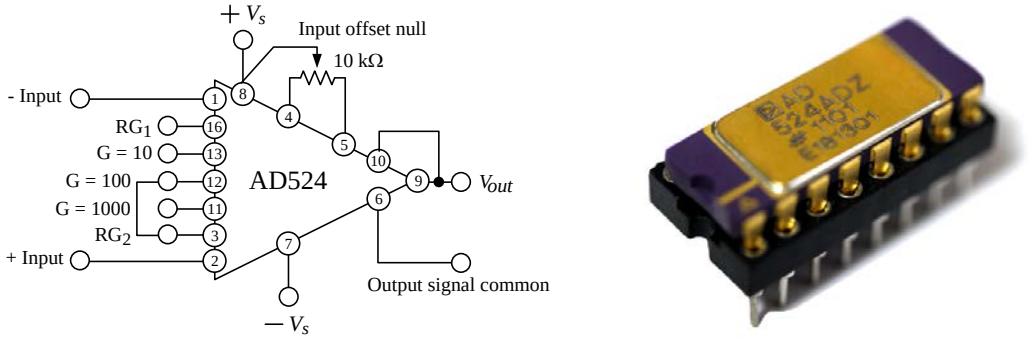

(a) (b)

Figure 9.2: Precision instrumentation amplifier:
(a) Operating connections;
(b) Typical of IC-AD254.

9.3.2 Voltage to Frequency Converter Circuit

Normally, the output signal of a Hall Effect sensor can be analyzed by using two methods: voltage analysis and current analysis. However, this study presents an analysis based on frequency domain by using MATLAB to enhance the efficiency of the new sensor module compare to the signal in the form of the voltage. The analysis of the frequency domain started by transforming the values in the pattern of the output voltage, which was amplified by the instrumentation amplifier into the time domain by the voltage to frequency converter (No. LM331N). This process was performed in the signal conditioning part to create the stable width of the pulse, as shown in the equivalent diagram in Figure 9.3. The operating fundamentals of the circuit can be explained when the output voltage of a Hall Effect sensor was amplified to be appropriate to be transformed into a pulse signal by giving the frequency. In this case, the frequency was first tuned to the value at 8 kHz calibrated by measuring the test specimen without a drilled hole on the surface of the sample material. The results from processing were performed by transmitting through the computer in order to transform them into the frequency domain using MATLAB software for ease of analysis.

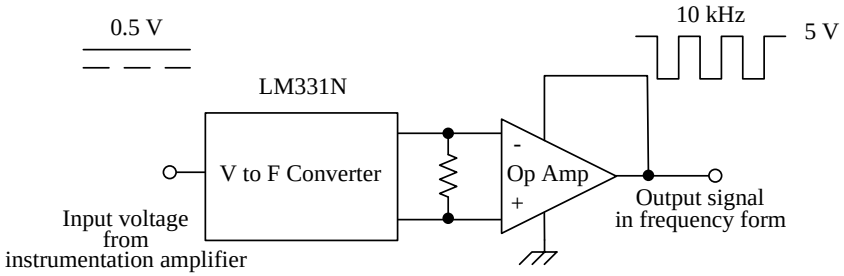

Figure 9.3: Diagram of voltage to frequency converter system.

9.3.3 Principle of MATLAB Software

MATLAB (matrix laboratory) is a high-level language which was developed by MathWorks, Inc. MATLAB is heavily used to compute technical matters such as numerical computing, data analysis, problem solving and graphic design. In the case of graphic design, MATLAB has powerful graphic tools and can produce perfect pictures in both two and three dimensions. It is also comprehensive in experimentation and algorithm development, computing of mathematical models, and includes instruments and control system simulation, especially image processing [40, 41].

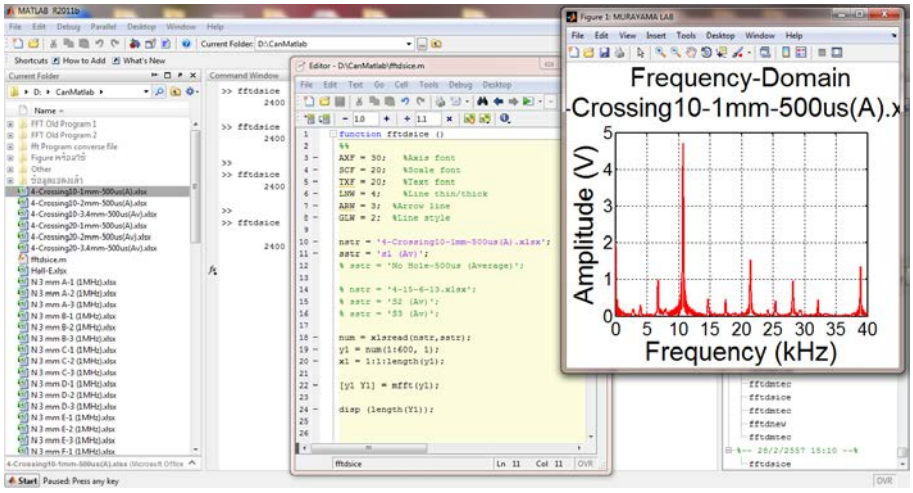

Figure 9.4: Execution of MATLAB software in order to transform time domain into the frequency domain.

The history of MATLAB started in matrix computation and matrix software. MATLAB was originally developed by Dr. Cleve Moler under the LINKPACK and EISPACK projects which were written using the FORTRAN language. In addition, MATLAB can perform operations from the command line or can create script and functional programs that perform repetitive tasks. Its basic data element is an array that does not require dimension, while low level languages require. It is a high performance language for technical computing and programming in an easy to use environment which is famous for research

[42]. The application of MATLAB for this study, MATLAB was used for transformation in the frequency domain analysis. Transformation is used to convert a time domain function to a frequency domain function. The most common transformation used in the frequency domain is the Fourier transformation; the example is illustrated in Figure 9.4.

9.4 Principle of Frequency Domain

The frequency domain is one of the methods used to control the signal processing unit due to long signal transmission and the high resolution of demodulation with less interference from other signals. The frequency change in this study was directly varied by the input of the voltage to frequency converter, which was derived from the conversion of the output voltage of a Hall Effect sensor into a pulse. It can also exhibit a stable width of a time domain as given in Equation 9-1. This output signal is then transformed to the frequency domain [43] by using the principle of Fourier transform [44] which can provide a precise high frequency via MATLAB.

$$f_o = \frac{V_H}{2.09\,(\mathrm{V})} \times \frac{R_s}{R_L} \times \frac{1}{R_t C_t} \tag{9-1}$$

Figure 9.5 shows a typical sample of frequency in the form of a time domain which was converted from the output voltage of the Hall Effect sensor.

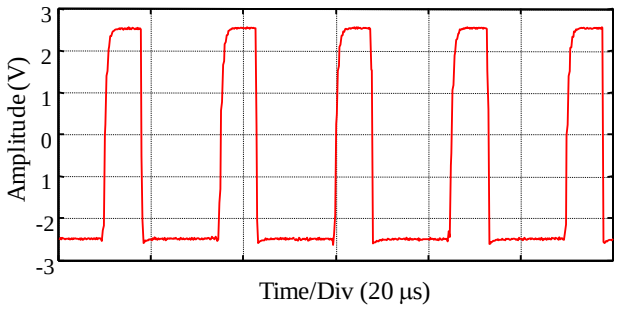

Figure 9.5: Typical frequencies in time domain waveform.

From the previous description of signal analysis based on frequency domain used MATLAB in order to computation the signal in frequency form by transforming the frequency in the form of time domain into the frequency domain, the sequence of processing can exhibit by flowchart as shown in Figure 9.6.

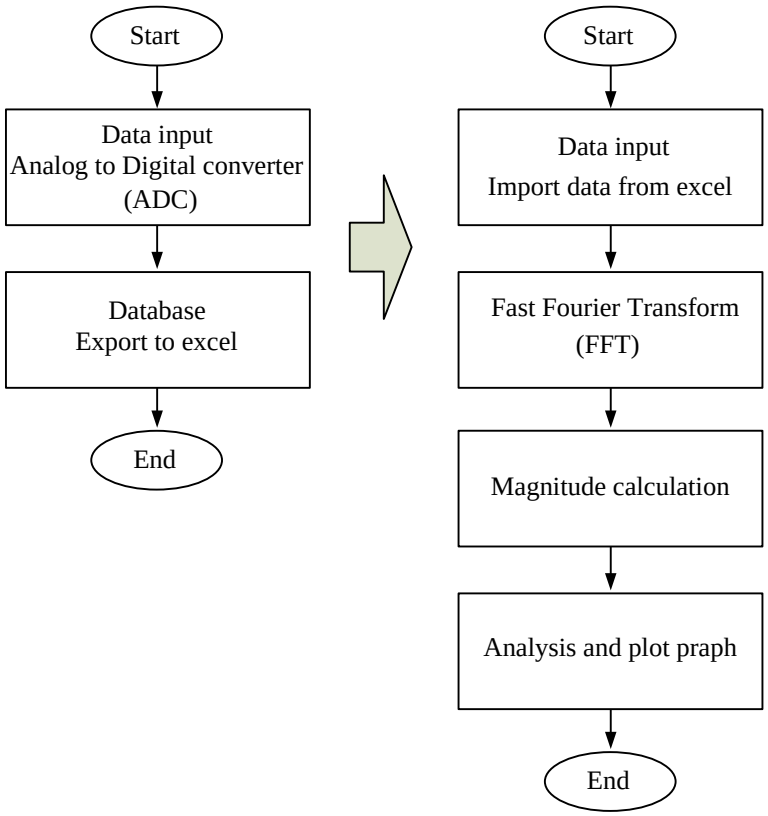

Figure 9.6: Flowchart of processing using MATLAB.

The process of frequency transforming from the time domain into the frequency domain in this study can be divided into two parts: the first is performed to transform the output signal in analog form into digital signal by using the analog to digital converter circuit (ADC) and then transmitting it through a computer in format of an excel file (.xlsx). This form of database collection is used for further analysis, while the second is performed by reading the data of an excel file using MATLAB then calculated based on the principle of Fourier transform. Finally, we will also display the results from analysis of the graph pattern of both the time domain and the frequency domain. In addition, MATLAB version R2011b (7.13.0.564), 32-bit (win32) was selected for this study. While the time per division was at 20 μs, the frequency was at 20 kHz and then converted into the frequency domain based on the principle of Fourier transform as given in Equation 9-2. Figure 9.7 shows an example of a frequency domain waveform which was calculated using MATLAB software.

$$X(k) = \sum_{n=0}^{N-1} x(n) e^{\frac{-j2\pi nk}{N}} \tag{9-2}$$

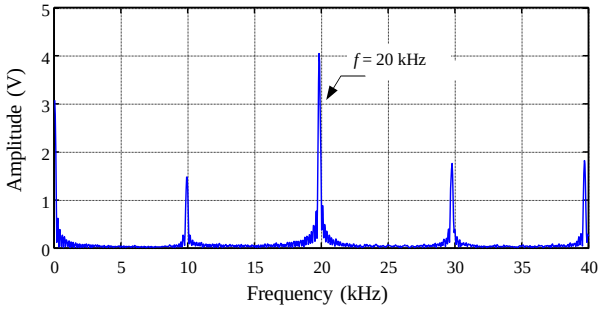

Figure 9.7: Frequency domain waveform calculated by MATLAB software.

Figure 9.8 illustrates an example of signal analysis in the frequency domain using MATLAB software to measure imperfections in the iron material of a Hall Effect sensor which was drilled at the centre on the surface of the specimen with a drilled hole diameter of 3 mm and a depth of 25 mm. In this case, the oscilloscope was to be set at a range of measurement of the time domain of both. The volts division and time division were 1 $V_{p\text{-}p}$ and 500 μs, respectively. It can be observed that the output voltage from an experimental Hall Effect sensor analyzed in frequency domain would provide high resolution compared to voltage analysis. Moreover, the frequency domain will also be available to clearly distinguish between the output signal and the harmonic. From the example of the experiment, the position of the drilled hole on the surface of specimen can be exhibited as 8.454 kHz compared to the position of material surface without drilled hole which was 8 kHz. Therefore, the difference between these positions would be exhibited at 454 Hz which has a high resolution for measurement of these variables.

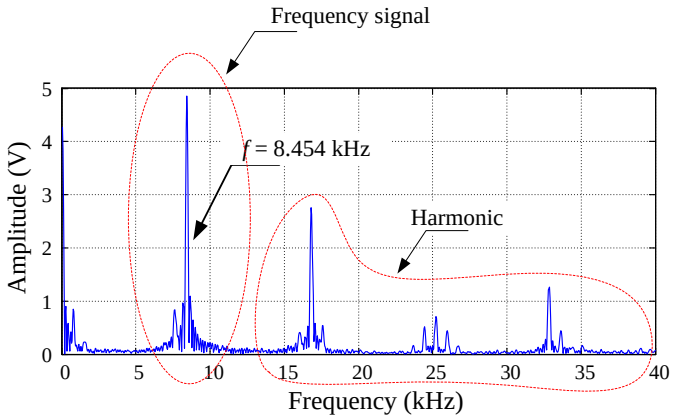

Figure 9.8: Frequency domain analysis in measurement of the material imperfection, 3 mm of diameter of hole with 25 mm of depth.

9.5 Experimental Results in Frequency Waveform

The process of measurement will start from the output signal of the sensor modules and was amplified 20 times by an instrumentation amplifier. The frequency was later converted to time domain at 8 kHz. Analysis of the frequency domain from the measurement and tests of specimens by using a sensor module, namely the 4-crossing Hall sensor was performed by placing the sensor module at the centre of drilled hole for measuring the diameter and depth of a hole on the specimen's surface. In an experiment without the hole on the surface of the sample material, the frequency of the Hall Effect sensor output was firstly tuned to the value at 8 kHz with 5 V_{p-p} of the amplitude.

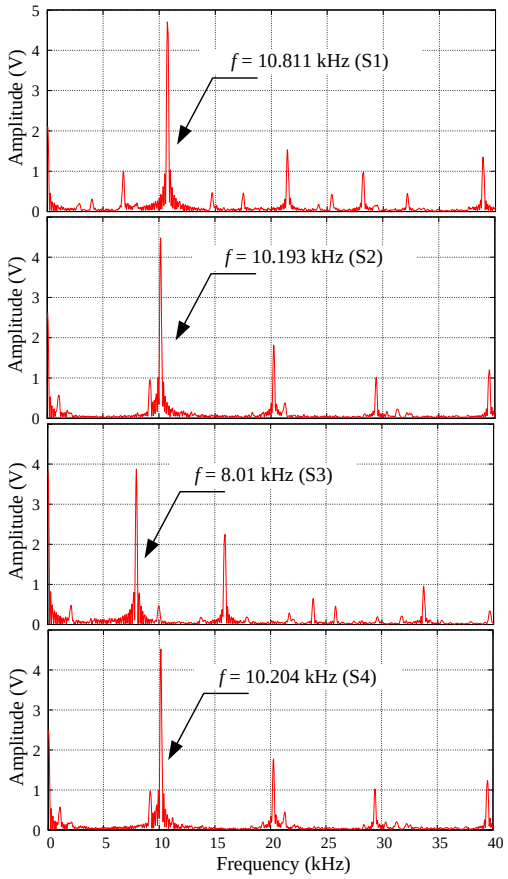

Figure 9.9: Comparison of frequency domain from each Hall generator under the same specific conditions (10-mm diameter and 1-mm depth).

The frequency variation in the time domain waveform would be increased relative to the deeper hole due to the frequency signal which was converted from the voltage signal in a way that was proportional to the output voltage. The frequency signal would also be proportional to the depth of the hole. Therefore, the frequency from the measurement would be varied by the depth and diameter of drilled hole. An analysis of the frequency

domain was performed by comparing the results of the measurement of a 10-mm and 20-mm diameter hole with various depths; i.e. 0 mm, 1 mm, 2 mm, and 3 mm. Four Hall generators were crosswise placed for enhancing the performance and resolution in measurement of a sensor module and especially in an estimation of the diameter of the hole. As the signals from four Hall generators can be taken to compare individually and calculate the actual size of a drilled hole, the results from measurement of a 4-crossing Hall sensor would be more accurate than that of a single Hall sensor. A Hall generator 1 (S1) was placed at the centre of drilled hole in order to compare the level of depth with a Hall generator 3 (S3) while a Hall generator 2 (S2) and Hall generator 4 (S4) were used for estimating the width of the hole.

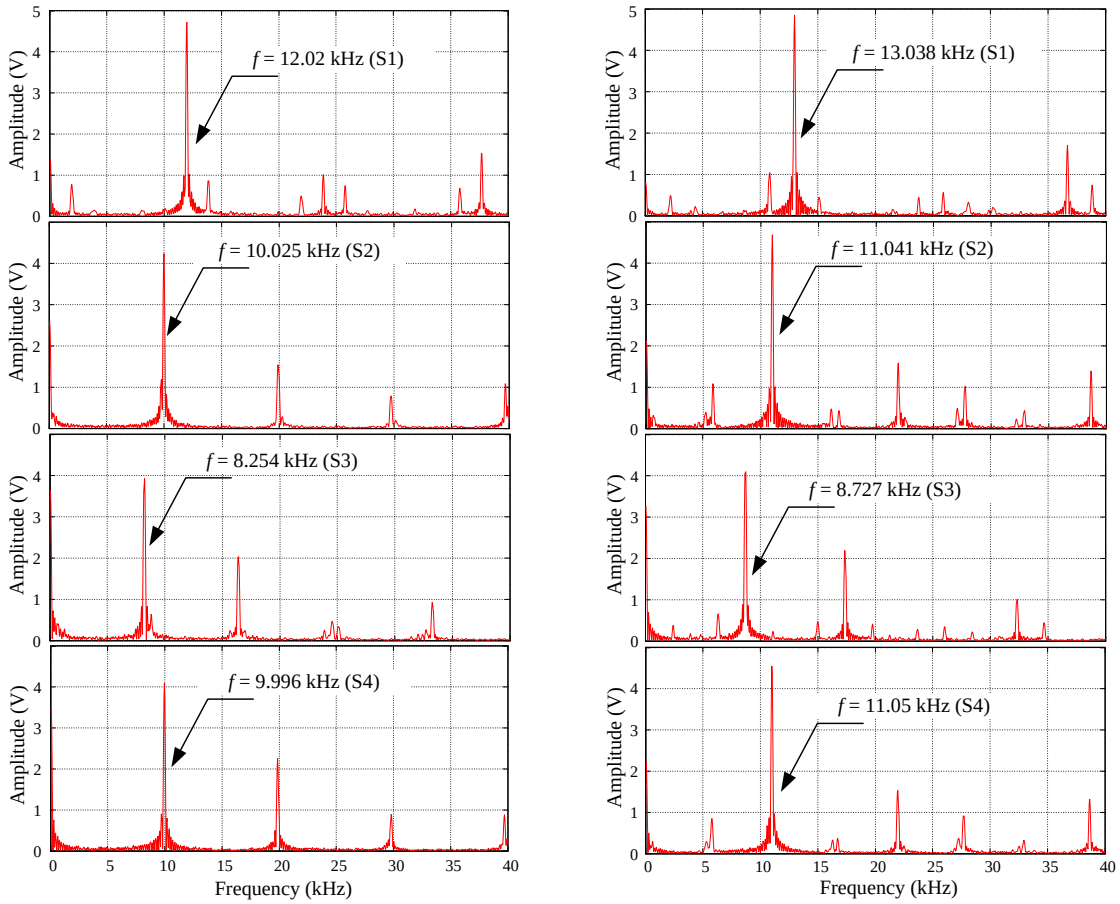

(a) (b)

Figure 9.10: Comparison of frequency domain from each Hall generator under the same specific conditions;
(a) The 10-mm diameter and 2-mm depth;
(b) The 10-mm diameter and 3-mm depth.

Figure 9.9 and 9.10 shows a comparison of output signals from 4 Hall generators in the frequency domain when measuring the 10-mm diameter drilled hole with 1-mm, 2-mm, and 3-mm depths. In this experiment, it could be noted that the 4-crossing Hall sensor module can estimate the width as well as the depth of the hole. The 4-crossing Hall sensor would be effective and appropriate for testing large holes and cracks. The application of several Hall generators installed together would be beneficial for determining the edge and the size of the hole or crack of the target. This is because the output of each Hall generator can be taken to determine the edge, the diameter of a hole or a crack, and also the depth which provides better results compared to a single Hall sensor. The experiment results of a sensor module based on frequency domain analysis that can clearly distinguish between the output signals from measurement and harmonic. This can be extremely helpful in evaluating the dimension of a drilled hole which can distinguish the signal easily. The difference of frequency between the deepest whole position which was the position of S1 and the shallowest depth of a hole (0 mm) was at the position of S3 of test specimen at 1 mm, 2 mm, and 3 mm of depth were about 2.801 kHz, 3.766 kHz, and 4.311 kHz, respectively.

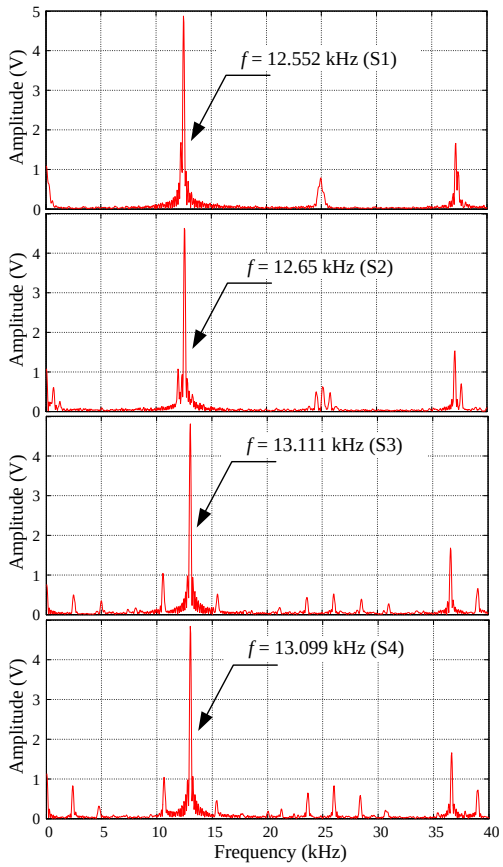

Figure 9.11: Comparison of frequency domain from each Hall generator under the same specific conditions (20-mm diameter and 1-mm depth).

Figure 9.11 and 9.12 shows the experiment results in the frequency domain from measuring the diameter of a drilled hole at 20 mm with various depths of 1 mm, 2 mm, and 3 mm. It was found that the variation of frequency from the measurement of each Hall generator would also be proportional to the diameters and depths of drill holes in the same direction. It can be observed that the average difference frequency between the deepest hole position and the shallowest hole (S1-S3) on the surface of test specimen was about 6.991 kHz, at 3 mm of depth.

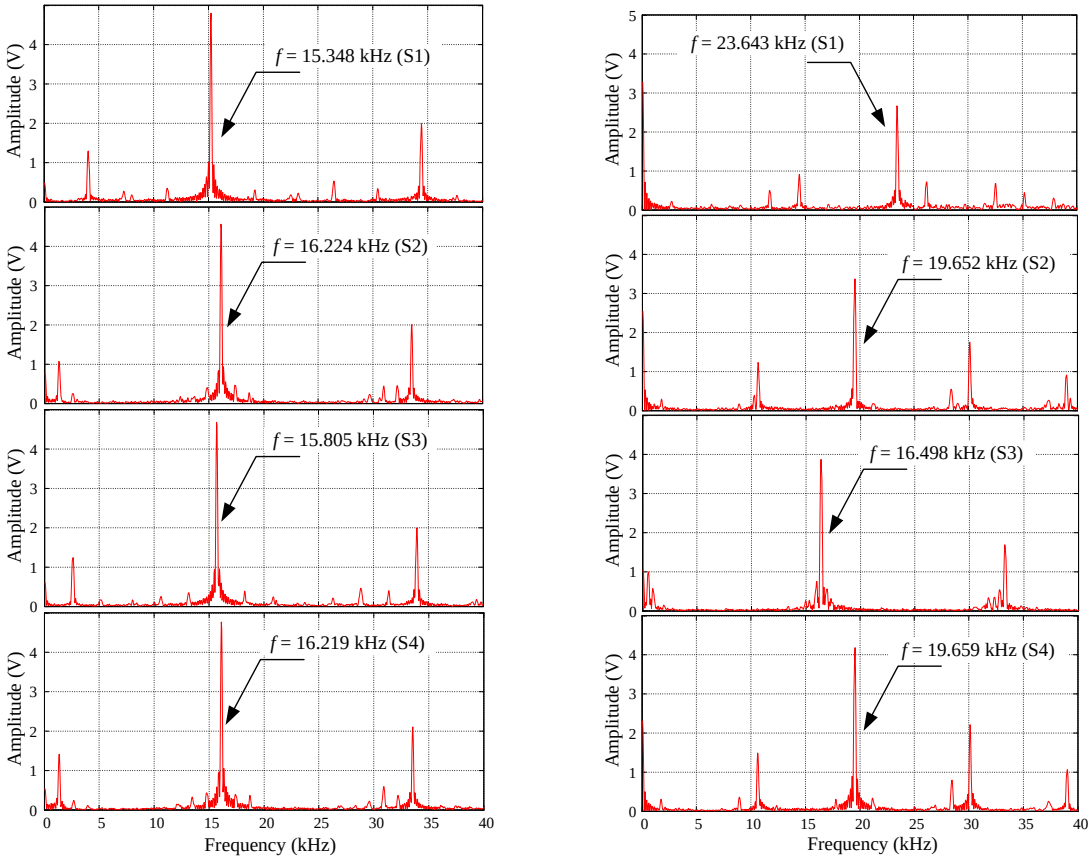

(a) (b)

Figure 9.12: Comparison of frequency domain from each Hall generator under the same specific conditions;
(a) The 20-mm diameter and 2-mm depth;
(b) The 20-mm diameter and 3-mm depth.

9.6 Error Analysis of Measurement

This section proposes the performance of the 4-crossing Hall sensor by considering each Hall generator that assembled the sensor module by comparing 10-mm and 20-mm diameter drilled hole with various depths; i.e. 0 mm, 1mm, 2 mm, and 3 mm. The results of the measurement can be used to guarantee the operation scope and limitations of the sensor module due to each Hall generator exhibiting the output signal which related to the dimension (size and depth) of the drilled hole. By the way, an experimental starting in this study will be performed by placing a Hall generator is named S1 at the centre position of the drilled hole.

Considering the measured results of the 4-crossing Hall sensor when measuring the 10-mm diameter drilled hole, it can be observed that the highest frequency was for the deepest hole (1 mm) which was the position of S1. The relationship between the frequency of the experiment and the width of the hole on the specimen surface is shown in Figure 9.13. On the other hand, the shallowest hole (0 mm) was at the position of S3. The positions of S2 and S4 exhibited the uniform frequency while implying the width of the drilled hole (chapter 5, section 5.4.2). The relationship between measurement results are shown in Table 9.1. The average of standard deviation from repeated measurements in order to test the repeatability of system which was equal to 0.007 kHz.

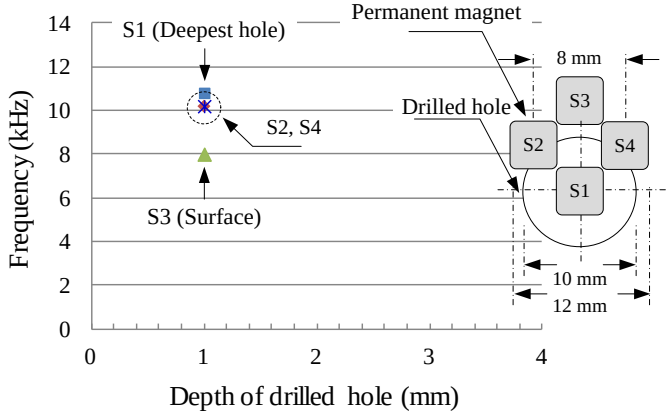

Figure 9.13: Relationship between frequency from each Hall generator measuring the hole with 10-mm diameter and 1-mm depth.

Table 9.1: Comparison of the results from each Hall generator measuring the hole with 10-mm diameter and 1-mm depth.

Hall generator	S1	S2	S3	S4
Output voltage (V)	2.01	1.9	1.5	1.91
Frequency (kHz)	10.811	10.193	8.01	10.204
SD of frequency (kHz)	0.011	0.005	0.006	0.004

Considering the relationship between the frequency and depth of drilled holes at 2 mm and 3 mm, it can be observed that the results from measurement were similar to that of the depth of a hole at 1 mm. The position of S1 will be exhibit the deepest hole in order to compare the level of depth with S3 (shallowest hole) while the position of S2 and S4 provided the same results, as both Hall generators (S2 and S4) were placed at the edge of drilled hole used for estimating the width of hole, as shown in Figure 9.14 and 9.15. Therefore, various by depths of holes are directly given in Table 9.2 and 9.3. The average standard deviation of different depths from repeated measurement in order to testing the repeatability of system was equal to 0.012 kHz and 0.009 kHz, respectively.

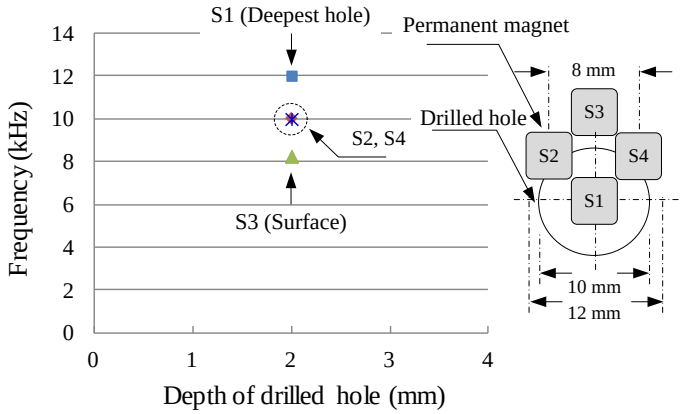

Figure 9.14: Relationship between frequency from each Hall generator measuring the hole with 10-mm diameter and 2-mm depth.

Table 9.2: Comparison of the results from each Hall generator measuring the hole with 10-mm diameter and 2-mm depth.

Hall generator	S1	S2	S3	S4
Output voltage (V)	2.26	1.86	1.55	1.86
Frequency (kHz)	12.02	10.025	8.254	9.996
SD of frequency (kHz)	0.02	0.01	0.004	0.013

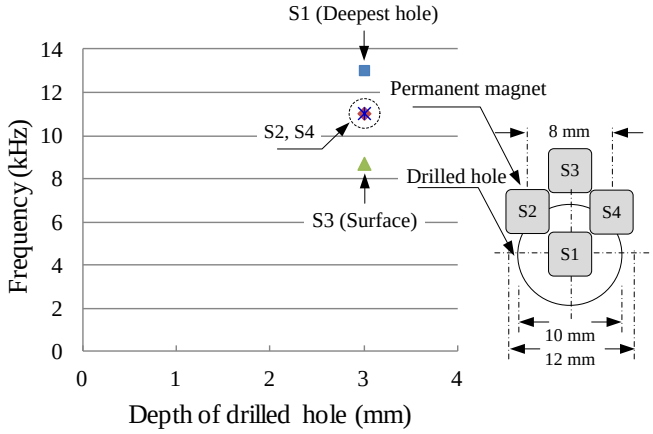

Figure 9.15: Relationship between frequency from each Hall generator measuring the hole with 10-mm diameter and 3-mm depth.

Table 9.3: Comparison of the results from each Hall generator measuring the hole with 10-mm diameter and 3-mm depth.

Hall generator	S1	S2	S3	S4
Output voltage (V)	2.45	2.04	1.62	2.05
Frequency (kHz)	13.038	11.041	8.727	11.05
SD of frequency (kHz)	0.016	0.013	0.003	0.005

Figure 9.16 shows the relationship of frequency from each Hall generator by comparing the results from measuring the drilled hole diameter at 10 mm with various depth of 1 mm, 2 mm, and 3 mm. From the results, it can be observed that S1 exhibited the deepest hole, S3 as reference value on the surface of test specimen. The position of S2 and S4 exhibited the uniform frequency, implying the width of drilled hole.

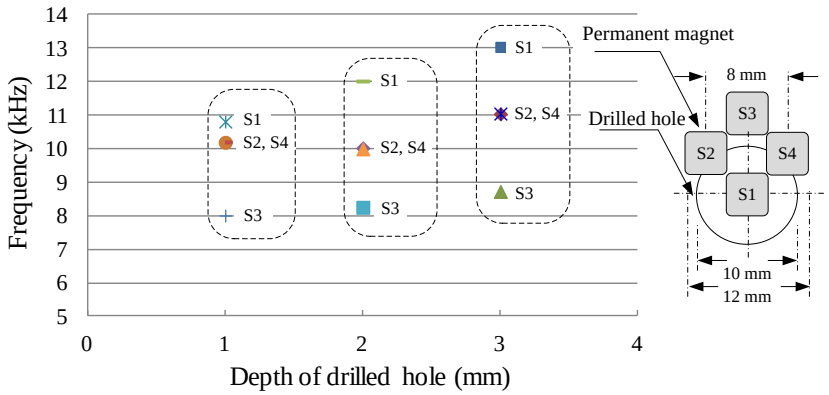

Figure 9.16: The relationship of frequency from each Hall generator at the holes with various depths (10-mm diameter).

Actually, the drilled hole with a diameter larger than a sensor module may cause errors in measurement. Especially, in case of the shallowest hole by 1 mm and 2 mm of depth with the same diameter of hole at 20 mm as shown in Figure 9.17 and 9.18. It can be noted that, the results from measurement can effectively provide the more accuracy at 3 mm of depth onward as shown in Figure 9.19. Therefore, the relationship of frequency and voltage signal from each Hall generator can be estimated to compare the level of depth with the standard deviation of frequency as shown in Table 9.4 - 9.6.

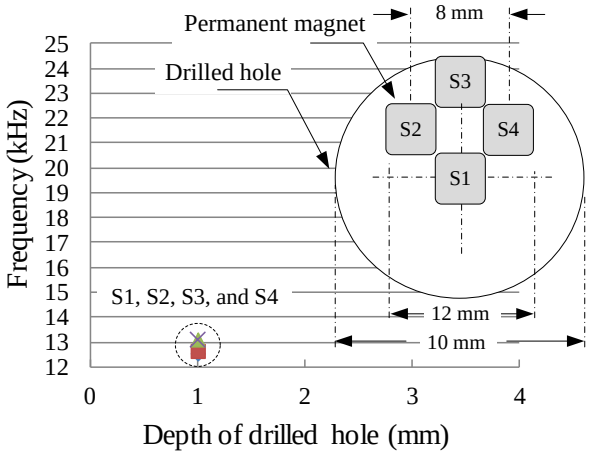

Figure 9.17: Relationship between frequency from each Hall generator measuring the hole with 20-mm diameter and 1-mm depth.

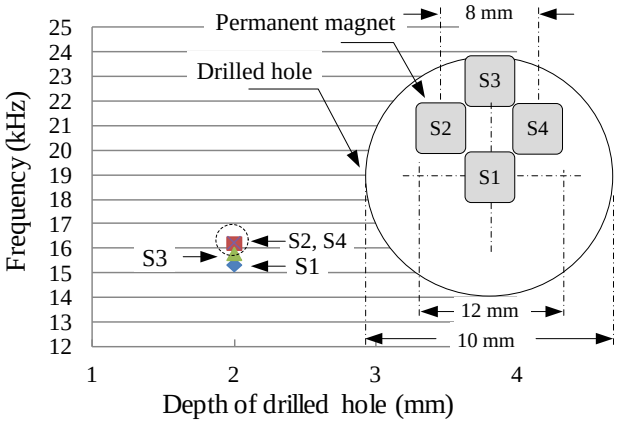

Figure 9.18: Relationship between frequency from each Hall generator measuring the hole with 20-mm diameter and 2-mm depth.

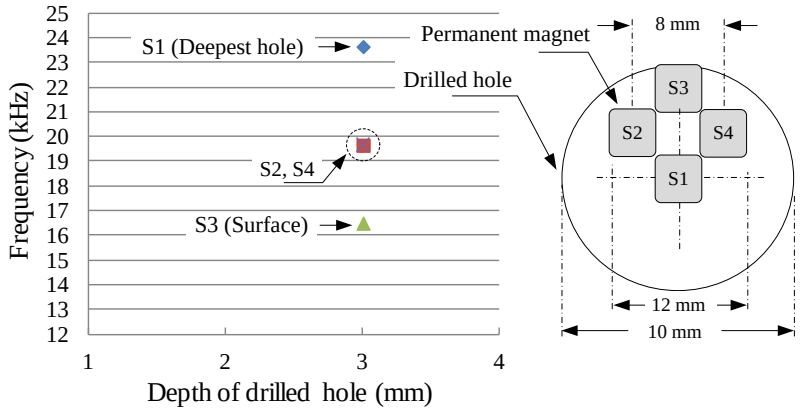

Figure 9.19: Relationship between frequency from each Hall generator measuring the hole with 20-mm diameter and 3-mm depth.

Table 9.4: Comparison of the results from each Hall generator measuring the hole with 20-mm diameter and 1-mm depth.

Hall generator	S1	S2	S3	S4
Output voltage (V)	2.34	2.44	2.42	2.44
Frequency (kHz)	12.552	12.65	13.111	13.099
SD of frequency (kHz)	0.002	0.024	0.006	0.01

Table 9.5: Comparison of the results from each Hall generator measuring the hole with 20-mm diameter and 2-mm depth.

Hall generator	S1	S2	S3	S4
Output voltage (V)	2.87	3.04	2.94	3.03
Frequency (kHz)	15.348	16.224	15.805	16.219
SD of frequency (kHz)	0.004	0.004	0.002	0.005

Table 9.6 Comparison of the results from each Hall generator measuring the hole with 20-mm diameter and 3-mm depth.

Hall generator	S1	S2	S3	S4
Output voltage (V)	4.4	3.67	3.13	3.68
Frequency (kHz)	23.643	19.652	16.498	19.659
SD of frequency (kHz)	0.005	0.004	0.004	0.008

Figure 9.20 - 9.22 shows the output signal in frequency of each Hall generator from experiments in specimens by comparing the results of drilled holes with diameters of 10 mm and 20 mm and various depths; i.e. 1 mm, 2 mm, and 3 mm, respectively. From the results of the experiment, it was found that frequency signals and voltage signals would be dependent on the dimension of drilled hole (diameter and depth) on the metal surface while the variation of output signals and will also be proportional to dimension of drilled holes. Therefore, development of a sensor module and signal conditioning in this study, which can be used in order to test metal imperfection are effectively and reliability.

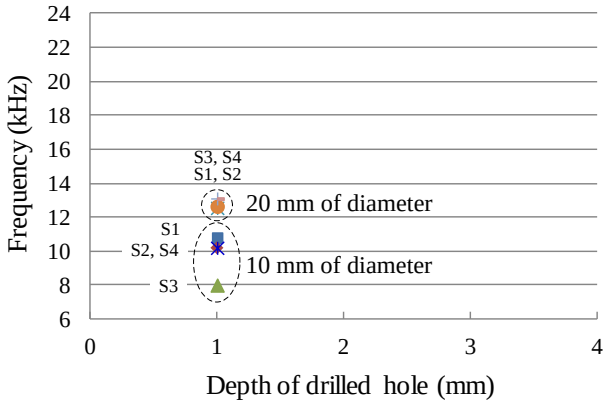

Figure 9.20: Comparison of frequency from each Hall generator at holes with the depth of 1 mm and the diameters of 10 mm and 20 mm.

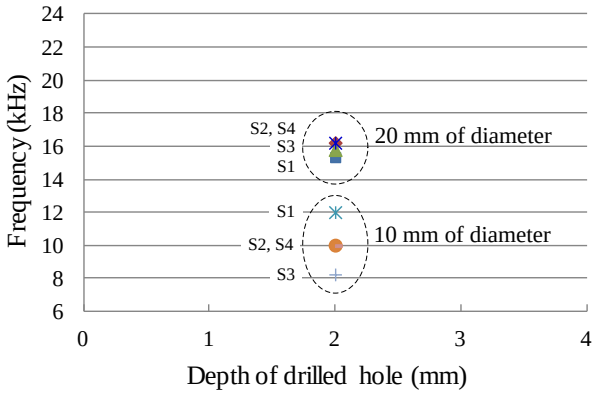

Figure 9.21: Comparison of frequency from each Hall generator at holes with the depth of 2 mm and the diameters of 10 mm and 20 mm.

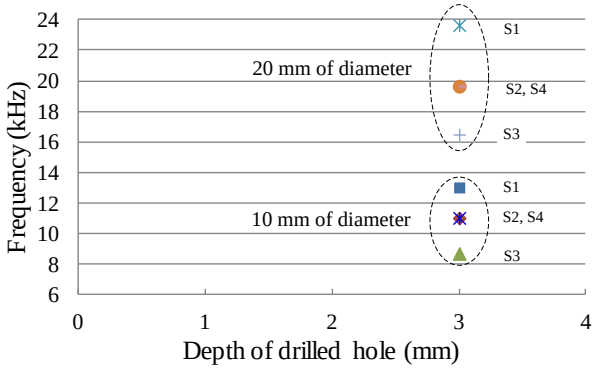

Figure 9.22: Comparison of frequency from each Hall generator at holes with the depth of 3 mm and the diameters of 10 mm and 20 mm.

From this experiment, it can be noted that the 4-crossing Hall sensor would be effective and appropriate for testing large holes and cracks. The application of several Hall generators which were installed together would benefit from determining the edge and the size of hole or crack of the target which can perform better than using only one sensor. Moreover, the individual output from each Hall generator could effectively provide the accurate position and diameter of drilled holes or fractures in materials.

9.7 Conclusion

The measurement of metal material imperfection based on frequency domain is one of non-destructive inspection. It was found that an analysis by frequency domain is the methodology which can be explicitly applied to detect the dimension of holes on a metal surface. In an experiment, the principle of frequency domain can precisely determine and distinguish the depth of drilled holes with 1 mm difference. It can be observed that, in the case of a large hole, 4-crossing Hall sensor would be most appropriate with optimum performance due to the smoothness and stability of output signals. The application of several Hall generators installed together would benefit from determining the edge and the size of hole of the materials which can perform better than using only one Hall generator. Therefore, the 4-crossing Hall sensor could exhibit high efficiency and reliability in measuring the drilled holes or the large fracture compared to single Hall sensor. This could contribute to the individual output from each Hall generator that could effectively provide the accurate position and diameter of drilled holes or fractures of materials.

Chapter 10

Performance Comparison of the New Sensor Module and the Electromagnetic Acoustic Transducer in NDT Measurement

10.1 Introduction

This chapter presents the completed experimental results to compare both performances of a special ultrasonic sensor and a new sensor module under the same measurement conditions in order to assess the effectiveness, the proper installation, the convenience of use, and the costs of both methods. A special ultrasonic sensor is generally called the Electromagnetic Acoustic Transducer (EMAT) which consists of a magnet and sensor coil. It was tuned to an ultrasonic wave with 1 MHz which can be injected and detected. The sensor coils were separated from the transmitter and the receiver and placed at two surfaces on the specimen to set the Lorentz force in a parallel direction of the specimen surfaces [5, 46]. This type of EMAT can generate the transverse wave (shear ware) for analyzing the wavelength of measurement [47]. In application, the output voltage from a new sensor module then amplified the difference to gain 20 times and was converted to the frequency domain for a better resolution at the specific set point of 8 kHz.

10.2 The Objectives

The conventional Hall Effect sensor is one of the appropriate methodologies for applying to the inspection of metal material completion. Normally, an analysis of output signal from a new sensor module can be analyzed and noticeably determined the small change of signal. Design of a sensor module considering the position of Hall generator and permanent magnet in this study aims to compare the efficiency of each sensor system between the new sensor module and the EMAT [5] method in terms of precision, reliability, suitability of drill holes detection under the same experimental conditions. Also, the simplicity of installation, system, and the measurement process will be observed at a lower cost. However, the test specimen was the 28-mm metal with the drilled hole diameters of 3 mm,

10 mm, and 20 mm. Each hole diameter with different depths, i.e. 1 mm, 2 mm, 3 mm, 23 mm, 25 mm and 26 mm, was prepared respectively. Therefore, test specimens considered the size and the depth of drilled holes on specimen surfaces as a case study to compare the output signal response in terms of efficiency and the measurement ability of both methodologies under specific conditions.

10.3 The Basic Idea

The basic system of EMATs requires the magnetic field to stimulate the sensor coil (transmitter and receiver). The driving of electromagnets would require the current source of 1 A to 10 A. The magnet as a stimulator would require the magnetic flux density and should be started from 0.2 T onward. However, driving a sensor coil to generate the specific frequency current would also be enhanced by a pulser. This pulser must be able to supply a high electric current to the sensor coil from about 1 A to 50 A, and the response signal from the receiver coil should be transmitted via low pass filter circuit and amplifier for analysis.

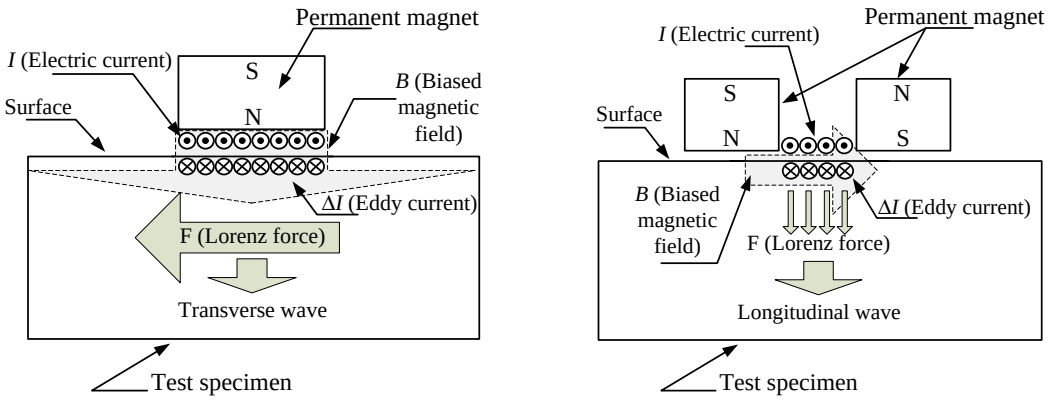

Figure 10.1: An EMAT for an ultrasonic wave the travels to vertical direction from the surface of a metal material;
(a) Transverse wave generated;
(b) Longitudinal wave generated.

The basic idea is to give as same force pattern as the oscillation pattern of an ultrasonic wave on the surface of the metal. This requires forces at every half wavelength of an ultrasonic wave that could be generated as illustrated in Figure 10.1, where Figure 10.1 (a) is the characteristic of a transverse wave, whereas the direction of Lorentz force is parallel to the surface of a metal surface. Figure 10.1 (b) shows the characteristics of a longitudinal

wave, while the direction of Lorentz force is vertical to the surface of a metal surface [48] where the wavelength also can be calculated by Equation 10-1.

$$\lambda = v/f \tag{10-1}$$

10.4 The EMAT Method

Test of specimen using ultrasonic wave based on EMAT method was performed by first determining the appropriate frequency (f = 1 MHz in this study). Transmitter and receiver were formed by oval coil as shown in Figure 10.2 and the characteristics of sensor coils as given in Table 10.1.

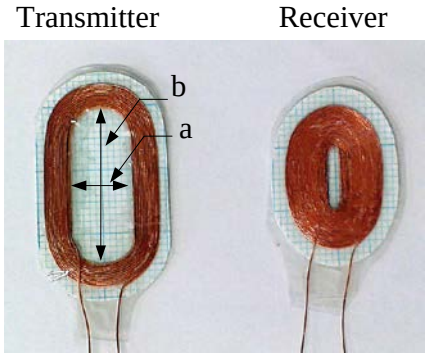

Figure 10.2: Sensor coils for experiment.

Table 10.1: Characteristics of sensor coils (transmitter and receiver) at 1 MHz.

Sensor coil	a (mm)	b (mm)	Turns	Diameter of wire (mm)	Impedance (Ω)
Transmitter	10	25	12	0.25	1.5432
Receiver	2	10	25	0.2	2.3236

Since the ultrasonic wave in this study was generated by EMAT method, therefore the major components would consist of sensor coils and magnetic flux density that used to stimulate the induction in the coils to generate the specific frequency. The operation of the EMAT method in order for most efficiency needs to be considered as the density of magnetic flux which was generated from the permanent magnets. In this study, the permanent magnets with the width and the length of 20 mm, and 10 mm of thickness were used and the magnetic flux density is equal to 0.5 T as a stimulator to both sensor coils; transmitter and receiver. Figure 10.3 illustrates the testing of the density of the magnetic flux of each point on the surface of permanent magnet by the fluxmeter. It was found that, the density of magnetic flux at each point would be unequal. Normally, the basic system of

EMAT can be divided into a permanent magnet used to stimulate the sensor coils into two, a transmitter coil and a receiver coil. Figure 10.4 shows the results of measurement in order to compare the magnetic flux density between the used single permanent magnet and the double permanent magnet. From the experimental results, it can be observed that the magnetic flux density in all points on the surface of double permanent magnet was found to exhibit high intensity rather than the single permanent magnet, which would cause the average value to be about 17.94 %. Figure 10.5 shows the difference in magnetic flux density between the double permanent magnet and the single permanent magnet on the transmitter, which would exhibit an average of about 0.09 T.

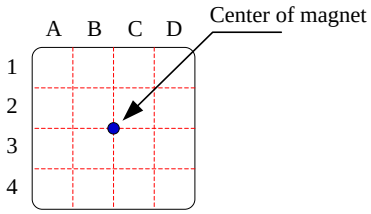

Figure 10.3: Testing points of a permanent magnet.

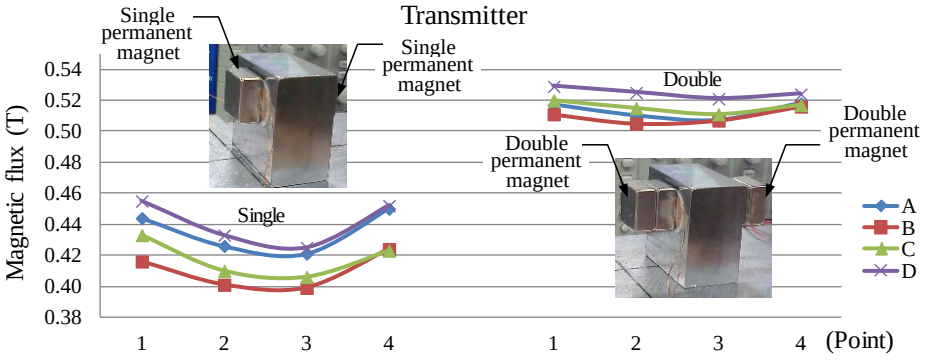

Figure 10.4: Comparison of the single and the double permanent magnet with transmitter coil.

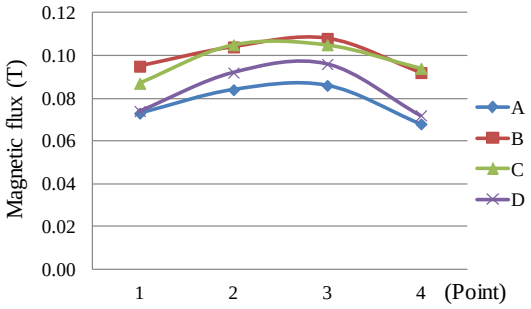

Figure 10.5: Different result between the single and the double permanent magnet (transmitter).

Figure 10.6 shows the experimental of permanent magnet used for stimulated of receiver coil in order to compare single permanent magnet and double permanent magnet. From experiment, it was found that the magnetic flux density at all points on the surface of double permanent magnet was found to exhibit high intensity unlike than single permanent magnet, which was similar to that of the permanent magnet in the transmitter, which would cause the average value to be about 17.23 %. Figure 10.7 shows the difference in the magnetic flux density between the double permanent magnet and the single permanent magnet on the receiver coil would exhibit an average of about 0.086 T. Moreover, the density of magnetic flux was exhibited most intensely at the centre of both magnets surfaces, as shown in Figure 10.8.

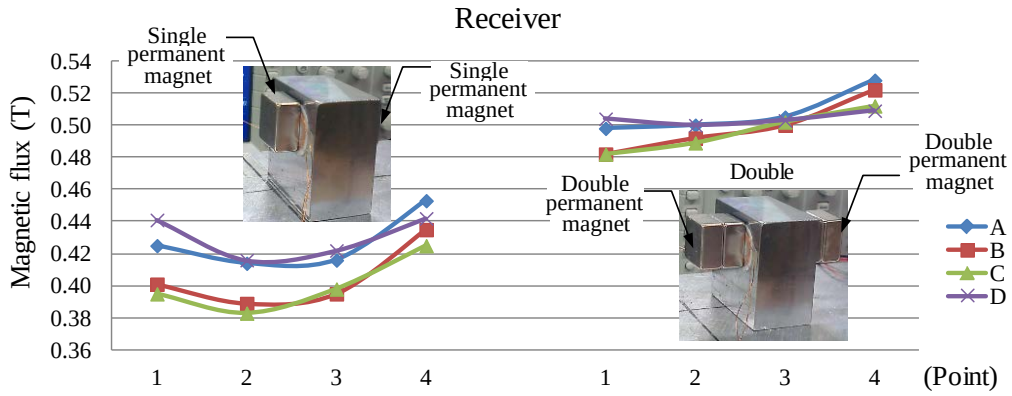

Figure 10.6: Comparison of the single and the double permanent magnet with receiver coil.

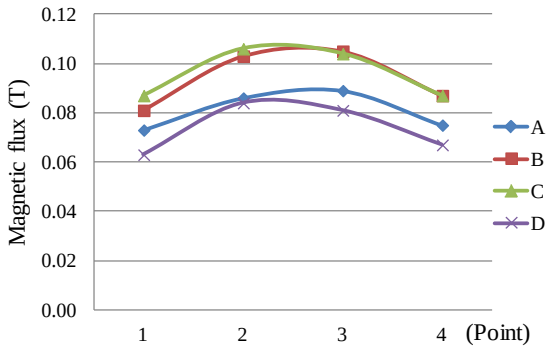

Figure 10.7: Different result between the single and the double permanent magnet (receiver).

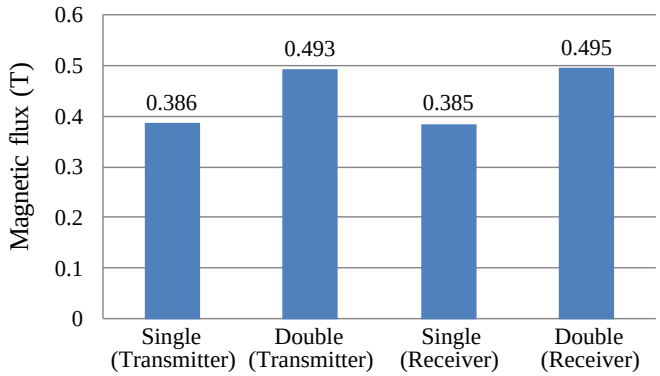

Figure 10.8: Comparison of the magnetic flux at the centre of permanent magnet.

Therefore, we can specify that the double permanent magnet will increase the density of the magnetic flux which was generated by the permanent magnet. The measurement system can be improved in terms of sensitivity and the ability to measuring the small size of a specimen in order to guarantee enhancing the performance of the sensor module and the reliability of the measurement results.

10.5 Experiment Setup

The experiment in this chapter can be divided into two sections; experiment with the new sensor module, and the experiment with EMAT, as follows:

10.5.1 Experiment of New Sensor Module

The new sensor module was placed at nine given points on the surface of the test specimen. The five-times repeated measurement was performed to assess the repeatability and reliability of the sensor system, starting from point A to point I. However, the output voltage from a new sensor module was then amplified by the difference to gain by 20 times and being converted to the frequency in the form of time domain by voltage to the frequency converter circuit. The set point frequency of voltage of 1.5 V was 8 kHz. The diagram of the experiment was given in chapter 9, section 9.3.

10.5.2 Experiment of EMAT

The specimens used in this study were steel cubes (48 mm of width and length, and 28 mm of thickness) with a density of 7.8 g/cm^3. The acoustic velocity of the transverse wave was 3.23 km/s and acoustic impedance was 450×10^4 g/cm^{2}s. At the centre of each cube, there was a 3 mm drilled hole at different depths (3 mm, 23 mm, 25 mm, and 26 mm). Nine points at the centre of specimen surface with 5 mm of distance between each point were determined. A test of a specimen using an ultrasonic wave based on the EMAT method [47]

was performed by determining the appropriate frequency (f = 1 MHz in this study). The sensor coil was used with the permanent magnet which generates the magnetic flux of 0.5 T, which was appropriate and sufficient for the testing specimen. However, driving a transmitter coil to generate the specific frequency would also be enhanced by a pulser. Each point was repeatedly tested 3 times starting from point A to point I to assess the repeatability and reliability of the sensor. The frequency signal from the experiment was finally filtered by a low pass filter before gaining and analyzing, respectively. A diagram of this experiment is illustrated in Figure 10.9.

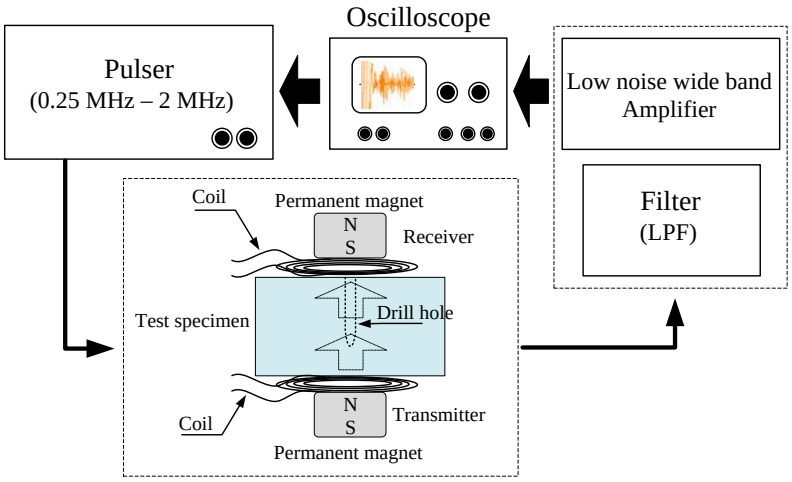

Figure 10.9: Experimental diagram of overall system for the EMAT.

10.6 Empirical Analysis

A test of a specimen in this study considered four different hole depths; namely, 3 mm, 23 mm, 25 mm, and 26 mm with the same diameter of drilled hole (3 mm) located at the centre of the same material property and dimensions, using only a single Hall sensor. The results were then compared to those of an ultrasonic wave generated from EMAT under the same conditions.

10.6.1 Empirical Analysis of the New Sensor Module in Frequency Domain

The experimental new sensor module will perform by converted the frequency in the form of the time domain into the frequency domain [39, 43]. Figure 10.10 shows the frequency of the 8.284 kHz from experiment of the specimen at point E with a depth of 3 mm. Considering the frequency converted from output voltage by the voltage to the frequency converter circuit, it can be noted that the relationship of the frequency variation and the depth of hole is similar to that of the voltage. Therefore, the frequency obtained from

measurement would exceed the set point (8 kHz) when measuring the specimen with a deeper hole depth as shown in Figure 10.11. Normally, we would consider only the frequency wave which exhibits the highest amplitude. The rest is harmonic or noise can be ignored.

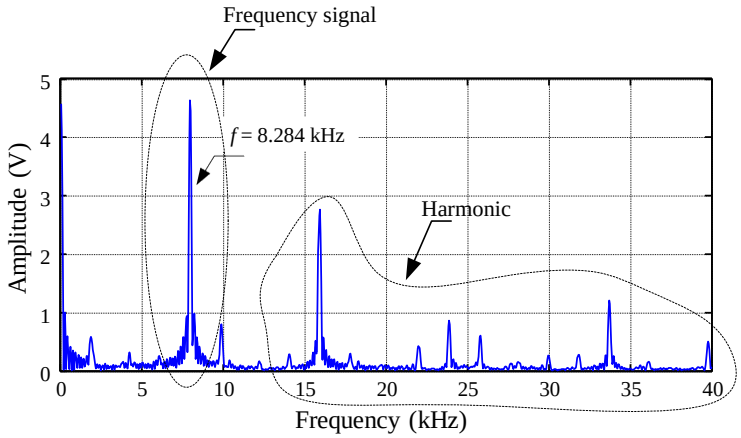

Figure 10.10: Waveform of frequency domain from experiment of specimen at point E with the depth of 3 mm.

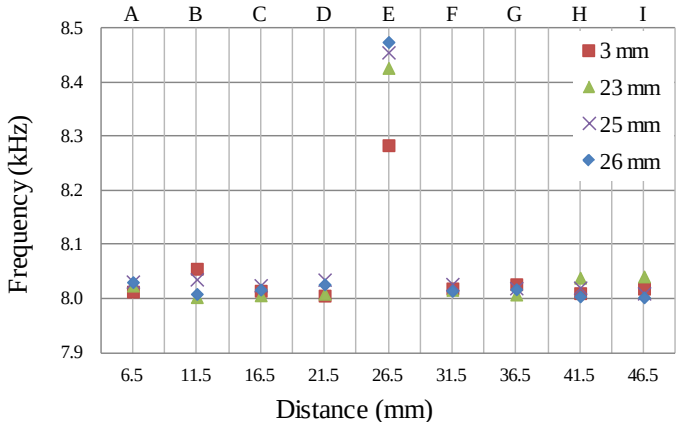

Figure 10.11: Frequency of output voltage from a new sensor module obtained from experiment of specimen with various depths.

A comparison of the output voltage and the frequency from experiments in 3-mm diameter holes with various depths, i.e. 3 mm, 23 mm, 25 mm, and 26 mm is illustrated in Figure 10.12 - 10.15. Considering point E, it can be observed that the output voltage of a new sensor module analyzed in the frequency domain would provide high resolution compared to voltage analysis. Furthermore, from the experiment results, it was found that the frequency signal variation and voltage signal from a new sensor module would be varied with regard to the depth of the drilled hole in the same direction.

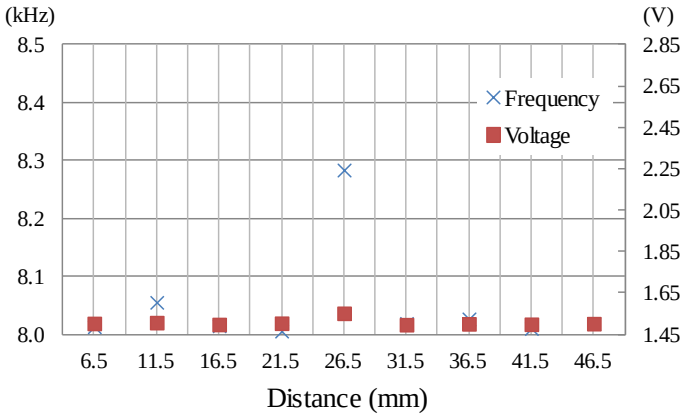

Figure 10.12: Comparison of output voltage and frequency in case of the 3-mm hole depth.

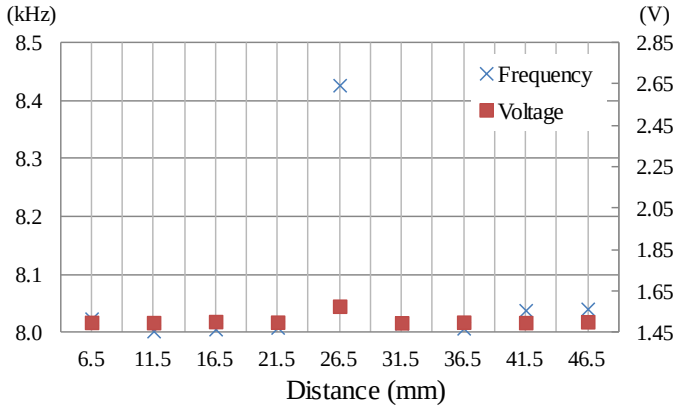

Figure 10.13: Comparison of output voltage and frequency in case of the 23-mm hole depth.

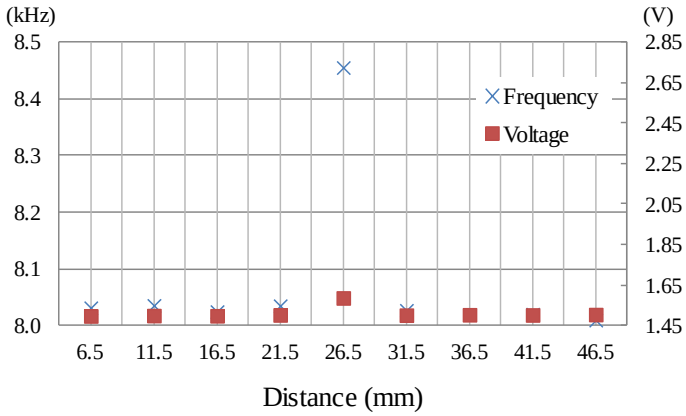

Figure 10.14: Comparison of output voltage and frequency in case of the 25-mm hole depth.

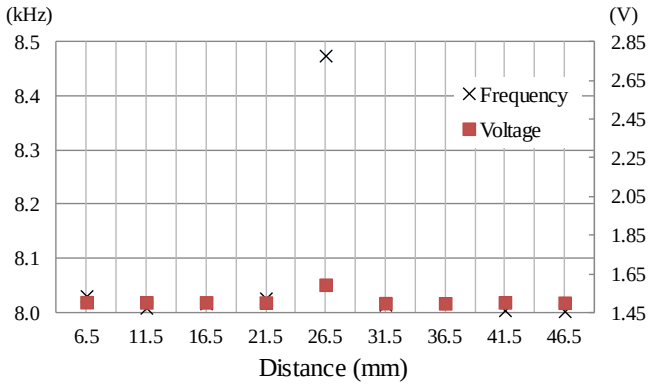

Figure 10.15: Comparison of output voltage and frequency in case of the 26-mm hole depth.

10.6.2 Empirical Analysis of the EMAT

In case of empirical study of the EMAT, the both sensor coils were placed at nine given points similarly to that of new sensor module. The sensor coil was used with the permanent magnet with the magnetic flux of 0.5 T, which was appropriate and sufficient for the testing specimen. In experiment, the sensor coil and permanent magnet were placed at nine specific points as shown in Figure 10.16.

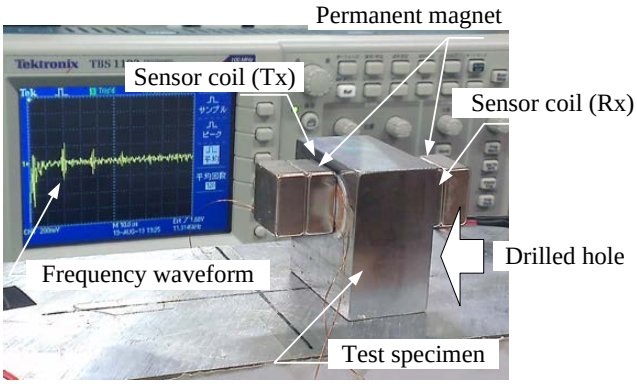

Figure 10.16: Placement of sensor coil and permanent magnet.

From the results of EMAT experiment at nine given points, with 28 mm of distance between transmitter and receiver, it was observed that at point E, the centre of specimen with drilled hole would respond differently to the measurement. The frequency waveform from measurement of 3-mm diameter hole with various depths (3 mm, 23 mm, 25 mm, and 26 mm) as illustrated in Figure 10.17 - 10.20. From repeated measurement at each given point starting from point A to point I to assess the reliability of the system and the variation of ratio between signal per noise (S/N) at different hole depths, it can be noted that the best ratio of signal per noise was at the reflecting range of wave at 2nd cycle. A comparison of the ratio at different depths is as shown in Figure 10.21.

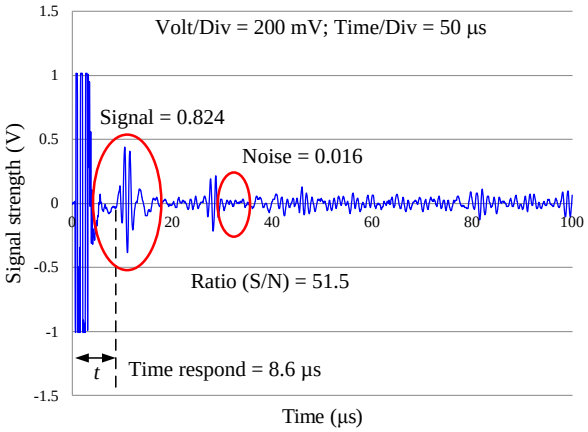

Figure 10.17: Waveform of ultrasonic wave from experiment of specimen at point E with the hole depth of 3 mm.

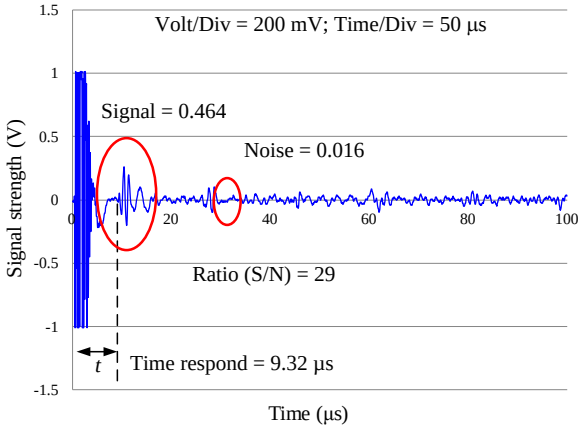

Figure 10.18: Waveform of ultrasonic wave from experiment of specimen at point E with the hole depth of 23 mm.

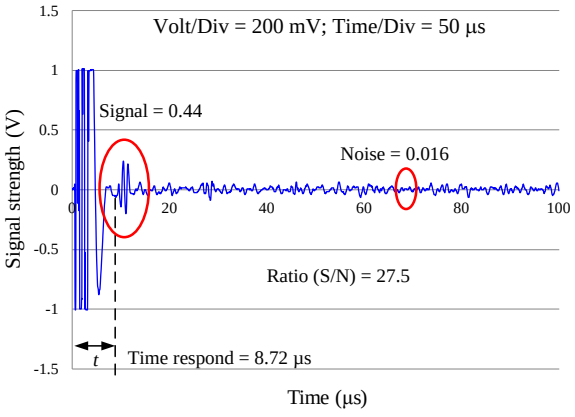

Figure 10.19: Waveform of ultrasonic wave from experiment of specimen at point E with the hole depth of 25 mm.

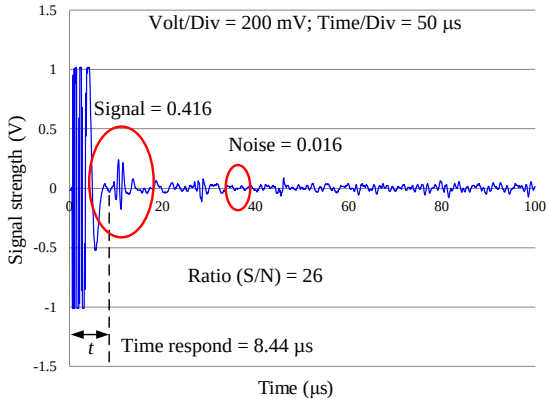

Figure 10.20: Waveform of ultrasonic wave from experiment of specimen at point E with the hole depth of 26 mm.

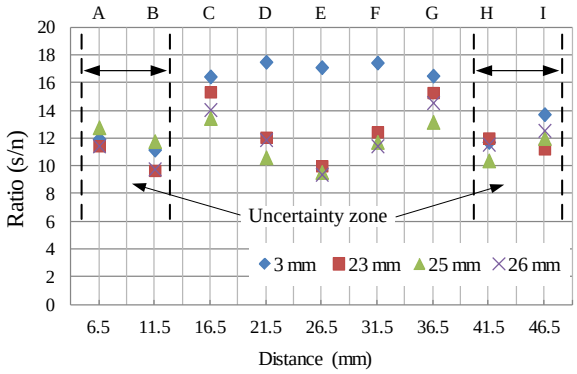

Figure 10.21: Comparison of ratio from experiment of specimen with various hole depths.

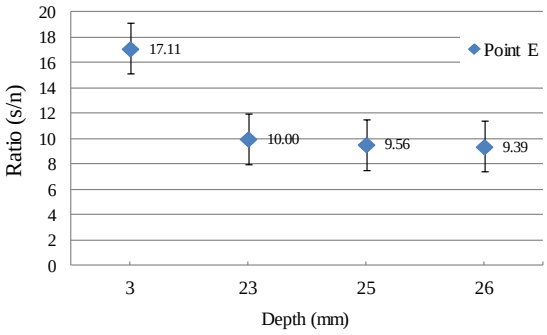

Figure 10.22: Comparison of ratio at point E.

From experiment, the uncertainty area was observed at point A to point B and point H to point I. The results from these points cannot be used for analysis as the sensor coils, both transmitter and receiver, were not fully placed on sensing area of coil. Figure 10.22 illustrates the comparison of the ratio only at point E (the centre of specimen) with various depths of hole. Therefore, the ratio at 3 mm, 23 mm, 25 mm, and 26 mm of depth were 17.11, 10, 9.56, and 9.36, respectively with a standard deviation of 0.49.

However, from an analysis of the ratio from experiments at various depths, it can be observed that the ratio from measurement would be inversely proportional to the depth as the rest of area's thickness having decreased, which causes poor reflection. Considering the time response from the wave reflection by comparing the results from the specimen with 4 drilled holes with those in the calculation (8.669 μs) to estimate the error and reliability of the system, the error from the measurement was about 4.51% as shown in Figure 10.23. Figure 10.24 shows the comparison of time responding specifically by the centre of 4 drilled holes and that by calculation using the specimen without a hole.

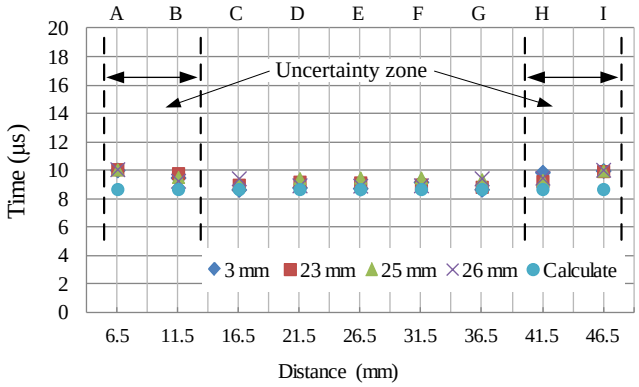

Figure 10.23: Comparison of time response from test specimen and that from calculation.

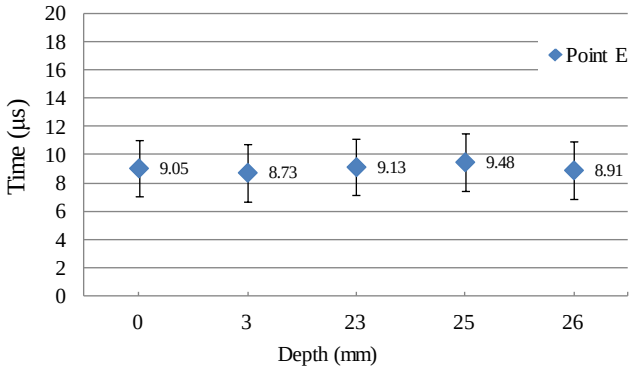

Figure 10.24: Comparison of time response at point E.

A comparison of the results from the testing of specimens using the new sensor module and EMAT, the results from EMAT are in the form of time response while those from the new sensor module are in the frequency domain. In this study, both methods were found applicable in the measurement of the specimen with the thickness of 28 mm. However, the application of EMAT would not be convenient for installation due to small size of the specimen compared to that of a new sensor module.

10.7 Uncertainty and Statistical Analysis

Analysis of the new sensor module based on frequency signal and EMAT method will be considering to repeatability of measurement [34] in the same experimental conditions, starting from point A to point I on the test specimen surface.

10.7.1 Repeatability of the New Sensor Module

An experiment for five-times repeated measurement was performed to assess the repeatability and reliability of sensor module used by a new sensor module as sensor device starting from point A to point I on the test specimen surface with various depths, as shown in Table 10.2 - 10.5. The average standard deviation of different depths from repeated measurement of each testing point on the surface of test specimens (3 mm, 23 mm, 25 mm, and 26 mm) were about 0.012, 0.011, 0.014, and 0.012, respectively. Therefore, the average standard deviation of any depth of drilled hole was calculated as being about 0.012 being regarded as very low value.

Table 10.2: Repeated measurement of each point with a 3-mm hole depth.

Times number	Test point (kHz)								
	A	B	C	D	E	F	G	H	I
1	8.005	8.094	8.009	7.998	8.288	8.044	8.033	8.005	8.031
2	8.006	8.051	8.032	8.007	8.283	8.006	8.033	8.01	8.031
3	8.019	8.049	8.028	8	8.286	8.007	8.041	8.021	8.004
4	8.008	8.043	8.003	8.01	8.281	8.036	8.008	8.014	8.015
5	8.028	8.041	8.001	8.013	8.28	8.003	8.018	8.002	8.01
Average	8.013	8.055	8.015	8.006	8.284	8.019	8.027	8.01	8.019
SD	0.01	0.022	0.014	0.006	0.003	0.019	0.013	0.008	0.012

Table 10.3: Repeated measurement of each point with a 23-mm hole depth.

Times number	Test point (kHz)								
	A	B	C	D	E	F	G	H	I
1	8.024	8.004	8.009	8.001	8.428	8.018	8.014	8.067	8.055
2	8.019	7.99	8.009	8.029	8.429	8.016	8.004	8.022	8.078
3	8.016	8.012	7.998	8.01	8.421	8.020	8.004	8.025	8.063
4	8.029	8.009	8.011	8.001	8.43	8.020	8.006	8.055	8.004
5	8.033	7.999	8.004	8.006	8.425	8.008	8.011	8.025	8.006
Average	8.024	8.003	8.006	8.009	8.426	8.016	8.008	8.039	8.041
SD	0.007	0.009	0.005	0.011	0.004	0.005	0.004	0.021	0.034

Table 10.4: Repeated measurement of each point with a 25-mm hole depth.

Times	Test point (kHz)								
number	A	B	C	D	E	F	G	H	I
1	8.02	8.002	8.013	8.028	8.451	8.03	8.021	8.027	8.03
2	8.046	8.07	8.032	8.07	8.453	8.017	8.015	8.027	8.005
3	8	8.059	8.038	8.019	8.454	8.01	8.016	8.019	8.005
4	8.051	8.026	8.02	8.034	8.459	8.048	8.013	8.005	8.008
5	8.041	8.022	8.021	8.025	8.459	8.03	8.032	8.024	8.001
Average	8.032	8.036	8.025	8.035	8.455	8.027	8.02	8.02	8.01
SD	0.021	0.028	0.01	0.02	0.003	0.015	0.008	0.009	0.011

Table 10.5: Repeated measurement of each point with a 26-mm hole depth.

Times	Test point (kHz)								
number	A	B	C	D	E	F	G	H	I
1	8.004	8.009	8.017	8.037	8.478	8.005	8.03	8.002	8.002
2	8.075	8.003	8.01	8.062	8.472	8.016	8.002	8.002	8
3	8.029	8.001	8.019	8	8.471	8.013	8.011	8	8.014
4	8.041	8.02	8.011	8.027	8.473	8.005	8.018	8.014	8.008
5	8.003	8.012	8.031	8.009	8.478	8.034	8.026	8.006	7.99
Average	8.031	8.009	8.017	8.026	8.474	8.015	8.017	8.004	8.002
SD	0.03	0.007	0.009	0.025	0.003	0.012	0.011	0.006	0.009

10.7.2 Repeatability of the EMAT Method

An experiment with the EMAT method to assess the repeatability and reliability of system was divided into two sections. The first was a variation of the ratio between signal per noise (S/N) and the second is a time response, which was conducted under conditions similar to that of the new sensor module.

10.7.2.1 Performance of the EMAT in Signal Ratio

In an experiment, three-times repeated measurement was performed to assess the repeatability and reliability of a measurement system using the EMAT method in case the variation of ratio between signal per noise at different hole depths, starting from point A to point I on the test specimen surface as shown in Table 10.6 - 10.9. The average standard deviation of different depths from repeated measurement of each testing point on the surface of test specimen (3 mm, 23 mm, 25 mm, and 26 mm) were about 0.638, 0.455, 0.963, and 0.567, respectively. The average standard deviation at any depth of drilled hole

was calculated at about 0.656, which is an alternative to using a new sensor module as a sensor device. Therefore, the generation of an ultrasonic wave using EMAT method would not be suitable for a small specimen. This means that the test specimen should have an adequately measured area for fully installing sensor coils and permanent magnets on the surface.

Table 10.6: Repeated measurement of each point using EMAT to assess the variation of ratio with a 3-mm hole depth.

Times	Test point (S/N)								
number	A	B	C	D	E	F	G	H	I
1	12.333	9.5	16.667	16.833	17.500	17.167	17.833	12.000	14.167
2	11.667	12.333	16.167	17.833	17.167	18.000	15.833	11.500	14.167
3	11.833	11.667	16.500	17.833	16.667	17.167	15.833	11.667	12.833
Average	11.944	11.167	16.444	17.500	17.111	17.444	16.500	11.722	13.722
SD	0.347	1.481	0.255	0.577	0.419	0.481	1.155	0.255	0.77

Table 10.7: Repeated measurement of each point using EMAT to assess the variation of ratio with a 23-mm hole depth.

Times	Test point (S/N)								
number	A	B	C	D	E	F	G	H	I
1	11.5	9.833	15.167	12.167	10.333	14	15.833	12	11.333
2	11.667	9.5	16.167	12.167	10	11.833	14.833	12.167	11.5
3	11.167	9.667	14.667	11.833	9.667	11.5	15.167	11.833	10.833
Average	11.444	9.667	15.333	12.056	10	12.444	15.278	12	11.222
SD	0.255	0.167	0.764	0.192	0.333	1.357	0.509	0.167	0.347

Table 10.8: Repeated measurement of each point using EMAT to assess the variation of ratio with a 25-mm hole depth.

Times	Test point (S/N)								
number	A	B	C	D	E	F	G	H	I
1	15.667	12.167	12.333	10.167	10.167	11	14.333	11	11.333
2	11.167	12.167	13.5	10.667	9.167	11.5	12.333	9.5	11.833
3	11.5	11	14.5	11	9.333	12.667	12.833	10.667	12.833
Average	12.778	11.778	13.444	10.611	9.556	11.722	13.167	10.389	12
SD	2.507	0.674	1.084	0.419	0.536	0.855	1.041	0.788	0.764

Table 10.9: Repeated measurement of each point using EMAT to assess the variation of ratio with a 26-mm hole depth.

Times number	Test point (S/N)								
	A	B	C	D	E	F	G	H	I
1	10.833	10.667	13.5	11.667	8.667	11.667	15	11.333	13
2	12.333	9.5	13.167	12	9.5	10.833	13.5	11.667	12.667
3	11.167	9.167	12.5	12	10	11.833	15.167	11.667	12
Average	11.444	9.778	13.056	11.889	9.389	11.444	14.556	11.556	12.556
SD	0.788	0.788	0.509	0.192	0.674	0.536	0.918	0.192	0.509

10.7.2.2 Performance of the EMAT in Time Response

Finally, considering the time response from repeated measurement with various hole depths on the surface of test specimen as shown in Table 10.10 - 10.13, the average standard deviation of different depths from repeated measurement of each testing point on the surface of test specimen were about 0.117, 0.306, 0.077, and 0.184 with the average standard deviation by calculation at any depth of any drilled hole was about 0.656.

Table 10.10: Repeated measurement of each point using EMAT to assess the variation of time response with a 3-mm hole depth.

Times number	Test point (μs)								
	A	B	C	D	E	F	G	H	I
1	10.04	9.36	8.6	8.76	8.76	9.36	8.64	9.96	10
2	10	9.56	8.52	8.76	8.64	8.8	8.64	9.56	10
3	10	9.52	8.8	8.84	8.8	9.36	8.68	10.04	9.92
Average	10.013	9.48	8.64	8.787	8.733	9.173	8.653	9.853	9.973
SD	0.023	0.106	0.144	0.046	0.083	0.323	0.023	0.257	0.046

Table 10.11: Repeated measurement of each point using EMAT to assess the variation of time response with a 23-mm hole depth.

Times number	Test point (μs)								
	A	B	C	D	E	F	G	H	I
1	10.08	10	8.76	10.04	9.32	9.52	8.8	9.52	9.92
2	10.04	10	9.36	8.76	8.72	8.76	8.84	9.36	9.88
3	10.08	9.36	8.8	8.76	9.36	8.68	8.84	8.8	10
Average	10.067	9.787	8.973	9.187	9.133	8.987	8.827	9.227	9.933
SD	0.023	0.37	0.335	0.739	0.359	0.464	0.023	0.378	0.061

Table 10.12: Repeated measurement of each point using EMAT to assess the variation of time response with a 25-mm hole depth.

Times number	Test point (μs)								
	A	B	C	D	E	F	G	H	I
1	10.04	9.52	9	9.52	9.56	9.56	9.36	9.36	10
2	10.04	9.52	9	9.52	9.56	9.56	9.36	9.36	10
3	10.08	9.52	9.2	9.28	9.32	9.32	9.36	9.2	9.92
Average	10.053	9.52	9.067	9.44	9.48	9.48	9.36	9.31	9.973
SD	0.023	0	0.115	0.139	0.139	0.139	0	0.0924	0.046

Table 10.13: Repeated measurement of each point using EMAT to assess the variation of time response with a 26-mm hole depth.

Times number	Test point (μs)								
	A	B	C	D	E	F	G	H	I
1	10.04	9.36	9.56	9.08	9.56	8.56	9.28	9.52	10
2	10.08	9.04	9.36	8.8	8.4	9.16	9.6	9.52	10.04
3	10.08	9.36	9.36	8.92	8.76	9.08	9.4	9.36	10.04
Average	10.067	9.253	9.427	8.933	8.907	8.933	9.427	9.467	10.027
SD	0.023	0.185	0.115	0.140	0.594	0.326	0.162	0.092	0.023

10.8 Conclusion

From the experiment with proximity sensors, namely EMAT and the new sensor module under the same conditions in order to compare efficiency, it can be observed that the ultrasonic wave generated by using the EMAT method would not be appropriate for small specimens. Therefore, the tested specimen should have an adequate area for fully placing sensor coils and permanent magnets in the sensing area. However, in this study, the specimen that caused the uncertainty of the measurement and high errors was small. In particular, there were errors at point A, point B, point H, and point I. Compared to the new sensor module, the results from a new sensor module were found to exhibit high accuracy and reliability with lower errors (less than 0.24 %) and standard deviation (about 0.014) in the measurement of small specimens. Moreover, the higher resolution of measurement at each position was observed due to a smaller size of a new sensor module as well as ease of installation, operation, and measurement compared to EMAT. However, the difficulty of measurement using a new sensor module would involve an inability to measure the thickness of the tested specimen, unlike the measurement using EMAT which can be

performed with high accuracy and reliability. Moreover, use of the new sensor module has benefits over that of the EMAT method due to there being less complexity in the system, lower costs and an easier and more convenient installation.

Chapter 11

Conclusions

11.1 Conclusion

The main findings of the study and conclusions addressing the research questions and objectives are summarised in this chapter. Some recommendations are also provided for further study of industrial application of a new sensor module in several variables measurement.

The usability of industrial instruments to be effectively with the accuracy, precision, and reliability would be depended on several environmental factors such as the variation of temperature, vibration in areas of measurement, and also the selection of equipment could not be reasonable for measuring some variables. These factors indirectly impacted on reliability of instruments and system. Furthermore, the improvement of measuring system to enhance the performance of the sensor device, namely a Hall Effect sensor, in this study may involve developing the sensor module in order to be suitable for detection and measuring the several variables in the industrial sector based on the principles of a Hall Effect sensor. Furthermore, an improvement of the measuring system to enhance the performance of the sensor device, namely Hall Effect sensor, in this study will consider developing the sensor module in order for it to be suitable for detection and measuring the several variables in industrial sector based on the principles of the Hall Effect sensor. This would including improvements in signal conditioning in order to processing the output signal and distinguishing the signals which have little variation.

11.2 Development of a New Sensor Module

Overall content in this study can be summarized in terms of concepts that are helpful for improvement and development of a conventional Hall Effect sensor as a new non-destructive measurement by proposing the algorithms and methodologies of a Hall Effect sensor. These studies can be divided into three parts:

The first presents the usability of a new sensor module to detect and measure several variables in the industrial sector by designing a new sensor module. The main objective of is to improve a conventional Hall Effect sensor in order to assess the ability of the sensor module and the reliability of the system by measuring lubricant viscosity and contamination in lubricant, angular displacement, non-destructive inspection and then comparing the efficiency of the EMAT method by measuring material imperfection using the methodology of non-destructive measurement.

The second presents the comparison of performance between advantage and disadvantage under the same specific conditions, such as comparing the efficiency of stimulation for activating the Hall Effect sensor between an electromagnetic field generated by Helmholtz coil and a magnetic field generated by a permanent magnet, with regard to the placement of Hall generator and a permanent magnet by comparing the array position and the cross position including the number of Hall generators and permanent magnets, and finally comparing the processing of signals by analyze the output signal of a new sensor module in terms of measurement of patterns of voltage signal and frequency domain.

The third presents the operation methodologies of a Hall Effect sensor, as follows:

a) Stimulation of a Hall Effect sensor by different methodologies of a magnetic field.
b) Influence of the placement of Hall generator and permanent magnet and the number of Hall generators per number of magnets.
c) Processing of output signal and analysis of the signal in terms of voltage signal and frequency domain.

11.3 Application of the New Sensor Module

This section summarizes the measurement of some variables in the industrial sector by applying a Hall Effect sensor as a sensor device in terms of a sequence of studies that start by considering a normal permanent magnet for measuring the lubricant viscosity and contamination in lubricant, the stimulation methodologies of a Hall Effect sensor with reference to a magnetic field. In the case of a magnetic field generated from a permanent magnet, the permanent magnet with different shape for assembling a sensor module such as flat-curve permanent magnet was chosen by applying for angular displacement, and also material imperfection in order to accords and relate the variables to measurement.

The performance of a new sensor module will be considered with reference to the stimulation methodologies of a Hall Effect sensor by comparing the Helmholtz coil and the permanent magnet. Then the placement of Hall generator and permanent magnet by will be compared between the array position and the cross position in order to measure material

imperfection. Finally, the methodologies of the new sensor module will be compared to the methodologies of EMAT.

11.3.1 Summary of Lubricant Viscosity and Contamination in Lubricant Using a New Sensor Module

The experiment established that the developed system could provide accurate and reliable results. The sensor module was developed for the measurement of contamination of the lubricant which has already been mentioned in this article. The principle of the magnetic field was measured using a new sensor module. It can be used to measure the amount of contamination of the metal (ferrous) in the lubricant. The reference standard for detecting the lubricant is NAS 1638. The results showed that the sensor can measure the amount of contamination of the metal, which is associated with changes in the magnetic field in the lubricant. This system can measure the contamination level since NAS 15, which can define the wear and tear of machinery, is sufficient to indicate proper drainage. The advantages of using the principles of measuring magnetic fields is that they are able to reduce errors due to the turbidity of the lubricant due to each brand and grading the clarity and intensity of colour as well, although care is when using the optical measurement. Measurement system can be improved in terms of sensitivity and ability of measuring the contamination at a lower level, NAS 15 by selecting the sensor that has high sensitivity to measure magnetic fields. Moreover, it can be updated to install on the machine that can measure in real time to prevent the damage of machinery.

In case of viscosity measurement, it was also observed that the output voltage from a new sensor module was smoothly and consistent varied considering the period of time of metal particles moving to a permanent magnet and reaching a stable point. Metal particles with various weights were added to 25 ml lubricants and then experimented on in order to estimate the appropriate weight to be used for testing. The appropriate weights of metal particles for experimentation would range from 0.1 g to 1 g. If the reference metal particles' weight was greater than 1 g, the output voltage from a new sensor module would be non-constant. However, the influence on the lowest viscosity of the lubricant was insignificant and the influence on the lubricant viscosity higher than 9,500 maps at -15 °C (Cranking) and 60,000 mPa.s at -20 °C (Pumping) was low. Therefore, we can estimate the ratio between weight of the reference metal particles (0.8 g) and the volume of the lubricant as ≈ 0.1019 ml per 25 ml.

11.3.2 Summary of Angular Displacement Using a Hall Effect Sensor with Helmholtz Coil

From an experimental study of an angular sensor position by analyzing the new sensor module output voltage, the relationship of Hall voltage and the density of electromagnetic field within the Helmholtz coil radius can be observed. Moreover, the experimental results from the new sensor module output voltage varied with the density and direction of the electromagnetic field generated by the Helmholtz coil. The deadband from testing varied between 2 deg to -3 deg according to the theory. However, the deadband would be dependent on magnetic field generated, whether by a Helmholtz coil or a permanent magnet. To reduce the effect of deadband, the use of a permanent magnet and an ADC with a 16-bit resolution are recommended. In terms of statistical analysis, the results from the developed system were highly accurate and reliable throughout the experimental range (95%). The maximum uncertainty was 0.734847 at -3 deg.

11.3.3 Summary of Angular Displacement Using Two Flat-Curve Permanent Magnets

From an analysis of magnetic field density variation on a new sensor module due to an inclined angle change, it can be noted that any point of a permanent magnet formally generates a different magnetic density. Therefore, the output voltage from a new sensor module can be used to determine the angle of inclination. The experiments were separated in into the range of -20 deg to 20 deg and the range of -6 deg to 6 deg. The monitoring system developed by an angular displacement system can provide the results with the best accuracy and reliability for observing ground level subsidence or industrial machine alignment for the inclined angle within the range of -6 deg to 6 deg with 0.01 deg of resolution per step. Moreover, the angular displacement system can be applied to monitor the level of land subsidence in areas such as industrial machine alignment and installation as well as examining the inclination of structure in civil engineering.

11.3.4 Summary of Material Imperfection Based on Time Domain

The Hall Effect sensor was chosen due to its high reliability and reasonable cost compared to other methodologies. Moreover, this sensor can simply connect to other electronic devices as output voltage is generated. From experiments with four sensor modules, it can be observed that a single Hall sensor would be appropriate for small drilled holes or small cracks on material surfaces in a slot shape rather than a round shape. In the case of large holes or cracks, a 4-crossing Hall sensor would be most appropriate for achieving optimum

performance compared to other modules because of the smoothness and stability of the output signals. The application of several Hall generators installed together would be beneficial for determining the edge and the size of the hole or crack of the target which can perform better than using only one sensor. However, from experiments on several modules, it can be noted that to achieve the optimum results, the module should be selected by considering the size of hole or crack in the target which should be larger or as small as the size of the Hall Effect sensor because the smaller the size of hole, the greater the potential error of measurement.

11.3.5 Summary of Material Imperfection Based on Frequency Domain

An analysis of the new sensor module output based on frequency domain is a methodology which can be explicitly applied to detect the dimension of holes (diameter and depth) on a metal surface. From this experiment, the principle of frequency domain can precisely determine and distinguish the depth of drilled holes with 1 mm difference. The appropriate placement of a Hall generator for measurement was experimented with in 2 cases, a single Hall sensor and a 4-crossing Hall sensor, in order to compare the reliability and accuracy of the results under the same conditions. It can be noted that the 4-crossing Hall sensor could exhibit high efficiency and reliability in measuring the drilled holes or the large fracture compared to a single Hall sensor. This could contribute to the individual output of each Hall generator that could effectively provide an accurate position and diameter of drilled holes or fractures in materials.

11.3.6 Summary of Performance Comparison of New Sensor Module and EMAT in NDT Measurement

Use of Hall generators installed together can provide a better outcome, which is the determination of the edge and size of a drilled hole as well as a crack in the surface of the material compared to the use of a single sensor. However, from experiments with each sensor module in this study, it can be noticed that a single Hall sensor would be appropriate for holes or cracks in the surface of a small specimen; while a 4-crossing Hall sensor would be effective and appropriate for testing large holes and cracks. It is because the output of each Hall generator can be compared for determining the edge or the diameter of a hole or crack, and also the depth, which provides better results compared to a single Hall sensor. Moreover, the frequency domain is one of the methodologies which can be adopted for analysis in order to enhance the effectiveness of the new sensor module application to make it more accurate and reliable as the measured signal is in the frequency form and which has considerable distinction in identifying small differences in signals from measurements of

the width and depth of holes. A single Hall sensor and a 4-crossing Hall sensor can clearly establish the different depth of hole by 0.5 mm. Compared to the efficiency of an ultrasonic sensor under the same conditions, it can be observed that the generation of an ultrasonic wave using the EMAT method would not be suitable for small specimens. Therefore, the test specimen should have an adequate measured area for fully installing sensor coils and a permanent magnet on the surface. Small specimens would increase uncertainty in measurement and also errors in comparison to the use of a new sensor module by which small specimens can be measured with higher accuracy, precision, and reliability (less than 0.24% of error with about 0.014 of standard deviation) as well as the distinction of each measured location. Also, the simplicity of installations, system, and measurement process at a lower cost can be observed. However, the use of a new sensor module is limited to detecting inner cracks and very thick materials.

References

[1] Ed. Ramsden, “Hall-Effect Sensor: Theory and Applications”, Elsevier Inc. 2006.

[2] K. Bienczyki, “Angle Measurement Using a Miniature Hall Effect Position Sensor”, Electrodynamic and Mechatronics, 2009. SCE 11 '09. 2nd International Students Conference, May 19-21, 2009, pp. 21-22.

[3] Y. Y. Lee, R. H. Wu, and S. T. Xu, “Applications of Linear Hall-Effect Sensors on Angular Measurement”, 2011 IEEE International Conference on Control Applications (CCA), Part of 2011 IEEE Multi-Conference on System and Control Denver, CO, USA. September 28-30, 2011, pp. 479-482.

[4] S. Tumanski and S. Baranowski, “Magnetic Sensor Array for Investigations of Magnetic Field Distribution”, Journal of Electrical Engineering, Vol 57. No 8/s, 2006, pp. 185-188.

[5] R. Murayama, and K. Ayaka, “Evaluation of Fatigue Specimens Using EMATs for Nonlinear Ultrasonic Wave Detection”, Journal of Nondestructive Evaluation, Vol. 26, Issue 2-4, 2007, pp. 115-122.

[6] T. Dogaru, C. H. Smith, R. W. Schneider, and S. T. Smith, “New directions in eddy current sensing”, Scopus, Vol. 18, Issue 6, 2001, pp. 56+58-62.

[7] C.S. Rangan, G.R. Sarma, and V.S.V. Mani, “Instrumentation Devices and System”, Tata McGraw-Hill, Publishing Company Limited, New Delhi, 2004.

[8] J. W. Dally, W. F. Riley, and K. G. McConnell, “Instrumentation for Engineering Measurements”, John Wiley & Sons, Inc., 1993.

[9] Honeywell Inc., “Hall Effect sensing and application; MICRO SWITCH Sensing and Control”, http://www.honeywell.com/sensing

[10] M. W. Bongard, R. J. Fonck, B. T. Lewicki, and A. J. Redd, “A Hall Sensor Array for Internal Current Profile Constraint”, Review of Scientific Instruments 81, 2010, pp. 10E105-1- 10E105-4.

[11] R. Murayama, Z. Yamaji, W. Sriratana, M. Kobayashi, and C. Jen, "Remote Sensing Sensor Using Giant Magnetostrictive Materials", Journal of the Japan Society of Applied Electromagnetics and Mechanics, Vol. 20, No. 2, June 2012, pp. 508-513.

[12] Ball P G, "Machine wear analysis: a rational approach to methods integration for maximum benefits", Lubrication Engineering, Vol.54, No.3, March 1998, pp. 18-22.

[13] B. W. Wilson, and G. Silvernail, "Automated in-line machine fluid analysis for marine diesel and gas turbine engines", International Condition Monitoring Conference, Mobile, Alabama, 2002, pp. 129-135.

[14] R. Guojun, T. Derong, and Q. Jinyu, "An on-line monitoring technique for contamination degree of diesel engine lubricating oil", Internal Combustion Engines, Vol. 32, June 2005, pp. 36-38.

[15] Bano, M. Strharsky, I. Hrmo, and Igor, "A viscosity and density meter with a magnetically suspended rotor", IEEE Scientific Instruments, Vol. 74, Issue 11, November 2003, pp. 4788-4793. doi: 10.1063/1.1614881

[16] V. Hiligsmann and P. Riendeau, "Monolithic 360 Degrees Rotary Position Sensor IC", IEEE Sensors Conference, Vienna, 24-27 October 2004, pp. 1137-1142.

[17] B. Lequesne, and T. Schroeder, "High-Accuracy Magnetic Position Encoder Concept", IEEE Transactions on Industry Applications, VOL. 35, NO. 3, 1999, pp. 568-576. doi:10.1109/28.767003

[18] Y. Y. Lee, R. H. Wu and S.T. Xu, "Applications of Linear Hall-Effect Sensors on Angular Measurement", 2011 IEEE International Conference on Control Applications (CCA), Denver, 28-30 September 2011, pp. 479-482. doi:10.1109/CCA.2011.6044465

[19] LEYBOLD DIDACTIC GMBH, "Helmholtz-Spulenpaar Pair of Helmholtz Coils", http://chemphys.purduecal.edu/~ncrelich/PortableDocuments/Leyboldfiles/55506DETelAtomicHelmholtz.pdf

[20] G. Arfken, "Mathematical Methods for Physicists", Academic Press, Orlando, 1985, pp.321-327.

[21] M. Hawkes, and A. Nehorai, "Effects of Sensor Placement on Acoustic Vector-Sensor Array Performance", IEEE Journal of Oceanic Engineering, Vol. 24, NO. 1, Jan. 1999, pp. 33-40.

[22] S. Tumanski, and S. Baranowski, “Magnetic Sensor Array for Investigations of Magnetic Field Distribution”, Journal of Electrical Engineering, Vol. 57. NO 8/S, 2006, pp. 185-188.

[23] S. S. Dhillon, K. Chakrabarty, and S. S. Iyengar, “Sensor Placement for Grid Coverage under Imprecise Detections”, Information Fusion, 2002. Proceedings of the Fifth International Conference, vol.2, Jul. 2002, pp. 1581-1587.

doi: 10.1109/ICIF.2002.1021005

[24] K. Skucha, P. Liu, M. Megens, J. Kim, and B. Boser, “A Compact Hall-Effect Sensor Array for the Detection and Imaging of Single Magnetic Beads in Biomedical Assays”, Solid-State Sensors, Actuators and Microsystems Conference (TRANSDUCERS), 16th International, Beijing, China, Jun. 5-9, 2011, pp. 1833-1836.

[25] S. Boukhenous, and M. Attari, “A Low Cost Instrumentation Based Sensor Array for Ankle Rehabilitation”, Biomedical Engineering Trends in Electronics, Communications and Software, Jan. 2011, pp. 69-78.

[26] M. H. Jones, “Tribologya key element in condition monitoring”, Proc Condition Monitoring, Oxford, 2011, pp. 20-29.

[27] Q. Meng, “Study on the On-line Oil Monitor Based on Optical Fiber Sensor”, Chinese Hydraulics & Pneumatics, Vol. 5, May 2006, pp. 34-37.

[28] F. Buiochi, R. T. Higuti, C. M. Furukawa, and J. C. Adamowski, “Ultrasonic Measurement of Viscosity of Liquids”, IEEE Ultrasonics Symposium, Vol. 1, 2000, pp. 525-528. doi: 10.1109/ULTSYM.2000.922604

[29] C. Lou, D. Xing, “Photoacoustic measurement of liquid viscosity”, IEEE Applied Physics Letters, Vol. 96, Issue 21, May 2010, pp. 211102-211102-3.

doi: 10.1063/1.3435462

[30] D. C. Crew, P. G. McCormick, and R. Street, “Measurement of magnetic viscosity in NdFeB”, IEEE Transactions on magnetics, Vol. 32, Issue 5, Part 2, September 1996, pp. 4356-4358. doi: 10.1109/20.538867

[31] Y. Dingxin, Z. Xiaofei, H. Zheng, and Y. Yongmin, “Oil Contamination Monitoring Based on Dielectric Constant Measurement”, Measuring Technology and Mechatronics Automation, Zhangjiajie, Hunan, 2009, pp. 249-252.

[32] A. Agoston, C. Otsch, J. Zhuravleva, and B. Jakoby, “An IR-Absorption Sensor System for the Determination of Engine Oil Deterioration”, Proceedings of IEEE, Sen-sors, Vol. 1, 2004, pp. 463-466.

[33] Z. Pang, N. Shi, G. Meng, and W. Li, “Development of in-line oil contamination sensor for lubricant of scraper conveyor reducer”, Electronic Measurement & Instruments (ICEMI '09), 9th International Conference, Beijing, 2009, pp. 4-808-4-812.

[34] United Kingdom Accreditation Service, “The Expression of Uncertainty and Confidence in Measurement”, United Kingdom Accreditation Service, London, 1997.

[35] “Viscosity Classifications”, http://www.tribology-abc.com/abc/viscosity.htm#top

[36] “COMSOL 3.2b Release Notes”, COMSOL AB, 2005. http://www.i-ath.com.sg/download/updates/comsol/comsol32a/comsolrelease32a.pdf

[37] D. Holder, “Design and Construction of a Helmholtz Coil Magnetic Test Cell”, U.S. Army Missile Command, 1992.

[38] T. C. Akinci, “Time-Frequency analysis of the current measurement by Hall Effect sensor for electric arc welding machine”, ISSN 1392-1207, Academic Journal, Mechanika, Vol. 85, Issue 5, 2010, pp. 66-71.

[39] “Practical Introduction to Frequency-Domain Analysis”, http://faculty.kfupm.edu.sa/ES/akwahab/Frequency_Domain.htm

[40] J. William and Palm III, “Introduction to MATLAB for Engineers”, McGraw-Hill Companies, Inc., 2011.

[41] B. R. Hunt, R. L. Lipsman, and J. M. Rosenberg, “A Guide to MATLAB for Beginners and Experienced Users”, Cambridge University Press, 2006.

[42] E. B. Magrab, S. Azarm, B. Balachandran, J. H. Duncan, K. E. Herold, and G. C. Walsh, “An Engineer’s Guide to MATLAB-with Application from Mechanical, Aerospace, Electrical, Civil and Biological Systems Engineering”, Pearson Education, Inc., 2011.

[43] G. Kerschen, V. Lenaerts, “A Frequency Domain Versus a Time Domain Identification Technique for Nonlinear Parameters Applied to Wire Rope Isolators”, Journal of Dynamic Systems, Measurement, and Control, Vol. 123, 2001, pp. 645-650.

[44] R. N. Bracewell, “The Fourier Transform and Its Applications”, McGraw Hill, New York, 1999.

[45] H. N. Norton, “Sensor and Analyzer Handbook”, Prentice Hall, Inc., Englewood Cliffs, NL 07632, USA., 1982.

[46] D. E. Bray and R. K. Stanley, “Nondestructive Evaluation”, CRC Press, New York, 1997.

[47] D. Greve, I. J. Oppenheim, H. Sohn, C. P. Yue, and W. Wu, “An Inductively Coupled Lamb Wave Transducer”, IEEE Sensors Journal, Vol. 7, No. 2, 2007, pp. 295-301. doi:10.1109/JSEN.2006.886904

[48] R. Murayama, M. Kobayashi, K. T. Wu, and C. K. Jen, “Noncontact Driving System Using Induction-Based Method and Integrated Piezoelectric Ultrasonic Transducers”, Journal of Sensor Technology, June 2012, 2, pp. 60-67. doi:10.4236/jst.2012.22009

Acknowledgment

The author wishes to express his eternal gratitude and deep appreciation to Prof. Riichi Murayama for important teachings, who is more than advisor and chairman of the dissertation committee, for his valuable guidance, constructive suggestions, and incessant encouragement throughout the study period. He is thankful to his interest in the progress of his thesis at all times.

The author would like to extend his special gratitude to Prof. Shi-Jie Zhu, Prof. Xing-Zheng Wu and Prof. Fumio Akagi, the committee members for their valuable suggestions and very good comments about this thesis.

He is also greatly indebted and he would like to express his sincere thanks and gratitude to King Mongkut's Institute of Technology Ladkrabang (KMITL), for budget, scholarship support and the worthy support during his study period. He is grateful to Assoc. Prof. Kitti Tirasesth, his to give a chance for continuous study in doctoral level, which prepared him for the challenges of studies in Japan. Without his everything supports including guidance, it is impossible to success by himself.

Moreover, heartfelt thanks are given to Fukuoka Institute of Technology (FIT), for research support and budget for international conference also everything available for his study at FIT.

In addition, he is grateful to Satomi Harada-sensei and Fumie Yuki-sensei, for educating Japanese. A special thank goes to Mr. Mori Cho, Mr. Hiroshi Chikamatsu, and all staff of International Affairs at Fukuoka Institute of Technology, for their continuous support and help.

Furthermore, he also would like to thanks him colleague, Mr. Jie Weng, Mr. Kenshi Matsumoto, and, Mr. Worachat Duangsuwan, them as master’s degree student in same laboratory, for practical advice and everything support during his study at FIT.

Thank are due to Department of Instrument and Control Engineering, Faculty of Engineering, King Mongkut's Institute of Technology Ladkrabang, for the worthy support during his study period.

Special gratefulness is extended to his parents, his wife, and friends for their never-ending encouragement and patience. Support and tremendous sacrifices have encouraged the author in all his worthwhile pursuits throughout the life and the author would like to dedicate this thesis to them.

List of Papers

Journals Papers

1. W. Sriratana, R. Murayama, and L. Tanachaikhan, "Application of the HES in Angular Analysis", Journal of Sensor Technology (JST), Vol. 2, No. 2, June 2012, pp. 87-93. doi:10.4236/jst.2012.22013

2. R. Murayama, Z. Yamaji, W. Sriratana, M. Kobayashi, and C. Jen, "Remote Sensing Sensor Using Giant Magnetostrictive Materials", Journal of the Japan Society of Applied Electromagnetics and Mechanics, Vol. 20, No. 2, June 2012, pp. 508-513.

3. W. Sriratana, and R. Murayama, "Analysis of Land Subsidence Using the HES", Journal of Electromagnetic Analysis and Applications (JEMAA), Vol. 4, No. 7, July 2012, pp. 310-316. doi:10.4236/jemaa.2012.47043

4. W. Sriratana, and R. Murayama, "Elimination of Oil Residual inside the Copper Pipe Using Ladder Technique", Engineering (ENG), Vol. 5, No. 1, January 2013, pp. 8-15. doi:10.4236/eng.2013.51002

5. W. Sriratana, and R. Murayama, "Application of Magnetic Field Method for Measuring Lubricant Viscosity", Advanced Materials Science and Technology, Periodical of Materials Science, Vol. 750, 2013, pp. 116-124. dol:10.4028/www.scientific.net/MSF.750.116

6. W. Sriratana, R. Murayama, and L. Tanachaikhan, "Synthesis and Analysis of PZT Using Impedance Method of Reactance Estimation", Advances in Materials Physics and Chemistry (AMPC), Vol. 3, No. 1, 2013.

7. W. Sriratana, and R. Murayama, "Measurement of the Lubricant Properties Using Hall Effect Sensor: A Study on Contamination and Viscosity", Engineering (ENG), Vol.5 No.4, April 2013, pp. 386-393. doi: 10.4236/eng.2013.54051

International Conference Papers

1. R. Murayama, Z. Yamaji, W. Sriratana, M. Kobayashi, and C. Jen, "Remote Sensing of an Ultrasonic Sensor Using Giant Magnetostrictive Materials", The 20th MAGDA Conference in Pacific Asia, Kaohsiung, Taiwan, 14-16 November 2011.

2. R. Murayama, W. Sriratana, M. Kobayashi, and C. Jen, "Nondestructive Testing Using Giant Magnetostrictive Materials as an Ultrasonic Sensor", The ICEM15-15th International Conference on Experimental Mechanics, Proto, 22-27 July 2012.

3. W. Sriratana, and R. Murayama, "Analysis of Lubricant Viscosity Using Magnetic Field Method", The Eight International Forum on Advanced Material Science and Technology (IFAMST-8), Fukuoka, 1-4 August 2012.

4. W. Sriratana, and R. Murayama, "Lubricant Viscosity Measurement Using Hall Effect Sensor", The Society of Instrument and Control Engineers (SICE Annual Conference 2012), Akita, 20-23 August 2012.

5. W. Sriratana, and R. Murayama, "Application of Hall Effect Sensor: A Study on the Influences of Sensor Placement", The 22nd IEEE International Symposium on Industrial Electronics (ISIE 2013), Taiwan, 28-31 May 2013.

6. W. Sriratana, and R. Murayama, "Analysis of Hall Effect Sensor Placement Based on Frequency Domain", The Society of Instrument and Control Engineers (SICE Annual Conference 2013), Nagoya, 14-17 September 2013.

7. W. Sriratana, and R. Murayama, "Performance Comparison of Hall Effect Sensor and EMATs in Measurement of Specimen with Various Hole Depths", International Conference on Experimental Mechanics (ICEM 2013) and The Twelfth Asian Conference on Experimental Mechanics (ACEM 12), Bangkok, 25-27 November 2013.

8. R. Murayama, and W. Sriratana, "Development of A Guide Wave Inspection System using A Polarized Shear Wave-EMAT and Evaluation of its Performance", International Conference on Experimental Mechanics (ICEM 2013) and The Twelfth Asian Conference on Experimental Mechanics (ACEM 12), Bangkok, 25-27 November 2013.

Local Conference Paper

1. W. Duangsuwan, S. Kenji, U. Yutaka, W. Sriratana, R. Murayama, "Study of Non-contact Drive Ultrasonic Sensor using a Giant Magnetostrictive Material", Japan Society of Mechanical Engineers, Okayama, 8 -11 September 2013.